STABLE PARAFFIN COMPOSITES FOR LATENT HEAT THERMAL STORAGE SYSTEMS

A Thesis
Presented to
The Academic Faculty

By

Anne M. Mallow

In Partial Fulfillment
Of the Requirements for the Degree
Master of Science in the
George W. Woodruff School of Mechanical Engineering

Georgia Institute of Technology

December 2015

STABLE PARAFFIN COMPOSITES FOR LATENT HEAT THERMAL STORAGE SYSTEMS

Approved by:

Dr. Samuel Graham, Advisor
School of Mechanical Engineering
Georgia Institute of Technology

Dr. Kyriaki Kalaitzidou
School of Mechanical Engineering
Georgia Institute of Technology

Dr. Baratunde Cola
School of Mechanical Engineering
Georgia Institute of Technology

Date Approved: September 18, 2015

ACKNOWLEDGEMENTS

I wish to thank my advisor, Dr. Samuel Graham, for his technical guidance combined with remarkable patience during this thesis journey. I am grateful for the support of Dr. Baratunde Cola and Dr. Kyriaki Kalaitzidou shown through the use of laboratory equipment, mentoring, and serving on my thesis committee. I also appreciate the collaboration with Dr. Omar Abdelaziz of Oak Ridge National Laboratory, which has facilitated and advanced this research.

I would like to thank members of the EMRL group for their friendship as well as friends outside of the group including fellows of the Three Amigos plus Stephen. Furthermore, I want to acknowledge my family for their love, patience, and unwavering support.

I wish to express my gratitude to the NSF IGERT Program, ORNL GO! Program, and Mr. Antonio Bouza of the U.S. DOE Building Technologies Office for financial support of this research and my education. Additionally, special thanks to Mr. Bryan Leyda and Mr. Dana Ream of ERG Aerospace for experimental material and insightful discussions.

TABLE OF CONTENTS

LIST OF TABLES

LIST OF FIGURES

SUMMARY

Phase change materials (PCMs) have the ability to store thermal energy as latent heat over a nearly isothermal temperature range. Compared to sensible heat storage, properly chosen PCMs can store an order of magnitude more energy when undergoing phase change. Organic PCMs present several advantages including their non-corrosive behavior and ability to melt congruently, which result in safe and reliable performance. Because of these qualities, organic PCMs have been proposed for use in latent heat thermal storage systems to increase the energy efficiency or performance of various systems such as cooling and heating in buildings, hot water heating, electronics cooling, and thermal comfort in vehicles. Current performance is hindered by the low thermal conductivity, which significantly limits the rate of charging and discharging. Solutions to this challenge include the insertion of high conductivity nanoparticles and foams to increase thermal transport. However, performance validation remains tied to thermal conductivity and latent heat measurements, instead of more practical metrics of thermal charging performance, stability of the composite, and energy storage cost.

This thesis focuses on the use of graphite nanoplatelets and graphite foams to increase the thermal charging performance of organic PCMs. Stability of graphite nanoplatelets in liquid PCM is realized for the first time through the use of dispersants and control of the viscosity, particle distribution, and oxidation. Thermal charging response of stable graphite nanoplatelet composites is compared to graphite foam composites. This study includes a correlation of thermal conductivity and latent heat to material concentration, geometry, and energy storage cost. Additionally, a hybrid PCM storage system of metal foam combined with graphite nanoplatelet PCM is proposed and evaluated under cyclic thermal conditions.

CHAPTER 1: INTRODUCTION

1.1. Background

In combination with the advancement of efficient and cost effective energy solutions, waste heat recovery technologies are being developed to reduce energy consumption and carbon dioxide emissions. It is estimated that more than half of the energy produced each year is rejected as waste heat into the environment [1]. This low-grade heat is produced by machines, electrical equipment, and industrial processes as a response to the inefficient operation of these systems. By developing methods to better harness this energy, it can either be immediately utilized in other industrial and domestic processes to enhance numerous thermodynamic cycles or stored for later usage.

Though high temperature (>200°C) waste heat is often re-used to perform work or provide heat to buildings and processes [2], lower temperature heat is released into the environment due to the quality of the heat or the inability to use it to do work. Furthermore, any of the high temperature energy that cannot be used immediately is also released due to the limited employment of energy storage technologies. Not only is this wasted energy worth billions of dollars each year, but the environmental effects of this excess heat is coupled to the environmental effects of the greenhouse gases released during the production of that energy. In a recent study published in Nature Climate Change, the heat generated by everyday activities, such as heating buildings or powering vehicles, has a significant warming effect, which influences major atmospheric systems [3]. This waste heat causes winter warming by as much as 1°C across large areas of northern North America and northern Asia [3], a finding that helps to explain the disparity between observed warming in the last half-century and the amount of warming that computer models have been able to explain.

It is apparent that waste heat recovery systems are fundamental to the global effort towards reduced energy consumption and associated greenhouse gas emissions to combat global warming. The development of more efficient, cost effective, and clean sources of energy such as the conversion of heat to power has been an area of much research and technological development [4-7]. As depicted in Figure 1.1 and Figure 1.2, technologies such as combined heat and power (CHP) and electricity co-generation have been developed to use surplus heat to generate electricity. However, a crucial link between waste heat production and utilization remains: thermal energy storage. Waste heat recovered from thermodynamic systems must be immediately applied to existing energy needs or the heat is lost to the environment. Energy storage is a crucial hurdle to overcome in the effort to bridge the gap between energy generation and consumption.

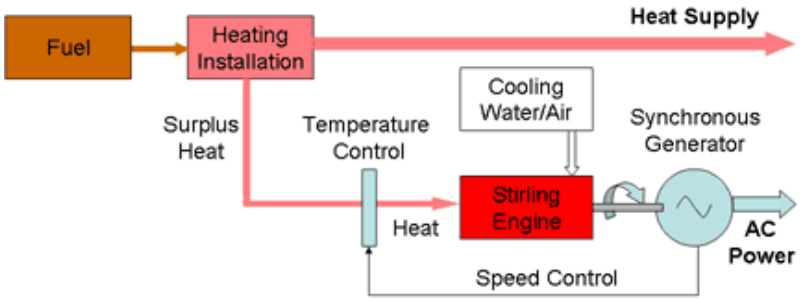

Figure 1.1 Combined heat and power (CHP) [7].

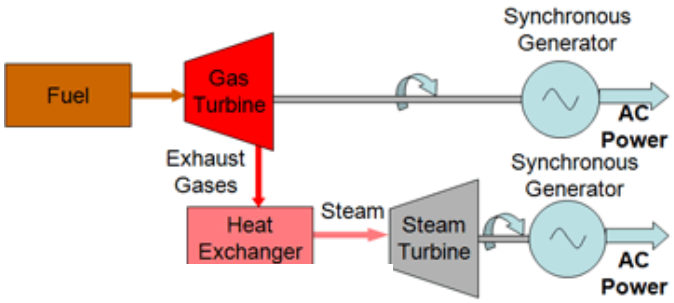

Figure 1.2 Electricity co-generation [7].

1.2. Thermal Energy Storage

The development of thermal energy storage is critical to the success of any intermittent energy source in meeting energy demand. Not only does this technology allow for decoupling supply from demand, but it also reduces energy costs, increases flexibility of operation by avoiding partial load operation or operation at other suboptimal times, and shifts demand over time to reduce peak loads [8]. Since the ability to store thermal energy is required for using waste heat and renewable energy in heating and cooling systems effectively, enhancement in thermal energy storage systems is imperative.

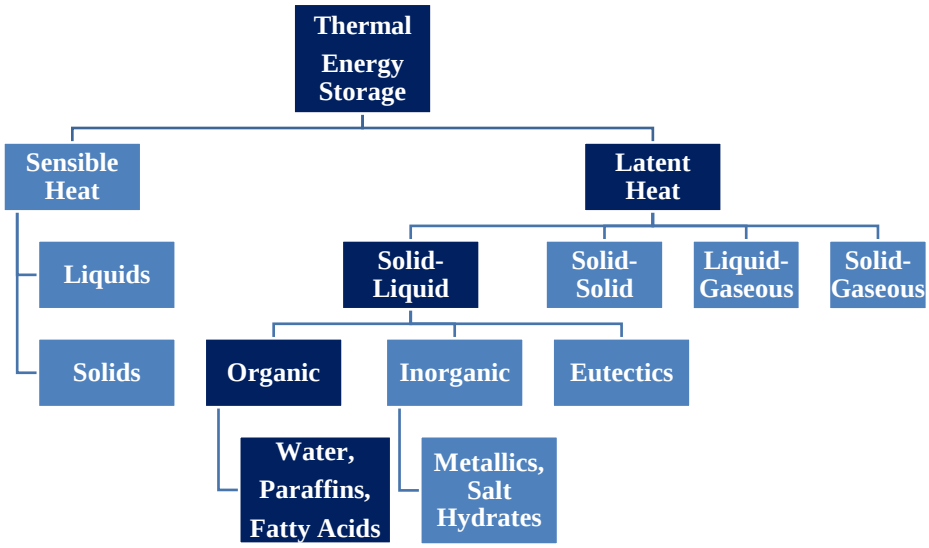

Figure 1.3 Classification of thermal energy storage materials [9-11].

As Figure 1.3 depicts, the two primary methods of storing thermal energy are sensible heat and latent heat. Sensible heat, measured as the specific heat value [$kJkg^{-1}K^{-1}$], is the heat stored in a substance by raising the temperature of the solid or liquid as depicted in Figure 1.4 as areas A, C, and E. The amount of heat stored depends on the specific heat of the medium, the temperature change, and the amount of storage material as described by Equation 1,

$$Q = mC_{av}(T_f - T_i) \quad (1)$$

where,

Q = quantity of heat stored [kJ]

C_{av} = average specific heat between T_f and T_i [$kJkg^{-1}K^{-1}$]

m = mass of heat storage medium [kg]

T_f = final temperature [K]

T_i = initial temperature [K]

Latent heat is the thermal energy associated with the phase change of a material, measured as latent heat of fusion (freezing/melting, [$kJkg^{-1}$]) or latent heat of evaporation (condensation/vaporization, [$kJkg^{-1}$]). As shown in Figure 1.4, an ideal material absorbs heat at a constant temperature when transitioning from solid to liquid (B) and liquid to gas (D), and releases energy at a constant temperature when it is undergoing the opposite change of states. The storage capacity of a latent heat storage system with a phase change medium is given by Equation 2,

$$Q = m\left[C_{sp}(T_m - T_i) + a_m \Delta h_m + C_{lp}\left(T_f - T_m\right)\right] \quad (2)$$

where,

Q = quantity of heat stored [kJ]

a_m = fraction melted

C_{sp} = average specific heat between T_i and T_m [$kJkg^{-1}K^{-1}$]

C_{lp} = average specific heat between T_m and T_f [$kJkg^{-1}K^{-1}$]

Δh_m = heat of fusion per unit mass [$kJkg^{-1}$]

m = mass of heat storage medium [kg]

T_f = final temperature [K]

T_i = initial temperature [K]

T_m = melting temperature [K]

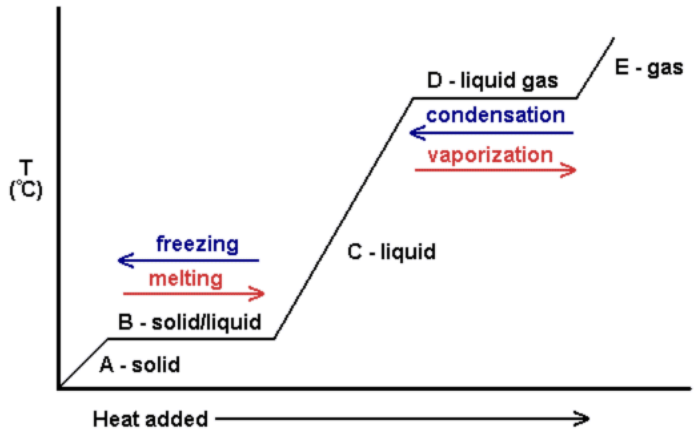

Figure 1.4 Phase change diagram [12].

Of the forms of thermal energy storage discussed above, latent heat thermal storage systems (LHTSS) are considered the most promising due to their ability to provide high energy storage density (5 to 14 times higher than sensible heat systems [11, 13]), while storing heat over a nearly isothermal temperature range corresponding to the phase-transition temperature [10, 11, 14]. They are especially superior when the temperature difference between storing and releasing heat is small to maximize the amount of heat stored during the phase change. For example, consider two systems operating between two different operating conditions: 25°C to 60°C and 50°C to 60°C. One system stores sensible heat in water and the other stores sensible and latent heat in paraffin. Assuming the representative properties listed in Table 1.1, the total energy stored in each system can be calculated using Equations 1 and 2. As the Table 1.1 displays, although paraffin outperforms water in both cases, the difference is more significant for the lower operating temperature range.

Table 1.1 Water and paraffin parameters and energy storage.

	Latent Heat [kJkg^{-1}]	Sensible Heat [kJkg^{-1}K^{-1}]	Melting Temperature [°C, K]	Energy Stored 25°C-60°C [kJkg^{-1}]	Energy Stored 50°C-60°C [kJkg^{-1}]
Water	335	4.2	0, 273	147	42
Paraffin	189	2.1	54, 327	263	210

Latent heat storage materials, referred to as phase change materials (PCMs), can store and release heat during various changes in phase: solid–solid, solid–liquid, liquid–gas, solid–gas. Solid-liquid PCMs are most widely used in the development of LHTSS. Although solid-solid phase change materials, which store energy through crystalline structure changes, offer the advantage of less stringent container requirements and limited volume change, they also have lower latent heat values. Liquid-gas and solid-gas PCMs have comparable latent heat values to solid-liquid PCMs, however, they require advanced storage containers that can handle the large volume changes. Solid-liquid PCMs have become a central focus in the development of latent heat thermal storage due to their comparatively high latent heat values and minimal volume change during phase transition, which reflects in ease of container and system design [11, 15]. The use of solid-liquid PCMs provides a cost-effective and environmentally friendly system for easy and efficient thermal energy storage and release, which can be designed to operate at various temperatures.

1.3. Solid-Liquid Latent Heat Storage Materials

As Figure 1.3 depicts, there are three main classifications of solid-liquid PCMs: organic, inorganic, and eutectic. Organic PCMs can be further classified as paraffins (alkanes) or non-paraffins. Paraffins are typically straight hydrocarbon chains (CH_3-(CH_2)-CH_3), which release or absorb large amounts of heat when the crystal structure shifts due to a temperature change. In

general, both the melting point and latent heat of fusion increase with the number of carbon atoms or chain length [10]. Non-paraffins include esters, fatty acids, alcohols, glycols and even water. Each of these materials exhibit unique properties unlike paraffins, which have very similar properties.

Inorganic PCMs can be further classified as salt hydrates or metallics. Salt hydrates are mixtures of inorganic salts and water forming a crystalline solid [10]. At the melting point, the hydrate crystals break into anhydrous salt, or a lower hydrate, and water. Metallics, a category that has yet to be seriously considered as a PCM technology, includes low melting metals and metal mixtures. The third category of solid-liquid phase change materials, eutectic PCMs, are a composition of two or more organic or inorganic components, each of which melts and freezes congruently, forming a mixture of the component crystals during crystallization [16]. Examples include: calcium chloride/water mixed with calcium bromide/water (inorganic) and naphthalene mixed with benzoic acid (organic).

Each of the above categories of PCMs has benefits and disadvantages for use in solid-liquid latent heat thermal storage systems. As described by Sharma *et al.* [10, 11], consideration of proper PCMs for use in LHTSS should be based on the following properties:

1) Thermal properties
    a) Suitable phase-transition temperature of material for desired operating temperature. For example, water melts at about 0°C, and, even though it has a high latent heat of fusion (335 $kJkg^{-1}$ [17]), this melting temperature is impractical for most applications.

b) High latent heat of fusion/energy storage density to minimize size of thermal storage system. Examples include paraffins (170-269 $kJkg^{-1}$), non-paraffins (86-259 $kJkg^{-1}$), and salt hydrates (68-482 $kJkg^{-1}$) [10]).

c) High thermal conductivity of both solid and liquid phases to assist the charging and discharging of energy of the storage systems

d) High specific heat to provide additional sensible heat storage

2) Physical properties

a) Favorable phase equilibrium (exchange of energy between solid and liquid phase without intervention).

b) Small volume change (expansion during melting, shrinkage during solidification) and low vapor pressure at operating temperatures to reduce containment issues.

3) Kinetic properties

a) Congruent melting to prevent phase segregation. Incongruent melting is specifically an issue for salt hydrates where the salt is not entirely soluble in the solvent. The resulting solution becomes supersaturated at the melting temperature, and the solid salt, due to its higher density, settles down at the bottom of the container and is unavailable for recombination during the reverse process of freezing.

b) High nucleation rate (self-nucleation) to avoid super cooling of the liquid phase. Another common problem with salt hydrates is that, at the fusion temperature, the rate of nucleation or crystallization is generally very low. To achieve a reasonable rate of crystallization, the solution has to be supercooled. This means instead of discharging energy at the fusion temperature, it is discharged at much lower temperature. To

overcome this issue, nucleating agents can be added ([13, 18], but this introduces cost and complexity to the system.

4) Chemical properties
    a) Long-term chemical stability
    b) Compatibility with construction materials to prevent corrosion
    c) Non-toxic and non-flammable
5) Economics
    a) Abundant and available
    b) Cost effective

Table 1.2 outlines specific advantages and disadvantages to each of the solid-liquid PCMs previously described. The melting temperature and latent heat values can either be determined with Differential Scanning Calorimetry (DSC) or Differential Thermal Analysis (DTA). In both methods, a sample is heated at a constant rate and the associated response to increase in temperature is compared to the performance of a reference material heated at the same rate. The latent heat and melting temperature of the sample can be determined based on the temperature difference over time between the sample and the known reference material. Samples of DSC curves are given in Figure 1.5. The term ‘sharper phase change temperature’ included in Table 1.2, refers to the difference in the response peaks as depicted by Figure 1.5. The difference between the sharper and symmetric curve of the fatty acid should be noted as compared to the paraffin DSC curve. Further discussion of the paraffin DSC curve can be found in Chapter 3.6.

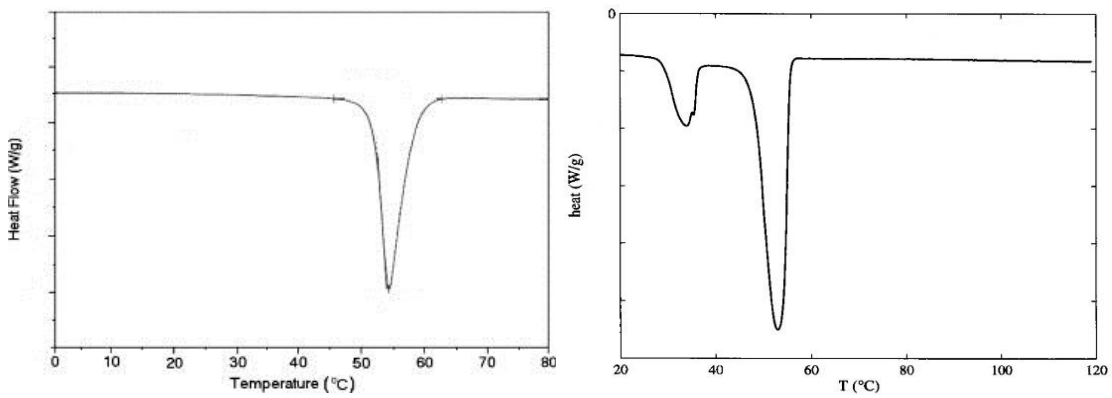

Figure 1.5 Fatty acid DSC curve [19] (left); Paraffin DSC curve [20] (right).

Enhancing properties of the various PCMs through improvements to the material or system design is necessary to exploit their characteristic high latent heat thermal storage capability in an efficient manner. By examining Table 1.2, it is apparent that no single material can have all the required properties for an ideal thermal storage media and that PCMs are suitable for a wide range of temperature applications.

Table 1.2 Characteristics of various phase change materials [10, 11, 15, 17, 21, 22].

	Advantages	Disadvantages	Melting Temperature Range [°C]	Latent Heat [$kJkg^{-1}$]
Organic	Cycle without phase segregation or degradation of latent heat; little or no supercooling; non-corrosive	Low thermal conductivity		
Paraffin (C_nH_{2n+2})	Low cost; chemically inert and stable below 500C; minimum volumetric change during melting	Non-compatible with some plastics; moderately flammable	6 - 76	170 - 269
Water (H_2O)	Low cost	Impractical melting temperature; high vapor pressure	0	335
Non-paraffin Organics/Fatty Acids	Sharper phase change temperature range than paraffin	Flammable; varying level of toxicity; low flash points; instability at high temperatures; high cost (2-2.5 times greater than paraffin); mildly corrosive	8 - 127	86 - 259
Inorganic	No degradation of latent heat			
Salt Hydrates	Sharper phase change temperature range and high thermal conductivity than organics	Phase (salt) segregation due to incongruent melting; supercooling of salt hydrates; corrosion	14 – 897	68 - 482
Metallics	High thermal conductivity	Cost, weight, corrosive	30 – 767	25 - 790
Eutectic	No segregation	Cost	15 - 82	95 - 218

1.4. Applications of Latent Heat Thermal Storage Systems

The first application of PCMs described in literature was used for heating and cooling of buildings (hot water production, assisted space heating, etc.) by Telkes (1975) and Lane (1983) [9, 11]. Since this initial introduction, PCMs have been widely studied for use in latent heat thermal storage systems to enhance the capabilities of various energy technologies [10]. Thermal storage of solar energy has become a significant topic of interest. By storing heat during the day, this energy can then be used during the night to reduce evening demand. Such a heat exchanger would use a PCM to store the collected solar heat, which would be later utilized with a heat transfer fluid, such as water or air, for pre-heating other energy processes (hot water, comfort heating, etc.). Additional applications of phase change materials include thermal management and protection of electronic devices [23], automotive engines [24], and spacecraft thermal systems [25], as well as to retaining thermal comfort in vehicles [26], motorcycle helmets [27], and even textiles [18]. High melting temperature PCMs can even be used in concentrated solar power systems [22].

In general, while high temperature PCMs (inorganic or eutectic; >200°C) can be used in solar power plants and other high temperature applications, the low temperature PCMs (organic, inorganic, or eutectic; <200°C) are mainly used in waste heat recovery systems and buildings for latent heat thermal storage. As Table 1.3 outlines, there are various applications for PCMs in residential, commercial, industrial, and institutional sectors. Some applications, such as PCM storage in gypsum boards or curtain walls, intend on using these materials to smooth temperature variations inside buildings [9]. Other uses, such as PCM integration in air ducts, heat pumps, and water heaters, utilize these materials as thermal storage materials for pre-heating or, conversely,

in electrical heating, as materials to assist with thermal management through cooling the electrical components.

Table 1.3 Potential implementation of thermal storage by PCMs [15].

Mode of implementation PCMs technology	Load Target	Objective	Sector
Distributed PCM storage in gypsum boards	Space heating and air-conditioning	Load shifting and conservation	All
Electrical heating units with PCM storage	Space heating	Load shifting and conservation	Residential, commercial, and institutional
Heat and cold PCM storage in air ducts	Space heating and air-conditioning	Load shifting	Commercial, institutional, and industrial
PCM air pre-heaters for heat pumps	Space heating	Load shifting and conservation	Residential, commercial, and institutional
Curtain walls with PCM system	Space heating	Conservation	Commercial, institutional, and industrial
Water heater with PCM storage	Water heating	Load shifting	Residential, commercial, and institutional

As evident by the previous discussion of the LHTSS applications, the development of any such system to store waste heat must possess at least the three following basic components [15]:

1. A latent heat storage material that undergoes a solid-to-liquid phase transition in the required operating temperature range
2. A proper containment system that houses the PCM
3. A heat exchanging surface for transferring heat from the heat source to the PCM and from the PCM to the heat sink

The continued advancement in the field of thermal storage is dependent on further development of latent heat storage materials to support the first basic component listed above.

Critical properties of these storage materials include the amount of thermal energy the PCM can store, as measured by latent heat, temperature at which the PCM melts, and the rate at which the PCM can transfer energy in and out of the system, which is partially dependent on thermal conductivity. After determining the operating temperature, optimizing the latent heat and the thermal charging rate allows for maximum response of the latent heat thermal storage system. Such optimization can be a result of either PCM selection, if the application has limited concern for specific advantages or disadvantages outlined in Table 1.2, or enhancing the characteristic properties of PCM if the application has constrained conditions such as being non-corrosive or chemically stable.

1.5. Thesis Outline

As summarized in Table 1.2, paraffins have been found to exhibit many desirable characteristics as PCMs for low temperature storage applications. This category of hydrocarbon materials, which ranges from hexadecane ($C_{16}H_{34}$) to hexacontane ($C_{60}H_{122}$), is known for being safe, reliable, and predictable. Paraffins are non-corrosive, non-toxic, and chemically and thermally stable; however, paraffins, such as those aforementioned, are expensive. With economic feasibility and commercial availability as system constraints, only technical grade paraffin, paraffin wax, is a practicable material for use in latent heat storage.

Paraffin wax is a mixture of many linear hydrocarbons obtained from petroleum distillation [11]. As a result of various hydrocarbon chain lengths, paraffin wax tends to have a small melting temperature range rather than a sharp melting point [15] as depicted in Figure 1.5. The disadvantage of most organic phase change materials, including paraffin wax, is their low

thermal conductivity, which results in longer transients for thermally charging and discharging the material.

To increase the rate of thermal charging and discharging, solutions such as extended surfaces, microencapsulation of the PCM, and introduction of high conductivity foams or nanoparticles within the PCM to increase the thermal conductivity of the composite have been proposed in literature. For a given PCM selected based on melting temperature, the amount of energy to be stored or the time interval over which the system is required to operate limits the choice of enhancement material. Solutions for thermal management of small electronics with pulsed operation are different than those for waste heat recovery from hot air ducts required to reclaim heat continuously. However, in general, such additions to the PCM system aim to minimize the impact on the stable, high latent heat capacity, and low cost PCM, while increasing the rate of thermal transport. This objective requires comparative experiments not only on the basis of thermal conductivity and latent heat measurements found in literature, but also focused on the of rate of thermal charging, stability of the enhancement material, and cost of the system.

Preliminary 2D finite element phase change simulations are presented below to demonstrate the potential impact of thermal conductivity on the rate of thermal charging for two different heat fluxes, 0.39 Wcm^{-2} and 1.55 Wcm^{-2}. The boundary conditions and thermal properties used in this simulation are presented in Figure 1.6.

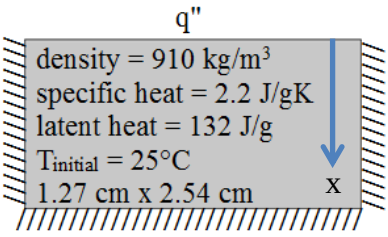

Figure 1.6 COMSOL geometry with boundary conditions and thermal properties

The temperature response at x=1.27cm is shown in Figure 1.7 and Figure 1.8 as a function of increasing thermal conductivity and magnitude of applied heat flux. Each system undergoes a sensible heating region followed by phase change at 55°C and then another sensible heating region. The thermal charging performance can be described based on the time that each system reaches the second sensible heating region. Both graphs indicate that the impact on thermal charging decreases as the thermal conductivity increases, especially for the lower heat flux.

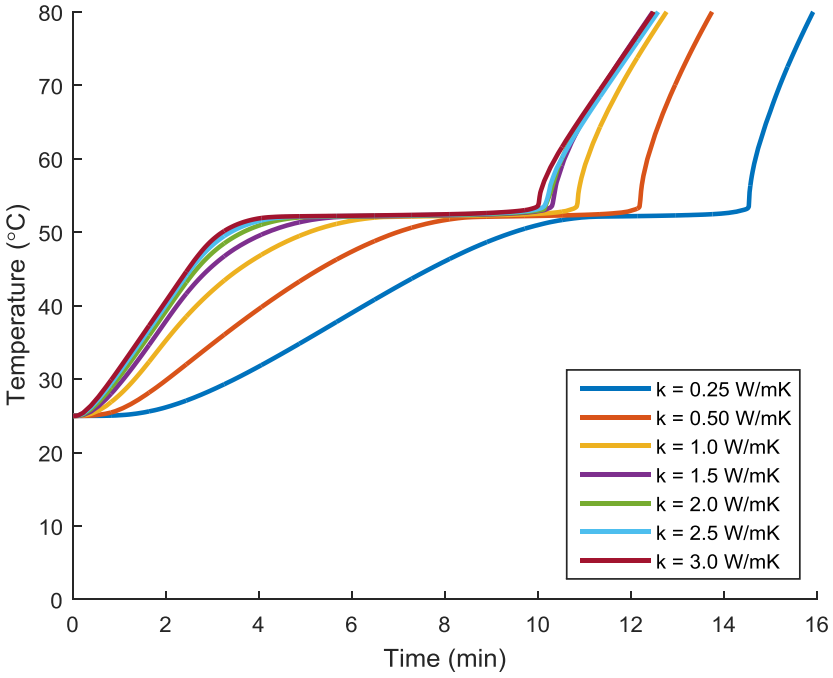

Figure 1.7 Temperature response under 0.39 Wcm^{-2}

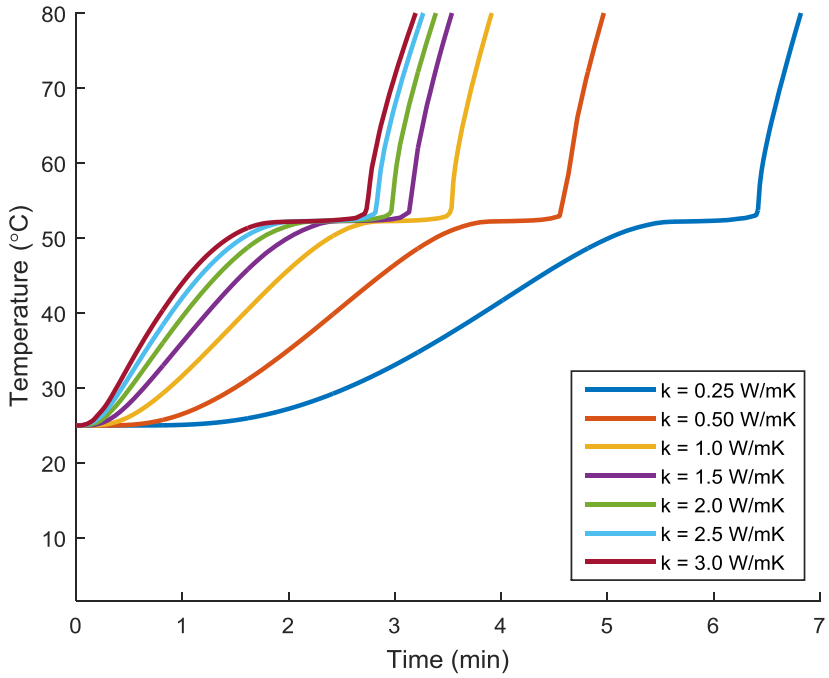

Figure 1.8 Temperature response under 1.55 Wcm^{-2}

This thesis seeks to study methods of thermal charging enhancement based on these performance metrics to contribute to the development of stable paraffin wax based latent heat thermal storage systems for low temperature waste heat reclamation. Chapter 2 provides an in-depth review of the thermal charging enhancement methods. This includes an explanation of the advantages and disadvantage of each approach followed by an introduction of the primary enhancement materials studied in Chapters 3 and 4. Chapter 3 focuses on the stability of the PCM enhancement material, and Chapter 4 discusses the impact of various materials on the rate of thermal charging and cost of the composites systems. These three metrics are also correlated to the thermal conductivity and latent heat of the composites to help elucidate the parameters that should be considered when evaluating the impact of thermal performance enhancement materials. Chapter 5 will conclude and propose future work to further the development of latent heat thermal storage systems for low temperature residential applications. By studying the

impact of various thermal charging enhancement methods, this work supports the efforts in developing organic, non-corrosive, non-toxic, chemically stable and low cost PCM for use in thermal energy storage systems.

CHAPTER 2: THERMAL CHARGING ENHANCEMENT REIVEW

2.1. Introduction

As discussed in Chapter 1, the primary concern facing the use of paraffin wax in latent heat thermal storage systems is the limited rate of thermal charging as a result of the low thermal conductivity of the PCM. The advantages of paraffin wax, precisely its organic, stable, and inexpensive nature, have led a focus on methods to increase the thermal performance of paraffin wax while maintaining its characteristically high latent heat. Such methods include the use of extended surfaces, microencapsulation of the PCM, and introduction of high conductivity foams or nanoparticles within the PCM to increase the thermal conductivity of the composite.

2.2. Extended Surfaces

Extended surfaces, specifically fins, provide additional surface to transfer heat in and out of the latent heat thermal storage system. Fins have been studied on both the inside and outside of the PCM cavity wall as presented in Figure 2.1.

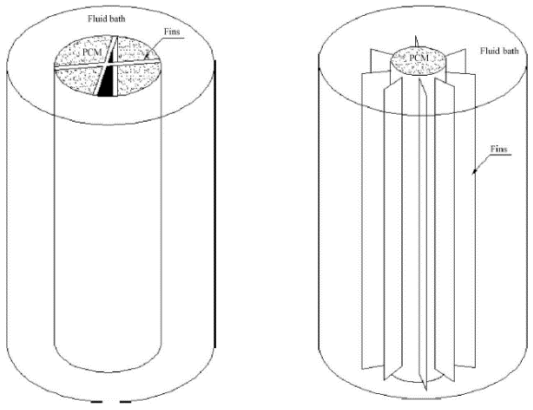

Figure 2.1 LHTS units with internal (left) and external (right) vertical fins [30].

Since the efficiency of the finned system increases when the heat transfer coefficient decreases, the location of the fins is generally based on the relative heat transfer coefficient. In most of the systems, the PCM side heat transfer coefficient is less than that of the heat transfer fluid side, and, thus, it is a general practice that fins are on PCM side [30]. Examples of fins published in literature, specifically annual and vertical fins, are depicted in Figure 2.2, and horizontal fins are shown in Figure 2.5 (left).

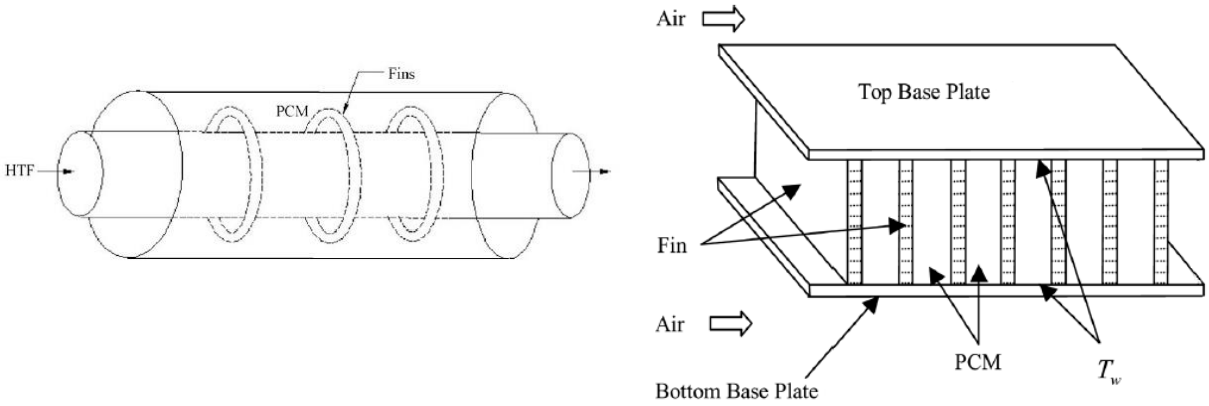

Figure 2.2 LHTS units with annual fins [31] (left); LHTS units with vertical fins [32] (right).

The two mechanisms of heat transfer that occur in latent heat thermal storage systems are conduction and natural convection. During melting, heat is transferred to the solid PCM by conduction and then by natural convection as the PCM liquefies. This is because the solid region moves away from the heat transfer surface, and the thickness of the liquid region increases near the heat transfer surface as shown experimentally in Figure 2.3. Since the thermal conductivity of liquid PCM is less than that of solid PCM (for example, $k_{liquidparaffin}$= 0.167 $Wm^{-1}K^{-1}$, $k_{solidparaffin}$ = 0.346 $Wm^{-1}K^{-1}$ for T_m = 64°C [14]), the heat transfer by conduction reduces as the charging process continues. Conversely, as the PCM solidifies during the discharging process, conduction becomes the dominant form of heat transfer [30].

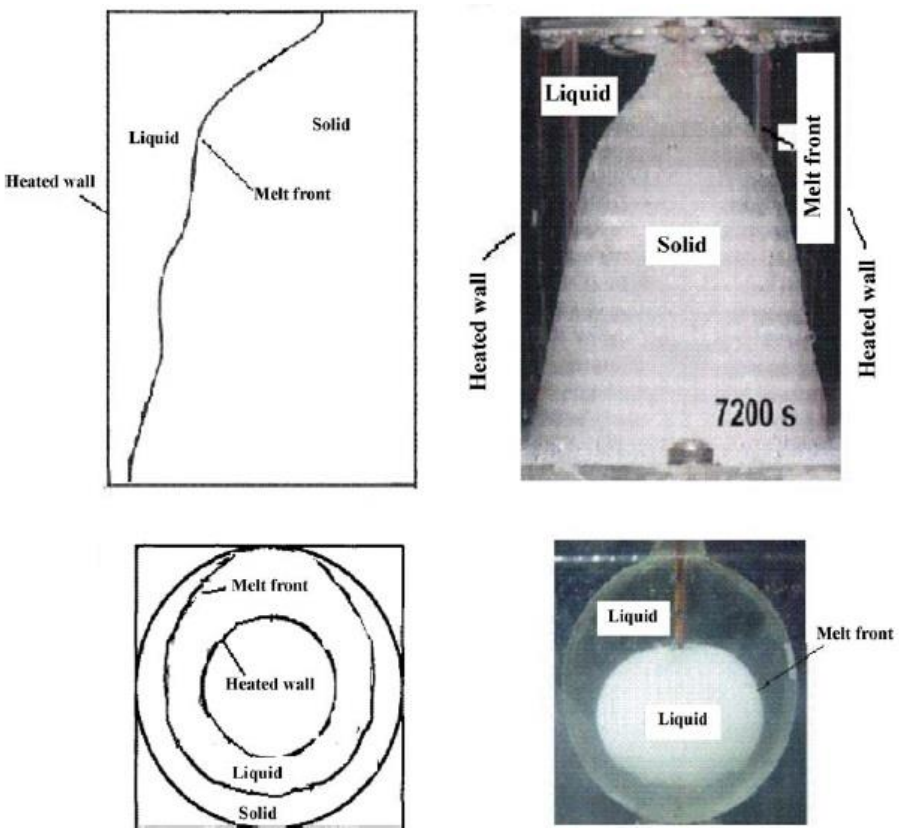

Figure 2.3 Natural convection dominated melting process: rectangular system (top left, [33]); cylindrical system (top right, [34]; (c) cylindrical annulus (bottom left, [35]; (d) spherical system (bottom right, [36]) adapted from [30].

As can be seen experimentally in Figure 2.3 and computationally in Figure 2.4, the location of the melt front is not uniform throughout the system as a result of its dependence on natural convection. Since the melting process in pure paraffin is dominated by natural convection, the presence of fins should be focused on improving the natural convection process (due to the lower thermal conductivity in the molten state) as well as the conduction rate [30].

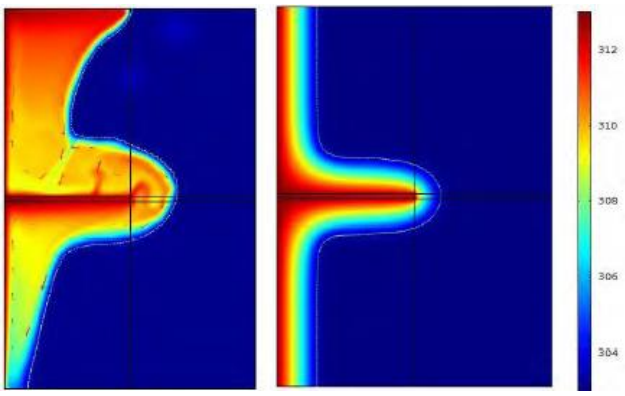

Figure 2.4 Temperature distribution for one fin system accounting for heat conduction and natural convention (left) and accounting for heat conduction only (right) [37].

When considering internal fins to increase the thermal performance of the LHTSS, the effect on each heat transfer mechanism and the associated impact on thermal response must be understood. For example, published literature has discussed the associated impact of the insertion of horizontal fins into a vertical cavity filled with paraffin wax as depicted in Figure 2.5. Issues addressed include how the fins interrupt the natural convection movement during melting (Figure 2.5 (right)), whether they actually inhibit the thermal charging rate or if the additional heat transfer surface compensates for impeding the natural convective motion, and how the additional heat transfer surface assists during solidification when conduction is the main mechanism of heat transfer. Published work has focused on understanding such tradeoffs with finned systems, including how heat transfer mechanisms during the phase change processes depend upon the configuration and orientation of the system and fins [30, 32, 38-43].

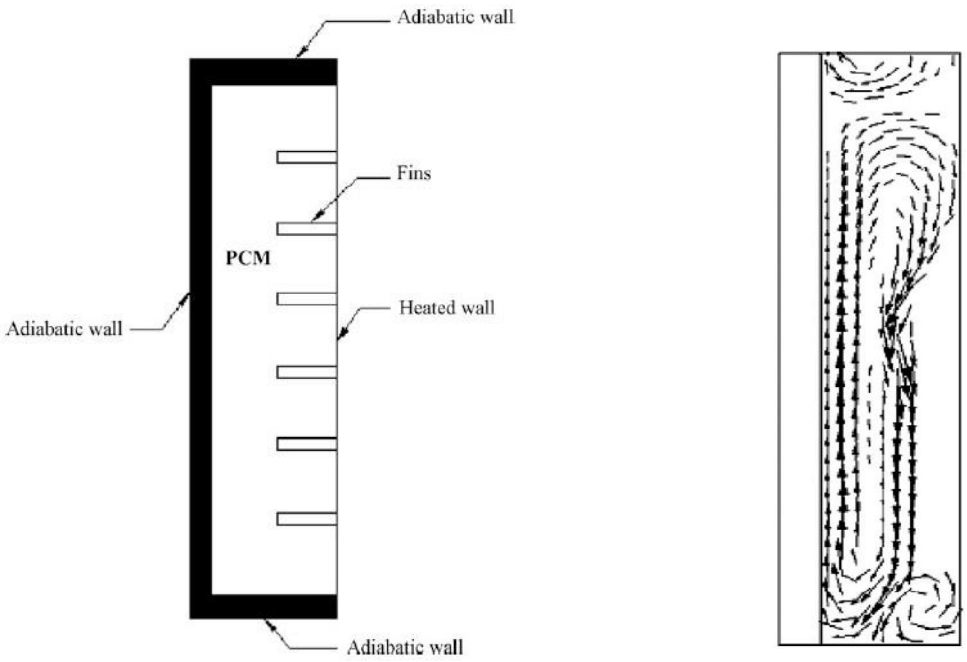

Figure 2.5 LHTS units with vertical fins [41] (left); fluid motion during melting [30, 44] (right).

Computational and experimental research has focused on the design of the finned systems to understand the relationship between the orientation of the heated wall(s), finned structures, and the entire unit. Additionally, studies have looked at the relationship between the number, dimension, and orientation of the fins in optimizing thermal charging and discharging as shown in Figure 2.6 and Figure 2.7.

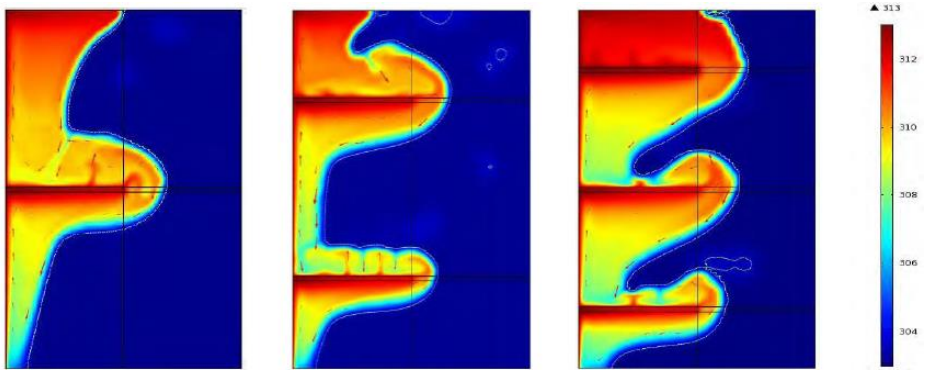

Figure 2.6 Temperature distribution and melting front for finned systems having 1 fin (left), 2 fins (middle), and 3 fins (right) [37].

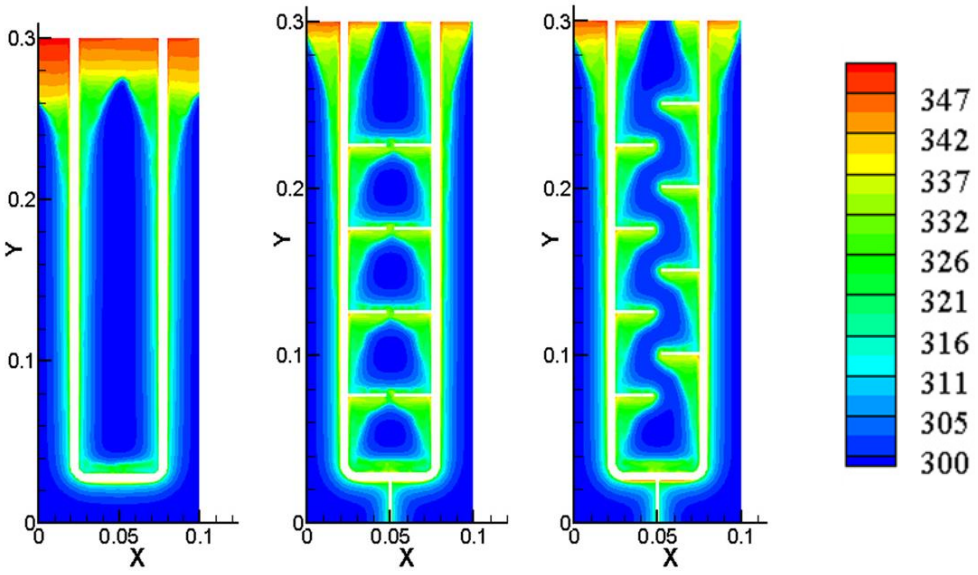

Figure 2.7 Temperature contour for U-tube design (left); U-tube with inline fins (middle); U-tube with staggered fins (right) after 300 seconds, temperature in Kelvin [45].

In general, the heat transfer enhancement is reported to increase with an increase in the number of fins, which corresponds to a decrease in the distance between the adjacent fins [31, 32, 41, 43]. However, an increase in the number of internal fins will not linearly contribute to an increase in thermal performance because natural convection is diminished within the smaller fin gap volume [46]. Additionally, as the number of fins increase, the total amount of latent energy stored by the system decreases since each fin replaces available space of the PCM.

Extended surfaces provide a simple and low cost (due to ease of fabrication) method of enhancing thermal performance of LHTSS [17]. However, this thermal enhancement technique also adds considerable weight to the system as well additional size constraints for the system to accommodate finned structures. Although fins provide a thermal performance enhancement, one of the main restrictions on performance remains the low thermal conductivity of the PCM. As Figure 2.7 indicates, although fins increase the thermal charging of the system, the temperature distribution is very disproportionate where portions of the paraffin do not rise about 300K after

300 seconds. Therefore methods of not only increasing the heat transfer area, but also reducing the maximum distance from the heat transfer surface to the paraffin have been explored.

2.3. Microencapsulation

Microencapsulation is one such method of improving the thermal performance of the PCM by minimizing the radial path length from the enhancement material to the paraffin. With this method, the paraffin wax becomes a core enveloped within a solid shell structure (Figure 2.8) made of wide range of materials including natural and synthetic polymers [30]. The shell of microcapsules can protect the core material from interacting with the carrier fluid, which enhances the stability of the PCMs, while potentially improving the heat transfer efficiency because of the large surface-to-volume ratio [47].

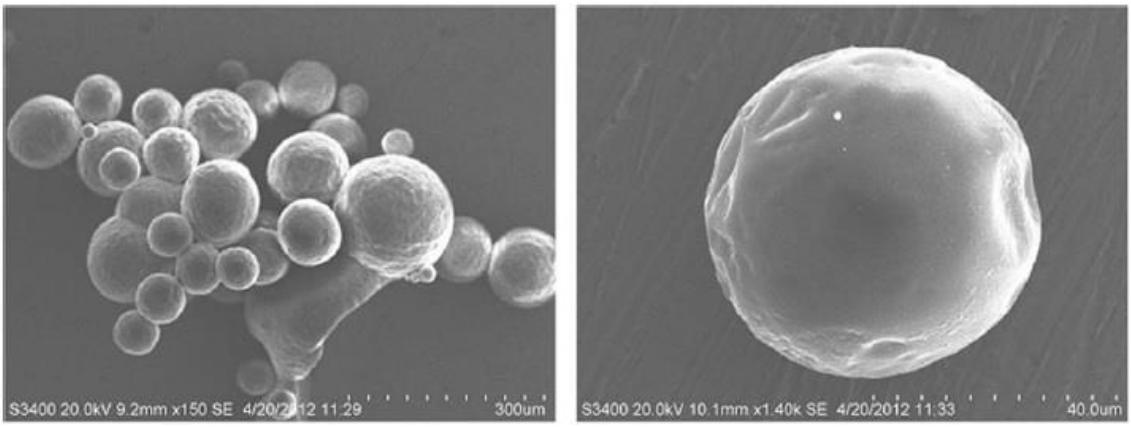

Figure 2.8 SEM photographs of microencapsulated paraffin wax in silicon dioxide [47].

Two main issues exist with microencapsulation: cost and material properties of the shell. Microcapsules can be prepared by several methods such as interfacial polycondensation, spray drying, coacervation, suspension polymerization, and in situ polymerization [47]. This additional processing adds considerable cost and production time to the system, especially when working with an inexpensive, commercially available material such as paraffin wax. Additionally, some

shell materials have been found to be flammable and release poisonous gas while others have poor mechanical properties, which results in cracking of the shell [47]. Various studies have shown that silicon dioxide [47, 48] and polymethylmethacrylate (PMMA) [49, 50] are viable options from a materials perspective, but were reported to reduce the latent heat by up to 49% [47, 49].

Based on these concerns, is it apparent that if a microencapsulated PCM should replace the relatively cheaper non-enhanced PCM, then a substantial heat transfer enhancement must be realized. It has been reported that the heat transfer performance is enhanced by up to 37% as compared to pure paraffin wax during constant heat flux tests [48, 50]. However, when considering the cost and reduction in latent heat, this improvement does not make economic sense when focusing on a system based on paraffin wax.

The final option to increase thermal performance by increasing thermal conductivity of the PCM is advantageous, specifically for the development of low cost, organic, effective, and commercial latent heat thermal storage systems. By increasing the thermal conductivity of the PCM, micro-scale methods are not necessary to minimize the distance from the heat source to the paraffin wax and fins will not be required to increase the heat transfer area.

2.4. Thermal Conductivity Enhancement

Thermal conductivity enhancement techniques have focused on saturating high conductivity porous materials with PCM or dispersing highly conductive particles in the PCM [30, 51, 52]. Aluminum, copper, and graphite are the most common materials used in literature to produce such highly conductive particles and porous foams to be incorporated in paraffin wax composite latent heat storage systems [53-61]. The intention is to increase the thermal charging

and discharging without the addition of considerable size, weight, or cost as well as help to more evenly distribute the heat throughout the system.

2.4.1. High Conductivity Metal Foams

Open-cell metal foams are commonly made by injecting a gas into molten metal, typically copper or aluminum, to form bubbles that produce interconnected pores of the foam. Paraffin can then be absorbed into the foam to form a high conductivity composite. Foams are characterized by two primary parameters: relative density and pore size. Relative density is the density of the foam divided by the density of the solid parent material of the struts. This parameter controls the ligament cross-section shape and size as seen in Figure 2.9.

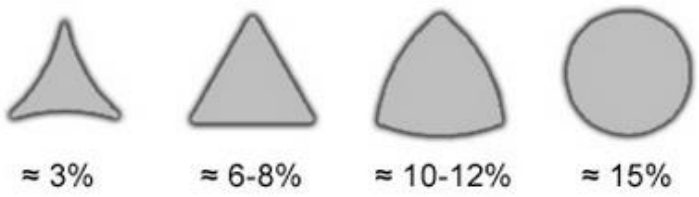

Figure 2.9 Ligament cross sections [62].

The second identification parameter for porous foams is pore density. Every gas bubble in the metal forms a cell consists of about 14 reticulated windows, as depicted in Figure 2.10. Each window is referred to as a pore. In any given bubble, the pores actually are of two or three different characteristic sizes and shapes, but for material designation purposes, they are simplified to an average size and circular shape [62]. The number of these pores in one inch of the foam then designates the foam pore density and is quantified by pores per inch (PPI). Examples of typical pores per inch include 5, 10, 20, 40 and 50 PPI.

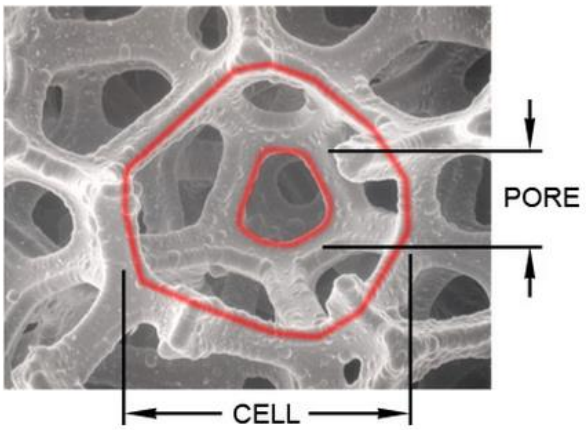

Figure 2.10 Structure of foams [62].

Both the pore density and the relative density have an influence on the specific surface area. As the pore density increases, the diameter of each pore decreases and the overall surface area of the foam increases. Similarly, as the relative density increases, the redistribution of aluminum within the foam ligaments results in an increase in the surface area. A high specific surface area allows for increased contact with the paraffin wax. The specific surface area as a function of pore density and relative density increase can be seen in Figure 2.11.

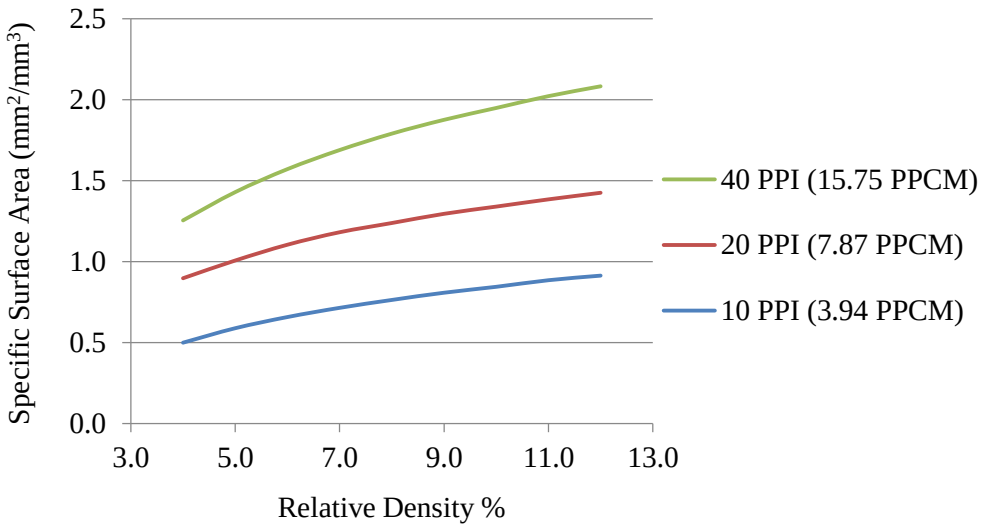

Figure 2.11 Specific surface area of Duocel® metal foams [62].

Metal foams are attractive thermal enhancement materials due to their stiffness/strength properties, high thermal conductivity, high surface area densities, and continuous interconnected pore structure [30, 63]. Research with PCMs integrated in porous foams describes the impact on thermal charging by measuring the decrease in melting time of the PCM [64, 65] or the decrease in temperature at the junction of the heat sink and the latent heat thermal storage system [66, 67]. Copper and aluminum foams have been computationally and experimentally studied [56, 59, 60, 66, 68]. Copper foams have been found to decrease the melting time of the PCM up to a factor of nine [60]. Similar experiments have been conducted with aluminum foams [64, 66], though the associated impact on thermal charging is less than copper foams due to the 50% decrease in bulk material thermal conductivity. However, this performance is countered by additional of cost and weight. Therefore, aluminum is more promising for the development of low cost LHTSS for residential applications.

2.4.2. High Conductivity Graphite Matrix

Graphite is known for its high thermal conductivity and low density, which make it a good candidate for improving thermal conductivity of paraffin wax. Additionally, this material has been suggested to decrease of volume change of paraffin during the solid to liquid phase change and offers no corrosion problems [69]. For some applications, graphite is of specific interest because of its anisotropic nature, which is proposed to allow the heat transfer to be focused in the direction of interest.

Paraffin wax can be enhanced with a matrix of graphite that is produced from various forms including: graphite powder, micron graphite flake, expanded natural graphite (EG), and compressed expanded natural graphite (CENG). Studies report on different methods of

producing the foams as well as the impact on the mass of graphite present in the sample volume, which is measured by bulk density (kgm^{-3}), on the thermal conductivity and latent heat of the composite. Graphite power and micron graphite flake are not commonly used because of their limited impact on thermal conductivity. For example, a graphite matrix of 417 kgm^{-3} produced from pressing graphite powder and saturated with paraffin wax exhibits a thermal conductivity of 1.1 $Wm^{-1}K^{-1}$ [70], whereas the thermal conductivity of paraffin has been reported to increase by more than an order of magnitude (from 0.2 $Wm^{-1}K^{-1}$ to 50-70 $Wm^{-1}K^{-1}$) with the addition of a CENG foam [71, 72]. The two most common and effective methods of EG and CENG will be further discussed.

2.4.2.1. Expanded Natural Graphite

Expanded natural graphite is produced from natural graphite flake that has been chemically treated and then thermally exfoliated. By introducing an acid, such as sulfuric or nitric acid, to the graphite flake, each of the layers of the graphite flake are chemically detached (Figure 2.12). Since each flake is held together by weak van der Waals bonds, the addition of heat (microwave or furnace) splits apart into a worm-like accordion structure (Figure 2.13) [73, 74]. The EG can then be mixed with paraffin wax to form a composite thermal storage system.

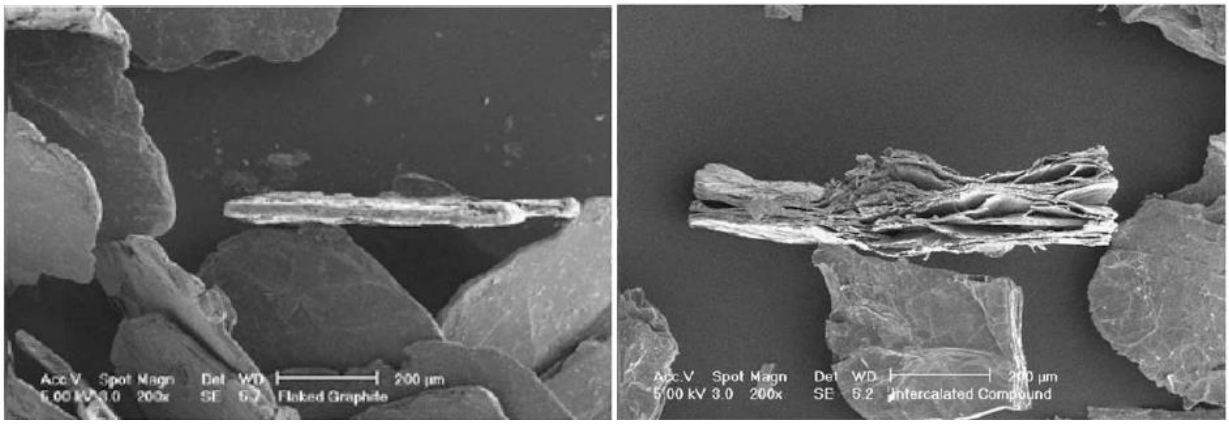

Figure 2.12 SEM photographs of flake graphite (left) and graphite intercalated compound after acid washing and drying (right), both with 200x magnification [52].

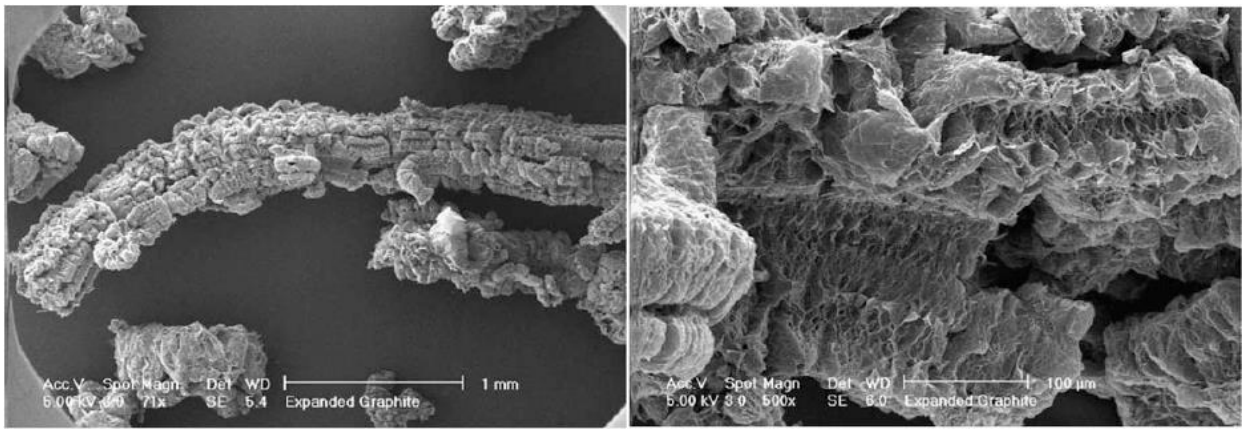

Figure 2.13 SEM pictures of EG at 71x magnification (left) and 500x magnification (right) [52].

The thermal conductivity enhancement and impact on latent heat have been discussed specifically by Sari and Karaipekli [74], Yin *et al.* [75], Xia *et al.* [76], and Zhang *et al.* [76]. Though expanded graphite offers improvement in thermal conductivity of the paraffin wax, this system does not take advantage of the anisotropic nature of graphite. By compressing the expanded natural graphite system, a significant increase in thermal conductivity can be realized.

2.4.2.2. Compressed Expanded Natural Graphite

Compressed expanded natural graphite is produced by compressing the expanded graphite into a compact porous foam. In doing so, the directional thermal conductivity of

graphite can be used to maximize the performance of the system. Paraffin wax can then be absorbed into the foam through capillary forces between the liquid PCM and the CENG to form a highly conductive composite [52]. One of the benefits of using this material is that the EG can be compacted into various shapes to form stable graphite matrices without using any binding materials due to the mechanical interlocking of the worms [52].

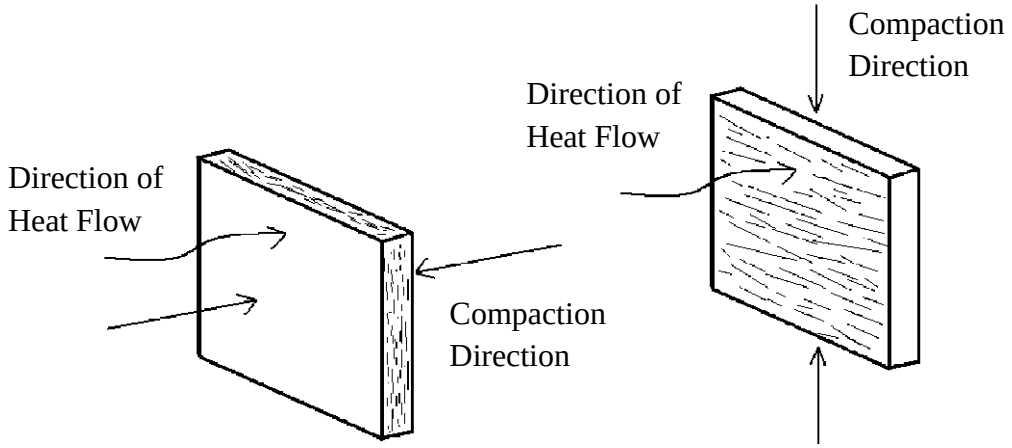

Figure 2.14 Schematic of compaction methods with respect to direction of heat flow during thermal conductivity tests [52].

As shown in Figure 2.14, thermal conductivity measurements can either be collected in the direction of compaction or perpendicular to the direction of compaction. The thermal conductivity of composites formed with CENG bulk densities greater than 50 kgm^{-3} are found to be impacted by the anisotropy of the compressed graphite as discussed by Mills *et al.* [52], Py *et al.* [72], Haillot *et al.* [71, 77] and shown in Figure 2.15; thermal conductivity of the sample in the compression direction is less than in the direction perpendicular to the compression direction. For example, the thermal conductivity CENG foam with a bulk density of 350 kgm^{-3} has been reported to be 70 $Wm^{-1}K^{-1}$ in the direction perpendicular to compaction, while it is 10 $Wm^{-1}K^{-1}$ in the compression direction [72]. Typical CENG foams range between 50 kgm^{-3} and 350 kgm^{-3},

the lower value a limit of mechanical strength of the matrix and the upper value limited by the permeability necessary to absorb PCM [72].

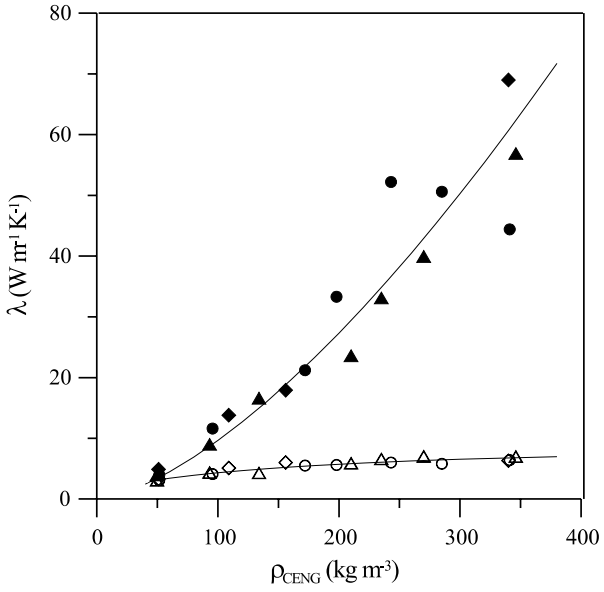

Figure 2.15 CENG thermal conductivities versus bulk graphite matrix density; perpendicular to compression (solid), parallel to compression (open) [72].

CENG foam is primarily considered a method of increasing thermal conductivity for paraffin wax due to its large thermal conductivity, high surface area to volume ratio, and small density. It also has the ability to be formed into various shapes and easily molded to the heat transfer surface, which allows contact between the composite and exchanger wall without the use of expensive thermal epoxies. However, disadvantages to using CENG for thermal conductivity enhancement are introduced due to the production technique. As the EG is compacted, some of the pores will be closed during compression forming voids of trapped air that are impenetrable by PCM. By studying the amount of PCM absorbed by the sample compared to the theoretical maximum, Py *et al.* [72] found that the higher the bulk density, the greater the volume of closed pores. Additionally, the time to saturate a matrix of graphite with paraffin takes longer than an

open cellular material [52]. Furthermore, graphite is not as rigid as metal and may not be adequately robust for certain applications.

There are two general issues with both metal and graphite foams: the impact on latent heat of the system and the time and energy intensive nature in their production. The impact on latent heat is not directly discussed in literature reviewing aluminum foams as thermal conductivity enhancement materials, though this issue is reviewed in work with CENG foams. Latent heat of the PCM not only decreases due to the addition of EG, but also because of voids formed during the compression process [72]; this is of specific concern for composites with a CENG foam bulk density above 100 kgm^{-3}. Additionally, the production of aluminum foam requires temperatures above the melting point of aluminum (660°C), and the production CENG between 50kPa (50 kgm^{-3}) and 700 kPa (350 kgm^{-3}) for compression [52].

These issues do not discredit high conductivity foams compared to fins or microencapsulation on the basis of cost, production time, or performance. However, another method of thermal conductivity improvement has previously been considered that is reported to have less impact on latent heat and does not require as much time or energy for processing. The following section will discuss this method - the addition of high conductivity nanoparticles to PCM for thermal conductivity enhancement.

2.4.3. High Conductivity Nanoparticles

Similar to highly conductive foams, nanoparticles of aluminum, copper, and graphite have been reported in literature [53-55, 78, 79]. When the performance of graphite nanoparticles is compared to that of denser materials such as aluminum or copper at similar concentrations [53-60], graphite is found to be the optimum thermal conductivity enhancement material. This is

due to its high thermal conductivity paired with low density and compatibility with paraffin wax, which allows for the largest conductivity enhancement with lowest material concentration [57, 80, 81].

As Jegadheeswaran and Pohekar summarize, the dispersion of particles is a simpler thermal conductivity enhancement method than PCM integration into porous material; porous material production can be both energy and time intensive, and the performance of the system is crucial on consistent and optimal pore size [30]. Additionally, the latent heat of PCM has been reported to be less affected by the introduction of particles than by the absorption into a porous matrix [30, 54]. The inclusion of graphite nanoparticles shows no decrease in latent heat capacity [81-83], whereas aluminum and graphite foams have been found to lower the latent heat capacity [61]. This is likely due to the structural limitations of aluminum and graphite foams, which require higher material concentrations than the percolation threshold of graphite nanoparticles.

Three geometries of graphite nanoparticles imbedded within PCM, typically paraffin wax, are found in literature: nanotubes, nanofibers, and nanoplatelets, though graphite nanoplatelets appear to be the most effective carbon filler [80-88]. Cui *et al.* [88] reported that carbon nanofibers were more effective than carbon nanotubes because of better dispersion with paraffin wax. Cheng *et al.* [83] reported a thermal conductivity improvement of about 30% with an 8 wt% graphite nanofiber/paraffin wax composite system; small improvement was also reported by Elgafy and Lafdi [87]. However, graphite nanoplatelets have exhibited over 200% increase in thermal conductivity with a 7 wt%/paraffin wax mixture [82]. No direct comparison of graphite nanofibers and graphite nanoplatelets has been found, however, it is posited that graphite nanoplatelets are superior to graphite nanofibers with respect to thermal conductivity

enhancement because of the increased surface area, which improves the conductive network within the composite PCM.

Graphite nanoplatelets (xGnP) are produced by using an ultrasonic processor to pulverize expanded graphite into graphite nanoplatelets that are <10nm thick with an average diameter of 15 μm (Figure 2.16) [82]. By further processing via ball milling, these nanoplatelets can be reduced to 1 μm in diameter [81]. Graphite nanoplatelets can then be mixed into paraffin wax, typically through constant shear mixing, to form a thermally conductive composite material.

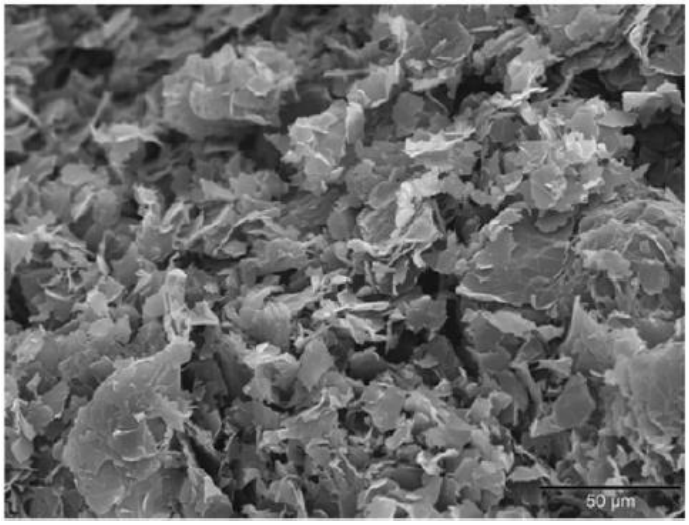

Figure 2.16 SEM of 15μm graphite nanoplatelets (xGnP-15).

The maximum thermal conductivity enhancmenet of 15 μm xGnP/paraffin composites has been reported to be 0.85 $Wm^{-1}K^{-1}$ with a 7 wt% xGnP system [81, 82]. With advanced processing via roll milling, Xiang and Drzal [81] were able to achieve 2.5 $Wm^{-1}K^{-1}$ with a 10 wt% xGnP system. Note that these thermal conductivity measurements were performed in the solid state. Though the thermal conductivity enhancement of foams outperforms graphite nanoplatelets, some authors suggest that xGnP is a more effective thermal conductivity

enhancement material because it enhances the conductivity without reducing the storage capacity as shown in Figure 2.17 [30, 81, 82].

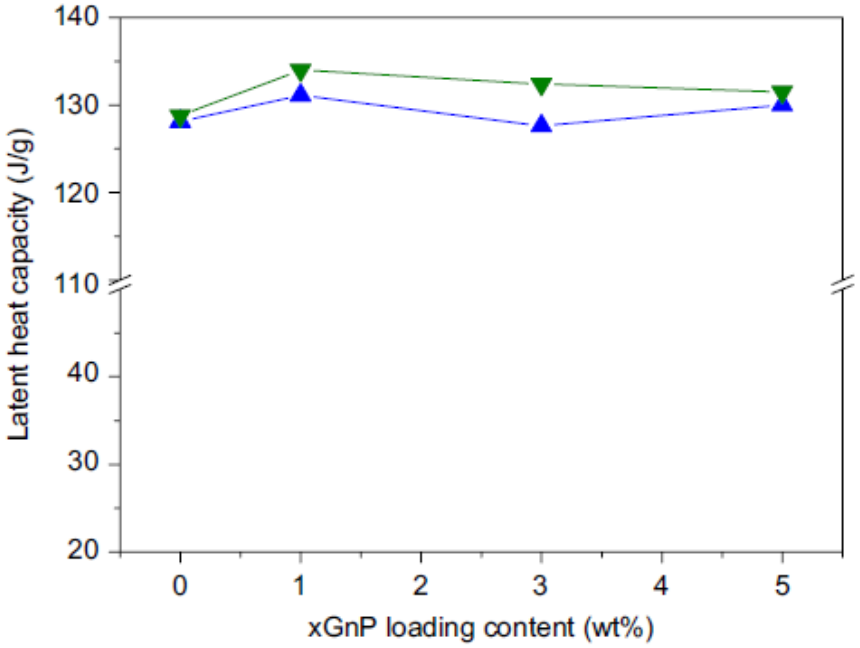

Figure 2.17 Latent heat storage performance of paraffin/xGnP composite PCMs [82].

Graphite nanoplatelet PCM composites are inexpensive and can be prepared with limited lab experience and equipment. Additionally, xGnP performance is not dependent on consistent pore size as are aluminum and graphite foams, and xGnP is reported to have less impact on the latent heat as well as natural convection occurring in the system than foams. The main issue with the use of xGnP to increase thermal conductivity is the stability of the nanoparticles in the liquid PCM. The stability of these suspensions during melting and solidification of the PCM is a concern as settling or sedimentation of the fillers will change the effective thermal conductivity. In an attempt to improve the stability, researchers have utilized dispersants, specifically sodium dodecylbenzenesulfonate (SDBS), which has shown some success in paraffin wax systems with aluminum and copper nanoparticles [58, 78]. No published research has been found that discusses the settling of graphite nanoparticles as a function of size and time. The only mention

of the settling of graphite particles found was in [80], which studied graphite nanofibers, not graphite nanoplatelets. It is noted that if the sample is subjected to multiple melting/solidification cycles, then the graphite nanofibers begin to agglomerate.

2.5. Research Outline

This thesis explores the use high conductivity materials in paraffin wax for thermal conductivity and thermal charging performance enhancement. The first phase of this research builds on past work with nanoparticles by acknowledging that effective thermal conductivity enhancement with highly conductive nanoparticles in paraffin wax is dependent on four main factors: base material, concentration (wt%), geometry of nanomaterial, and its stability within the PCM. Graphite has been shown to be the most effective enhancement material, while nanoplatelets with large diameters have been reported to be the optimum geometry in terms of thermal conductivity enhancement. This phase of work addresses the last factor, stability, along with the associated improvement in thermal performance through the following objectives:

1. Stabilization of graphite nanoplatelets (xGnP) in molten paraffin wax to prevent precipitation. The goal is to ensure that in the liquid state, the nanoparticles do not settle, therefore eliminating thermal charging enhancement from the xGnP.
2. Thermal charging performance experiments to understand how particles dispersed throughout the wax affect the rate of thermal charging. The goal is to understand if thermal conductivity is the dominate factor that must be addressed to improve performance or if the structure of the enhancement material must also be considered.
3. Explore potential uses of stable paraffin wax/xGnP composites in other systems such as aluminum foams to further increase rates of thermal charging.

Chapter 3 discusses the stability of graphite nanoparticles in liquid paraffin wax for use in cyclic charging. Stability of the nanoplatelets in the liquid state is imperative since settling of the particles eradicates the thermal charging enhancement of the system. Methods of stabilizing the graphite nanoplatelets through consideration of viscosity, chemical dispersants, mixing time, particle size, and oxidation are discussed. Samples are characterized through thermal conductivity and latent heat measurements.

Chapter 4 first discusses the impact of graphite nanoplatelets on rate of thermal charging under a constant heat flux boundary condition. To address the second objective of this research discussed above, the thermal charging of these graphite nanoplatelet composites is compared to the performance of two compressed expanded graphite composites, one with the same weight percentage and another with the same thermal conductivity as the xGnP samples. Though improved thermal conductivity is a proposed metric of PCM enhancement performance for LHTSS, is it not clear if this should be the only area of focus. To this end, a comparison is conducted on the impact of dispersed nanoparticles versus a porous network on the rate of thermal charging as a function of latent heat, graphite concentration, and thermal conductivity. Chapter 4 also discusses the third objective by comparing thermal charging performance of aluminum foams saturated with pure paraffin wax and a stable paraffin/xGnP composite to explore other uses of these composites. This includes a cyclic performance study.

Chapter 5 suggests further research guided by the work presented in Chapter 3 and Chapter 4. In general, by developing a stable xGnP/paraffin wax system and then investigating the impact of thermal conductivity and weight percentage as compared to other thermal conductivity enhancement materials, this work augments current knowledge of PCM thermal conductivity enhancement for use in latent heat thermal storage systems.

CHAPTER 3: HIGH CONDUCTIVITY NANOPARTICLES FOR THERMAL CHARGING ENHANCEMENT

3.1. Introduction

As discussed in Chapter 2, the use of high thermal conductivity nanoparticles for increasing thermal conductivity of paraffin wax is a simpler thermal conductivity enhancement method than PCM integration into porous material. Mixing nanoparticles into paraffin wax is less time and energy intensive than saturating either aluminum or CENG foam. Additionally, the latent heat of PCM has been reported to be less affected by the introduction of particles than by the absorption into a porous matrix [30, 54]. Large diameter graphite nanoplatelets have been shown to be the most effective thermal conductivity enhancement material. It has been summarized that graphite nanoplatelets may be more effective than CENG as they enhance thermal conductivity without reducing the storage capacity of pure paraffin wax [30].

While the use of graphite nanoplatelets has shown promise in the thermal conductivity improvement of paraffin wax, this enhancement is not only based on the type or size of material, but also the particle stability within in the system [58, 78, 80]. Yu *et al.* [58] reported that the thermal conductivity of PCM systems embedded with copper nanoparticles is greatest at the beginning and decreases as time increases due to settling of the particles. Long [78] also discussed the stability of aluminum nanoparticles in paraffin wax by observing the settling of the particles and recording the ratio of the height of the clear liquid to the total height of sample. Chintakrinda *et al.* [80] showed that when a graphite nanofiber/paraffin wax composite PCM is subjected to multiple melting/solidification cycles, the nanofibers begin to agglomerate and settle out. It is suggested that methods to prevent fiber agglomeration and eventual settling should be explored.

In an attempt to improve the stability, researchers have utilized dispersants, specifically sodium dodecylbenzenesulfonate (SDBS), which has shown some success in paraffin wax systems with aluminum and copper nanoparticles [58, 78]. This improvement has been recognized through a 60-minute thermal conductivity measurement where the thermal conductivity remained stable [58] and a 7-day observation of settling of the particles after which a ratio of 60% clear liquid to height of sample was noted [78]. Although dispersants have not been added to paraffin/graphite nanoplatelet systems with the sole intent of improving stability, xylenes have been reported to decrease the melt viscosity and facilitate uniform dispersion of graphite nanoplatelets for graphite concentrations above 6 wt% [81]. These results are encouraging, but an intense effort is required to improve the stability of the nanoparticles for eventual application.

In this chapter, the stability of waxes filled with graphite nanoplatelets is investigated. The settling rate of particles is analyzed using both visual inspection and capacitance sedimentation measurements. Correlations between the stability of the composites and factors such as nanoparticle size, mixing time of graphite and wax, the use of dispersants, oxidation of the wax, viscosity of the system, and length of hydrocarbon chain are reported. After providing insight into the factors that can be used to improve the stability of graphite filled paraffin wax composites, experiments will be conducted to understand the impact of wt% of graphite nanoplatelets on thermal conductivity.

3.2. Experimental Materials

Exfoliated graphite nanoplatelets (xGnP) were acquired from XG Sciences, Inc. xGnP-1 and xGnP-15 with an average diameter of 1 μm and 15 μm, respectively, and thickness in the 10-

20 nm range were used. Paraffin wax (n-docosane) and octadecylphosphonic acid (ODPA), which can be used as a dispersant, were purchased from Sigma-Aldrich Co. LLC and used as received.

Paraffin wax ($CH_3(CH_2)_xCH_3$) is a mixture of various linear hydrocarbon chains lengths and is commonly approximated as $C_{25}H_{52}$. Instead of using this common assumption, the number of carbon atoms in a sample of paraffin wax can be measured with nuclear magnetic resonance (NMR). NMR is able to characterize the chemical structure of a material based on energy emitted from a material as a result of exposure to an external magnetic field [89]. The NMR spectra for the paraffin wax used in following experiments is presented Figure 3.1. The two substantial peaks correspond to the CH_2 and CH_3 structures of the paraffin wax. The largest peak indicates that 50 protons are associated with CH_2, and since each proton is linked to 1/2 carbon, this indicates that there are 25 carbon atoms in the middle of the paraffin wax hydrocarbon chain. Similarly, the smaller peak indicates that 6 protons are associated with CH_3, and since each proton is linked to 1/3 carbon, this indicates that there are 2 carbon atoms on the each end of the chain. Therefore, the paraffin wax is measured to be $C_{27}H_{56}$.

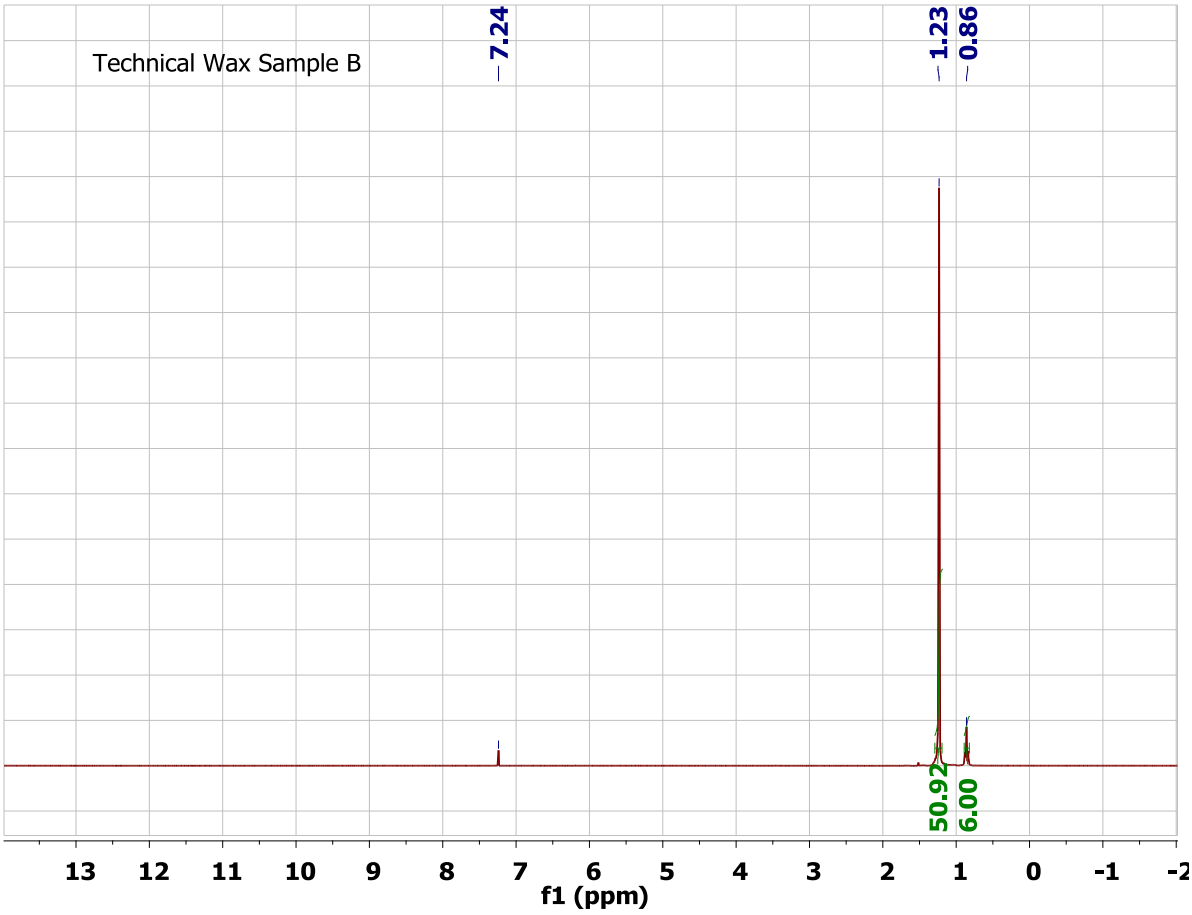

Figure 3.1 NMR spectra for paraffin wax.

Microcrystalline wax, MICROSERE© 5799A, was acquired from The International Group, Inc. and investigated as an alternative to paraffin due to its higher viscosity. Material properties for each wax are presented in

Table 3.1. Figure 3.2 and Figure 3.3 present the DSC curves for the latent heat of each wax during phase transition from solid to liquid and then from liquid to solid. The higher viscosity and higher melting temperature of the microcrystalline wax is a result of its branched hydrocarbon chain structure, as opposed to paraffin wax, which is composed of linear chains. A phase change material with an intermediate viscosity of 0.0115 Pa-s at 80°C was made by mixing 50% microcrystalline wax and 50% paraffin wax (50/50 mixture) to provide additional comparison during experimentation.

Table 3.1 Properties of base waxes used in experimentation.

	Temperature at end of melt [°C]	Viscosity at 80°C [Pa-s]	Thermal Conductivity [$Wm^{-1}K^{-1}$]	Latent Heat [Jg^{-1}]
Paraffin Wax - $C_{27}H_{56}$	57	0.0066	0.2807	148
Microcrystalline Wax	62	0.0287	0.2725	104

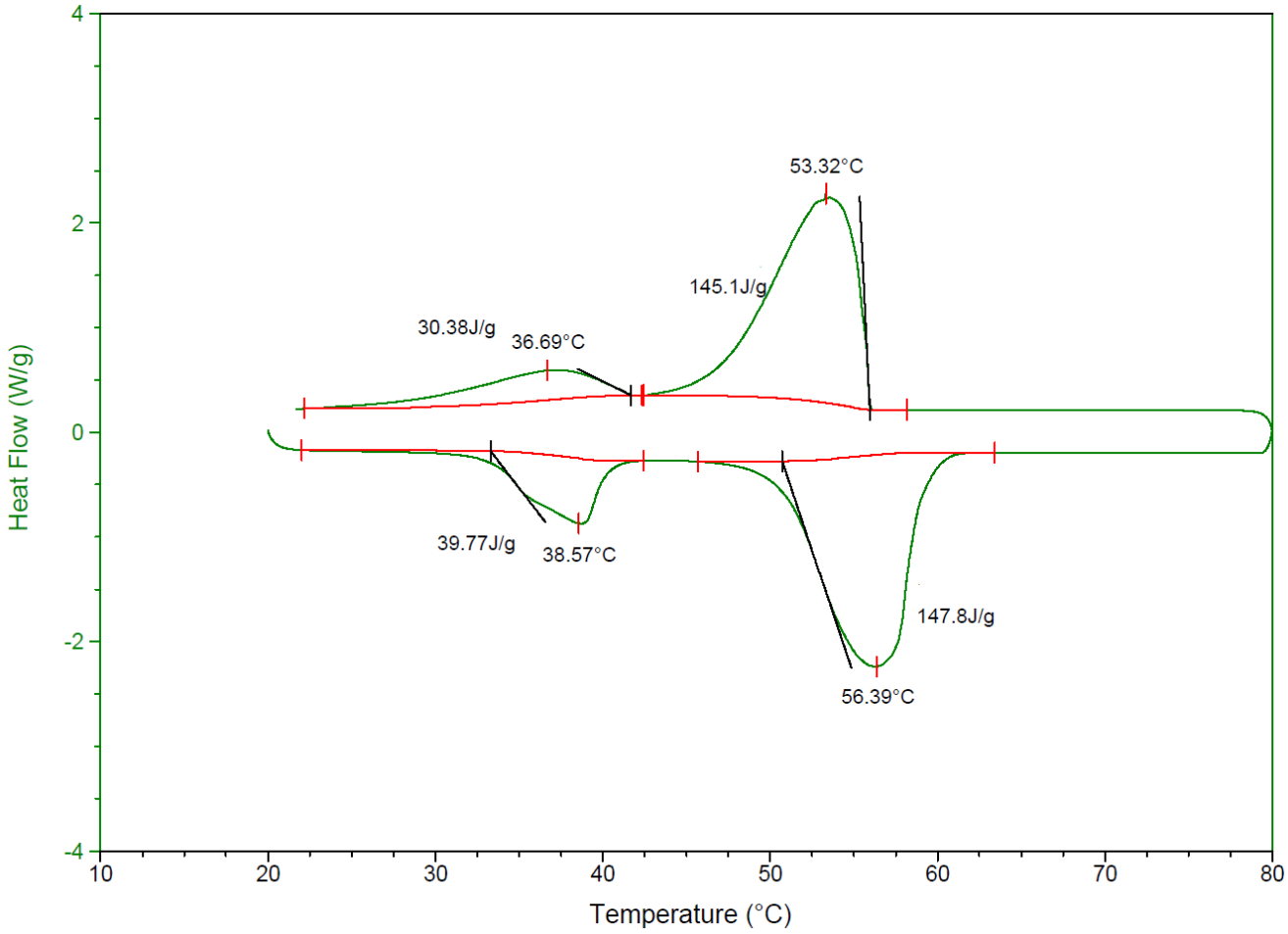

Figure 3.2 DSC curve of paraffin wax.

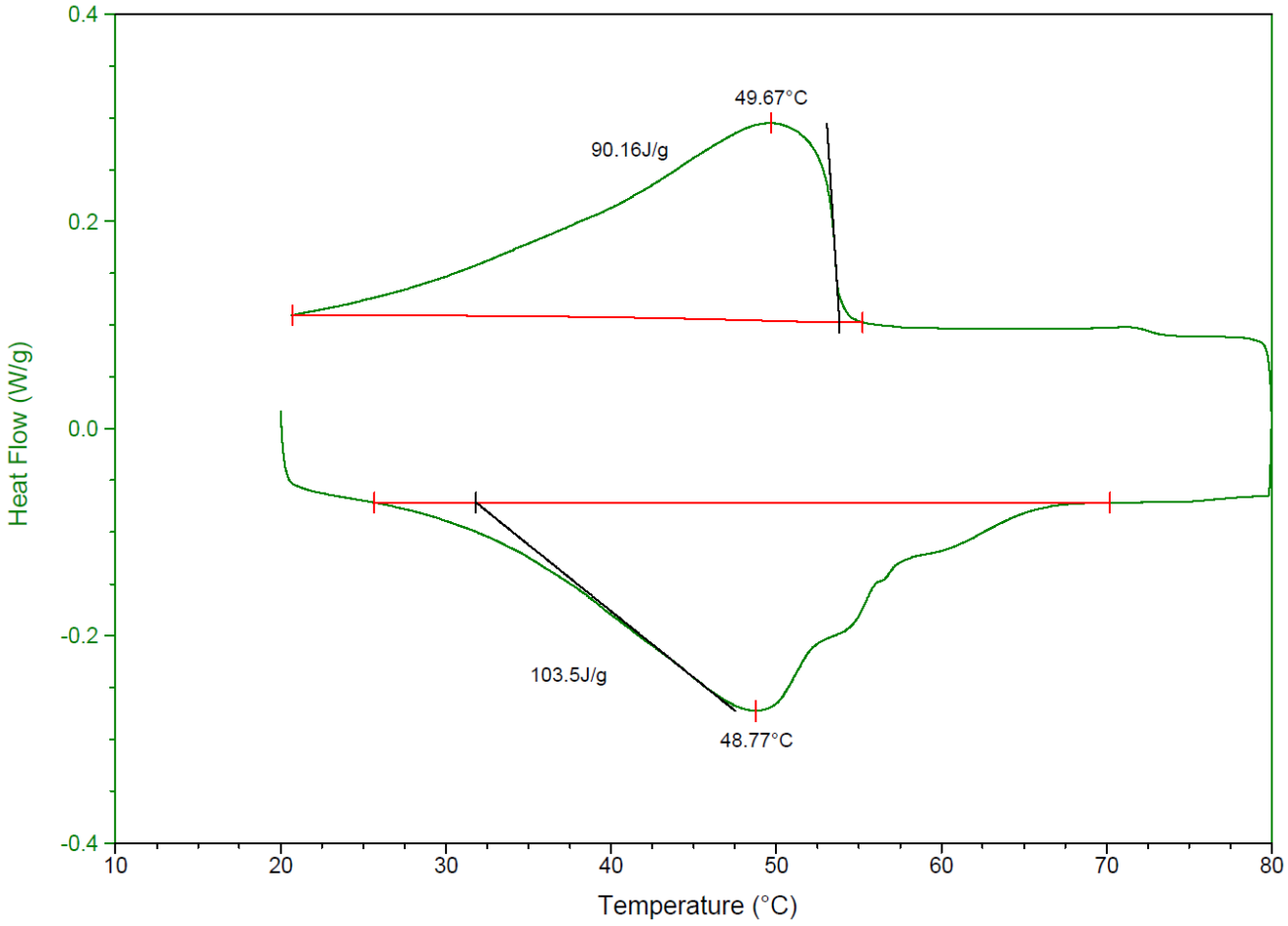

Figure 3.3 DSC curve of microcrystalline wax.

3.3. Sample Preparation

To prepare the xGnP PCM composites, wax was melted at 100°C, combined with xGnP in a 15 ml glass vial, and shear mixed on a stirring hot plate. xGnP composites used in stability experimentation contained 3 wt% of the corresponding graphite as this wt% corresponds to the percolation threshold for xGnP-15 [81, 82]. Composites were shear mixed at 500 rpm for 1 hour, 24 hours, 48 hours, or 96 hours, removed from the hot plate and then immediately sonicated in a room temperature water bath until solid and stored for later testing. These composites were used in four different tests:

1. Viscosity measurements - samples were briefly re-melted and poured into a 2.5 cm diameter disk.
2. Electrical properties measurements - samples were briefly re-melted and poured in cylindrical acrylic test containers having a volume of 2.5 cm^3 as shown in Figure 3.4.

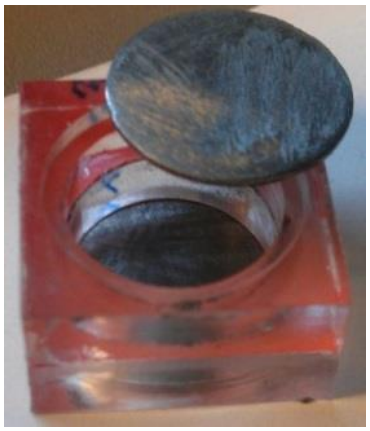

Figure 3.4 Test container for capacitance sedimentation measurements.

3. Thermal conductivity measurements – samples were briefly re-melted and poured into circular forms with a height of 1.9 cm and a width of 2.5 cm.
4. Melting temperature and latent heat measurements – samples were prepared by measuring 10.0 milligrams of each composite and placing in a metal pan as required by the DSC measurement.
5. Thermal charging measurements – samples were briefly re-melted and poured into experimental container, which will be discussed in Chapter 4.

The remaining portion of this chapter is divided into three sections. The first section will discuss methods of characterizing the experimental samples, specifically the rate of settling of the nanoparticles and the viscosity, latent heat, melting temperature, and thermal conductivity of the composite systems. The second section will focus on methods to improve the stability of

xGnP in liquid wax. The third section will discuss the impact of xGnP and ODPA on the thermal conductivity, latent heat, and melting temperature.

3.4. Sample Characterization

The settling of xGnP was characterized using a combination of visual inspection and electrical techniques in addition to measuring material properties such as the viscosity of the paraffin. Visual inspection was performed by melting the samples in a 15 ml glass vial on a hotplate at 80°C and monitoring over a period of time (Figure 3.5 (left)) as well as imaging the samples in the solid state after electrical measurements were conducted in the molten state (Figure 3.5 (right)).

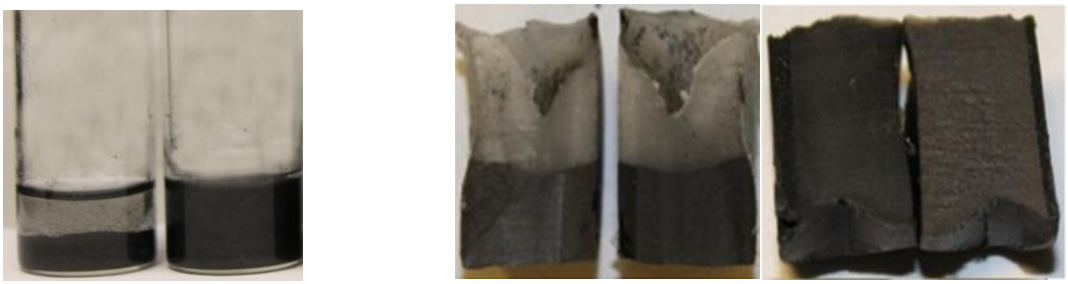

Figure 3.5 Examples of visual inspection in the liquid state (left) and solid state (right).

In addition to visual inspection, sedimentation of the particles was measured using a capacitance technique. Such a technique holds the advantage of being non-invasive while providing a more sensitive response than can be obtained using visual inspection [90]. A parallel plate capacitor system, as shown in Figure 3.4 and schematically in Figure 3.6, was designed to measure the change in capacitance of the system as the particles settle. This concept has been applied to measure the sediment in fluids such as water and glycerol, noting that a relationship exists between the sediment concentration and capacitance output [91-94]. Li *et al.* [91]

determined that suspended sediment concentrations, over a wide range, were correlated with the outputs of capacitance sensors.

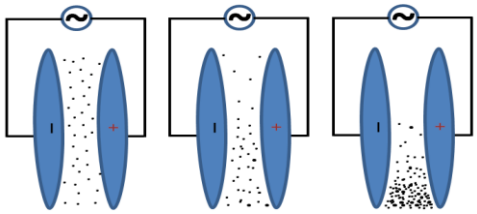

Figure 3.6 Capacitance sensor.

Test samples were poured into the acrylic 2.5 cm^3 containers and held at 80°C during testing. The capacitance as a factor of time for each molten sample was calculated from the impedance measured with a Solartron Analytical Model 1260A Impedance/Gain-Phase Analyzer at a constant 10,000 hertz over a range of time periods – 4 to 72 hours, dependent on the test. By setting a constant frequency (10,000 Hz) and measuring the magnitude of impedance over time, the change in capacitance was calculated with Equation 3,

$$C = \frac{1}{|z| \times 2 \times \pi \times f} \tag{3}$$

where,

C = capacitance of the sensor [farads]

$|z|$ = magnitude of the impedance [ohms]

f = frequency [hertz]

In addition to capacitance, the conductance was calculated as the inverse of the resistance recorded during the measurement. The shift from negative to positive conductance indicates the time when enough particles have settled and formed a conductive bridge between the parallel plates. The conductance was used as an additional comparison in the settling of the system. Examples of capacitance and conductance data are presented in Figure 3.7 and Figure 3.8. Figure

3.7 indicates that particles started settling out around 17 minutes, which corresponds to an increase in slope. This behavior is also seen by the conductive pathway formed in Figure 3.8 at 17 minutes.

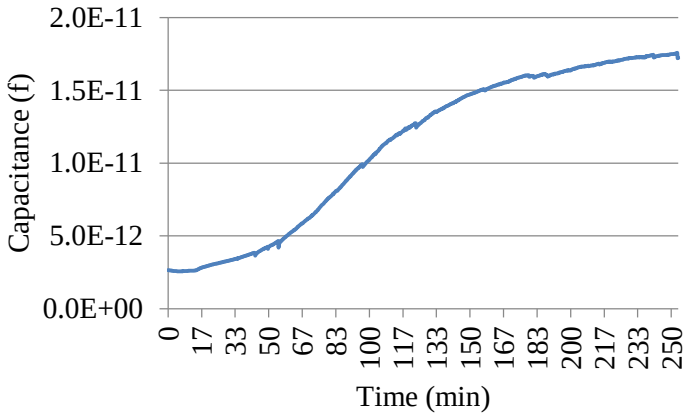

Figure 3.7 Example of capacitance data.

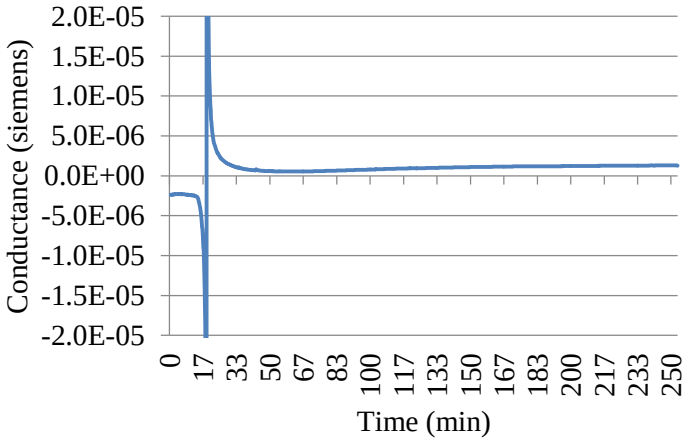

Figure 3.8 Example of conductance data.

The viscosity of the samples was measured using an ARES rheometer parallel plate (25 mm diameter) geometry with a plate separation distance of 1.5 mm. All samples were measured at 80°C with a shear rate of 300 sec^{-1}. Dispersion of the particles was also checked using a Hitachi VP 3700 variable pressure scanning electron microscope (SEM). Samples were melted and spread onto a sample holder with no additional treatment and then imaged at 15.0 kV at a

working distance of ~21 mm. Further characterization of the graphite and composites was performed chemically using x-ray photoelectron spectroscopy (XPS) and Raman spectroscopy. Since XPS measurements indicate the elements that exist within a material, graphite powder was measured using a Thermo K Alpha XPS to confirm the presence of surface oxygen groups available for chemical reaction with dispersants. Raman spectroscopy was used to confirm the interaction of graphite with ODPA. Previous research has shown a decrease in the ratio between the G' and G peak with the introduction of ODPA to graphene [95]. Raman spectroscopy was also used to confirm the oxidation of waxes as the oxidation of paraffin results in an increase in fluorescence background emission.

In the final section of this chapter, the use of a hot disk thermal analyzer (Hot Disk TPS2500S) to measure thermal conductivity of the pure waxes at 20°C will be discussed. Additionally, latent heat and melting temperature measurements with a TA Instruments Q2000 DSC by ramping from 20°C to 80°C at 5°C per minute will be presented. This technique measures the amount of heat needed to increase the temperature of a material as a function of temperature. The response of a sample material is compared to a reference material, both of which are simultaneously measured and maintained at the same temperature throughout the experiment. Measurement of the melting temperature and latent heat of composite samples will verify the impact that xGnP and ODPA have on these values.

3.5. Methods to Improve the Stability of Graphite Nanoplatelets (xGnP)

The following section discusses methods of improving the stability of xGnP in liquid paraffin wax. First, the impact of particle size, mixing time, viscosity, and hydrocarbon length will be discussed as it relates to the stability enhancement for a wax, xGnP system. Next, the

effect of ODPA on the stability will be analyzed followed by the influence of oxidization with and without ODPA as a dispersant.

3.5.1. Stability Enhancement for a Wax, xGnP system

For a wax and xGnP system, the effect of particle size, mixing time, viscosity, and hydrocarbon length was considered. Recall from Section 2.4.3 that two main sizes of xGnP with diameters of 15 μm and 1 μm are produced through ultrasonic processing. By mixing xGnP-1 and xGnP-15 composites with paraffin wax for 1 hour and heating to 80°C, it was clear from visual inspection that the 15 μm particle composite was less stable than the 1 μm composite after 30 minutes due to rapid settling of the particles. Figure 3.9 shows that the xGnP-15 composite has completely settled out after 30 minutes, while xGnP-1 particles remain suspended. This can also been seen from the capacitance data in Figure 3.10. The rate at which the particles settle is indicative of the slope of the capacitance lines. The rate of increase in the capacitance for the xGnP-15 sample peaks at 20 minutes; however the capacitance of the xGnP-1 sample continues rising after 60 minutes, again indicating the difference in settling rates of the two systems. It should be noted that while the xGnP-1 samples are inherently more stable, xGnP-15 composites are more desirable since larger particles provide a greater thermal conductivity enhancement as well as have a lower percolation threshold [6]. Thus, methods to improve xGnP-15 composites are of interest and much of the remainder of the reported work will focus on improving the stability of xGnP-15 composites.

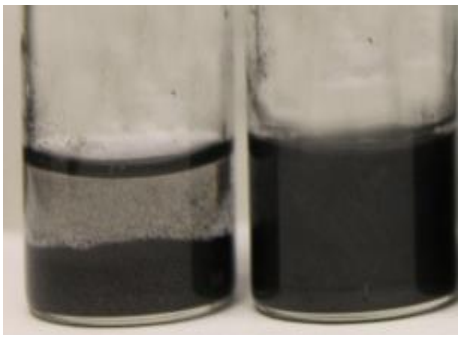

Figure 3.9 Comparison of xGnP-15 (left) and xGnP-1 (right) after 30 minutes.

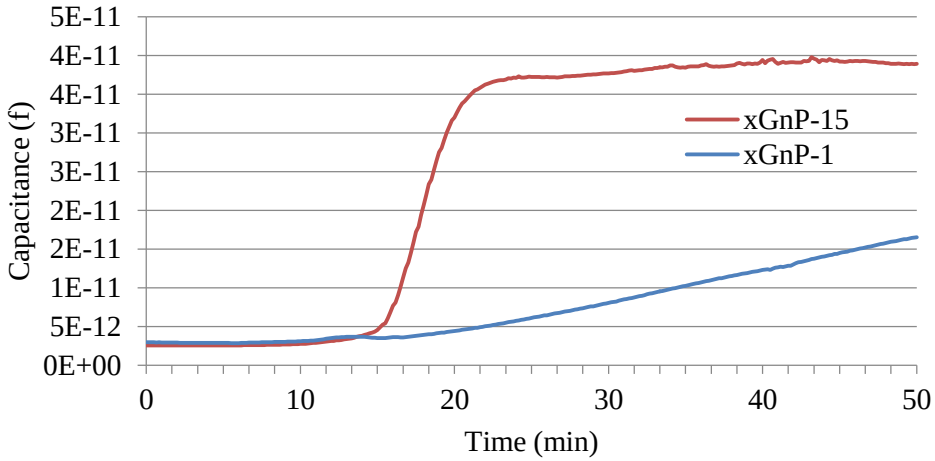

Figure 3.10 Capacitance of 3 wt% xGnP, paraffin wax, 1 hour mix.

Next, the effect of mixing time on the dispersion of the nanoparticles and on the stability of the system was investigated. The system composed of 3 wt% xGnP-15 was shear mixed for a period of 1 and 24 hours. Visual inspection of the systems, as shown in Figure 3.11, demonstrates that the xGnP-15 composite mixed for 24 hours is more stable than samples mixed for 1 hour. The results of the increased mixing time on the stability of the composite is believed to be due to the shear mixing breaking up graphite agglomerates into smaller particles that settle more slowly.

Figure 3.11 3 wt% xGnP-15, 50% paraffin/50% microcrystalline system (24 hour on left, 1 hour on right) after 2 hours in liquid state.

The effect of mixing time on xGnP-15 nanoplatelets was also studied with the capacitance technique for microcrystalline wax, paraffin wax, and the 50/50 wax mixture. Results are shown in Figure 3.12.

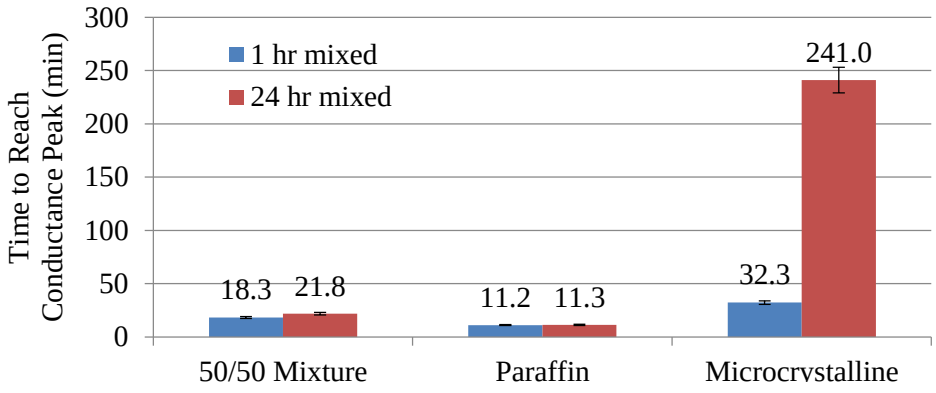

Figure 3.12 Conductance data for three wax systems mixed with xGnP-15.

As shown in Figure 3.12, the effect of mixing time on a system is dependent on the type of wax. Microcrystalline wax exhibits a 648% increase in time to reach a conductance peak with an increase in mixing time while the 50/50 wax mixture and paraffin wax display a 20% and 1% increase, respectively, as a result of increasing the mixing time from 1 hour to 24 hours. Additional experiments indicate that a mixing time beyond 24 hours does not improve the

stability of a composite system as no difference in the capacitance graphs is observed for systems mixed for 24, 48, and 96 hours.

It is apparent that the settling of the particles is affected by the physical properties of the wax. SEM images in Figure 3.13 show that, after 24 hours of mixing, smaller agglomerated particles are discernible as compared to a 1 hour mixing time. The images also indicate that shear mixing and ultrasonic sonication do not reduce the size of the particles. Therefore, it is concluded that smaller agglomerates lend to better dispersion and suggest why the longer mixed system is more stable. The trend that a longer mixing time leads to smaller agglomerates, and therefore better stability, was discussed by Moshkovith *et al.* [96] in regards to fullerene nanoparticles. It was found that as mixing time increases from 0 to 80 minutes, the fraction % of smaller aggregates increased, while the fraction % of larger aggregates decreased.

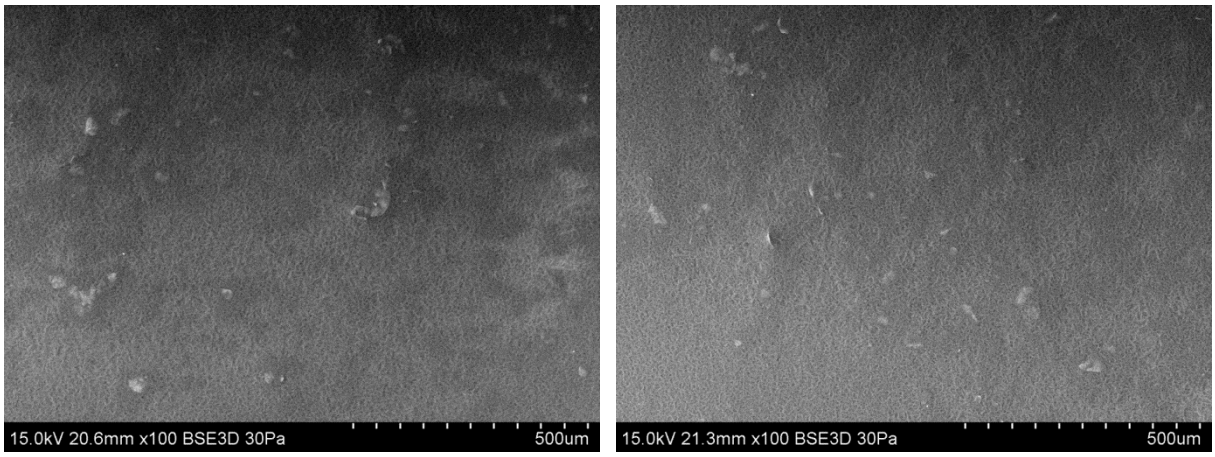

Figure 3.13 SEM images of xGnP-15/paraffin wax composite after 1 hr mix (left) and 24 hour mix (right).

To understand how wax material properties affect the stability, the impact of viscosity on the settling time was investigated. After viscosity baseline measurements were performed for paraffin, microcrystalline, and the 50/50 wax mixture, viscosity measurements for each of the xGnP-15 systems were completed at 80°C as presented in Figure 3.14. For both the 50/50

mixture and paraffin systems, the introduction of 3 wt% xGnP-15 results in a viscosity increase of about 25% from that of the pure material, while the microcrystalline system exhibits an 80% increase in viscosity.

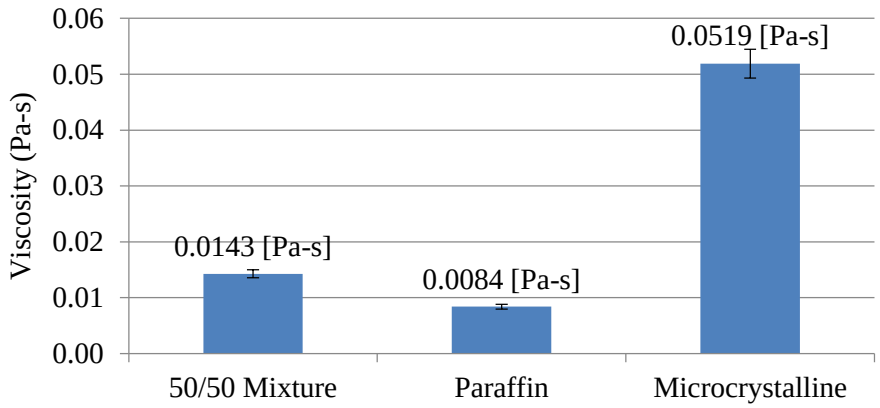

Figure 3.14 Viscosity data for wax, xGnP-15 systems.

By reviewing data in Figure 3.12, it is evident that the mixing time plays a role in the stability of the system as well as the viscosity. For example, the microcrystalline wax/ xGnP-15 system, with a viscosity of 0.0519 Pa-s, shows an increase in stability by a factor of 7.5 based on the time to reach a conductive pathway from 1 to 24 hour mixing. The 50/50 mixture wax/ xGnP-15 system, which is 260% less viscous than microcrystalline wax, exhibits an increase in stability by a factor of 1.2 from 1 to 24 hour mixing. The reduction in viscosity results in a decrease in the time to reach a conductive pathway due to the precipitation of the xGnP. Additionally, the reduction in viscosity reduces the impact of mixing time on the settling of the xGnP.

The results of the stability tests of the paraffin and microcrystalline wax systems mixed with graphite indicate that a high viscosity wax, which is indicative of the length or branching of the hydrocarbon chain, plays an important role. In addition, sufficient time is required to disperse

and break up agglomerated particles in order to improve stability especially for highly viscous waxes. To further increase stability, additional chemical modifications may be necessary and will be explored in the next section.

3.5.2. Stability Enhancement for a Wax, xGnP system with Dispersant

Two dispersants were investigated as possible stability enhancing agents, sodium dodecylbenzenesulfonate (SDBS) and octadecylphosphonic acid (ODPA). SDBS was tested since it has been previously shown to be effective with aluminum nanoparticles [78], but was found to have no effect on the stability of the xGnP as shown in Figure 3.15**.**

Figure 3.15 Settling comparison of ODPA (left) and SDBS (right) after 30 minutes.

ODPA was used because it was posited that the paraffin hydrocarbon chain (Figure 3.16 (left)) would form an affinity with the hydrocarbon end of the ODPA to increase stability and that the hydroxyl groups of the ODPA (Figure 3.16 (right)) would interact with the oxygen groups of the graphite.

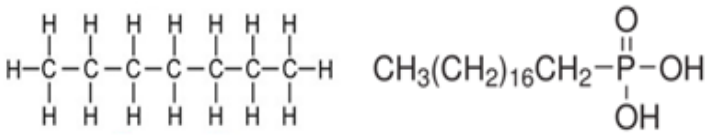

Figure 3.16 Chemical structure of paraffin (left) and ODPA (right).

To confirm the possible hydroxyl group interaction, XPS measurements were completed to ensure that oxygen was present on the surface of the graphite. As indicated in Table 3.2, from measurements of two different xGnP samples, there is about 3 atomic % of oxygen present on the surface of the graphite. Following the confirmation of oxygen on the surface of the graphite, Raman spectroscopy measurements were completed on a system of xGnP and ODPA that had been washed in ethanol, after which the ethanol was evaporated. Based on past work by Prado et al [95] and Ferrari [97], the G'/G peak was expected to decrease while the initial G peak would be larger than the G' peak. Results presented in Table 3.3 and Figure 3.17 confirm that the ODPA and graphite are interacting based on the reduction of the G'/G peak due to the presence of ODPA.

Table 3.2 XPS results.

	Graphite (Sample 1)	**Graphite (Sample 2)**
At. % C1s	94.18	94.20
At. % O1s	2.93	2.75

Table 3.3 Raman spectroscopy results.

	G peak	**G' Peak**	**G'/G**
Graphite	557 cm^{-1}	328 cm^{-1}	59%
Graphite with ODPA	1145 cm^{-1}	636 cm^{-1}	55%

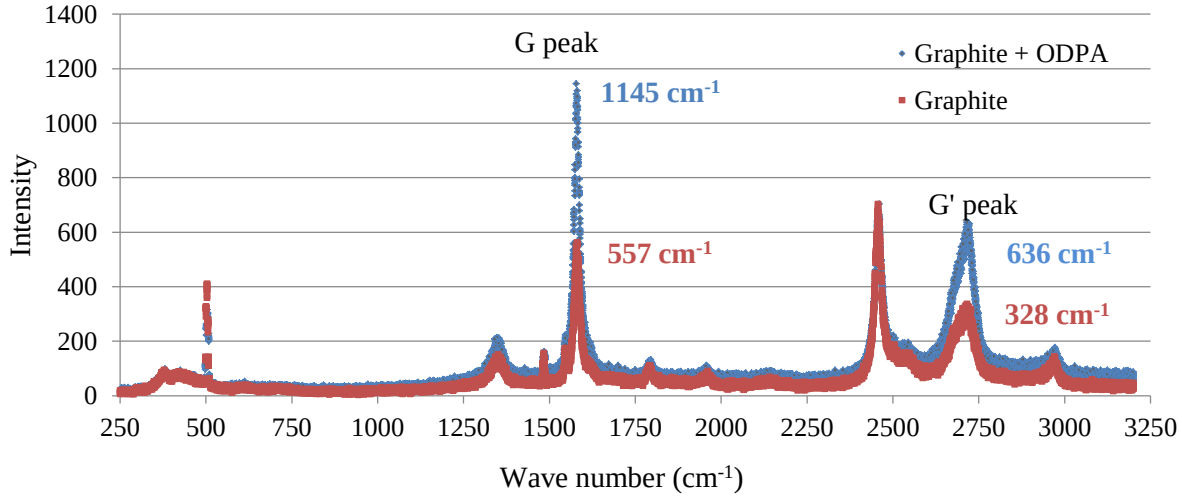

Figure 3.17 Raman data of graphite before and after being mixed with ODPA.

After confirming that the ODPA and graphite were interacting, visual inspection and capacitance measurements were completed after ODPA was shear mixed into the xGnP/paraffin wax system. Note that 5 wt% ODPA was chosen as an experimental amount to see how the addition of a dispersant impacted the stability. Results showed that ODPA increased the system's stability. As expected, the 1 hour mixed samples exhibited inferior stability to the 24 hour mixed samples. In addition, the more viscous, microcrystalline wax performed better than the less viscous wax systems. Images are presented of the 24-hour mixed microcrystalline wax with and without ODPA; Figure 3.18 (right) indicates that the sample with no ODPA settled before the sample that contained ODPA. Capacitance data also supports this conclusion: the increased rate of settling is translated into a greater rate of change of the capacitance in Figure 3.19.

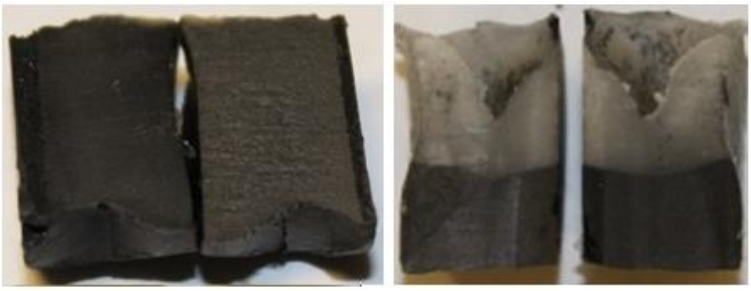

Figure 3.18 3 wt% xGnP-15, microcrystalline, 24 hour mix after 10.3 hours: 5 wt% ODPA (left) and 0 wt% ODPA (right).

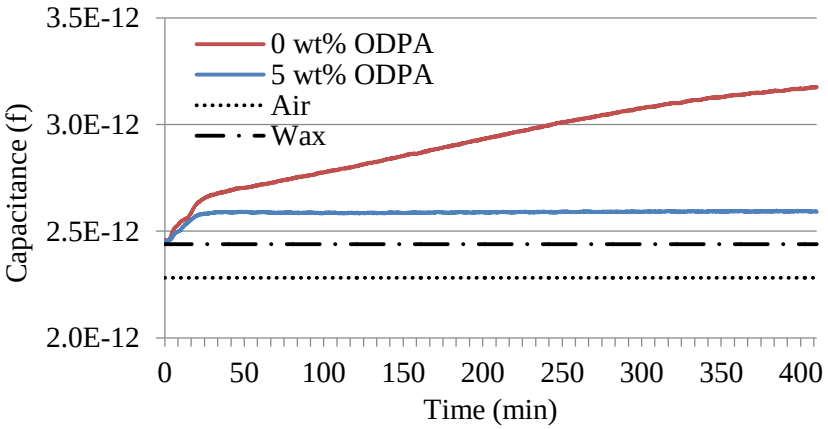

Figure 3.19 Capacitance data for 3 wt% xGnP-15, microcrystalline, 24 hour mixed systems in Figure 3.18.

Viscosity measurements were also performed on systems with and without ODPA. It was found that the addition of ODPA increases the viscosity of the system as seen in Figure 3.20. Based on the results with a wax, xGnP-15 system with no ODPA, it could be surmised that the increase in viscosity is the sole contributing factor to the increase in stability. Though the increase in viscosity should not be disregarded, this reasoning can be disproved by recalling that Raman spectroscopy confirmed that the ODPA and graphite were chemically bonded. Additionally, as can be seen from the pictures superimposed on Figure 3.20, which were taken after a settling study of 3.5 hours, Sample 2 has a higher viscosity than Sample 5 but also settles first. This confirms that the ODPA is improving stability due to chemical reactions with the graphite, not only the increase in viscosity.

Table 3.4 Sample ID for 3 wt% xGnP-15 systems for Figure 3.20.

ID	wt% ODPA	wt% Wax	Type of Wax	Mixing Time [hr]
1	5.0%	92.0%	Microcrystalline	1
2	0.0%	97.0%	Microcrystalline	1
3	5.0%	92.0%	Microcrystalline	24
4	0.0%	97.0%	Microcrystalline	24
5	5.0%	92.0%	50/50 Composite	1
6	0.0%	97.0%	50/50 Composite	1
7	5.0%	92.0%	50/50 Composite	24
8	0.0%	97.0%	50/50 Composite	24
9	5.0%	92.0%	Paraffin	1
10	0.0%	97.0%	Paraffin	1

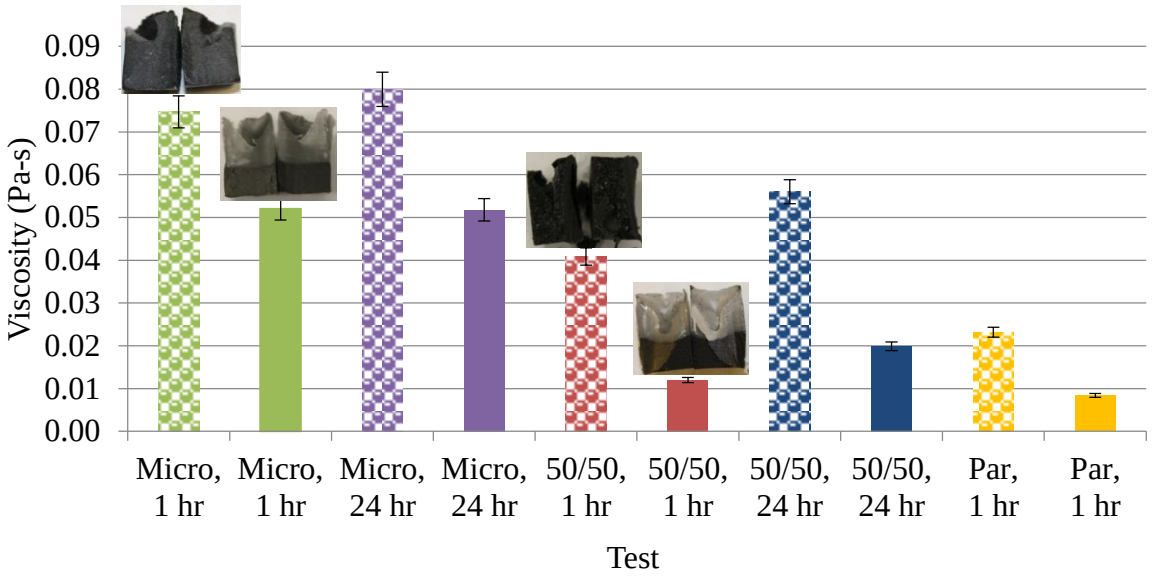

Figure 3.20 Viscosity of 3 wt% xGnP-15 samples with and without ODPA.

The addition of ODPA increases the stability of the xGnP wax system. Prior results indicate that an increase in viscosity and mixing time increases stability; this is further supported in the above work with ODPA. The less viscous wax systems tend to settle faster than the microcrystalline wax system. Additionally, the effect of 1 hour and 24 hour mixing time is realized: the 1 hour mix is less stable than the 24 hour mix. From visual inspection, the ODPA was visible in cross sectioned samples after 1 hour of mixing, but not after 24 hours of mixing suggesting better dispersion of ODPA in the wax. This also presents an explanation for the improved stability of the 24 hour mixed system.

3.5.3. Stability Enhancement for an Oxidized Wax, xGnP system

As the previous section summarizes, the introduction of ODPA increases the stability of the xGnP-wax system due to the chemical interaction with xGnP. Experimentation with oxidized wax was completed as an additional method to introduce potential chemical interaction between the graphite and wax. To oxidize the wax, it was placed in an oven at 150 °C in air for 6 days.

Raman spectroscopy confirmed oxidation due to the increase in fluorescent background emission as shown in Figure 3.21.

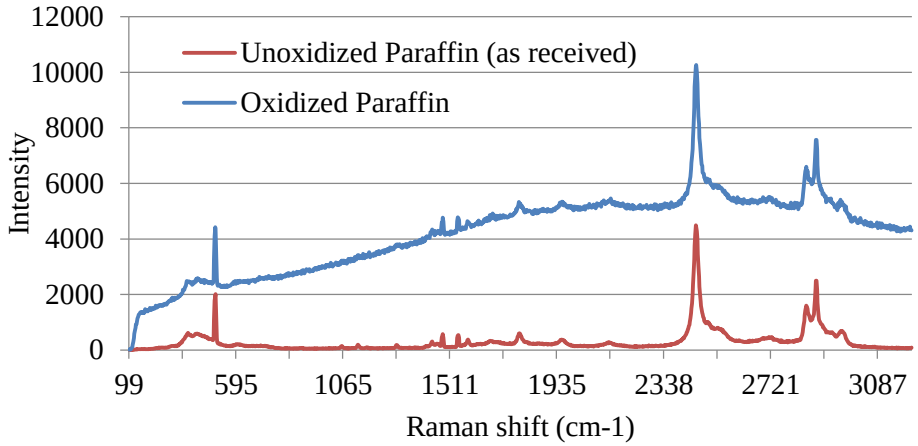

Figure 3.21 Raman spectra of oxidized and unoxidized wax.

Initially, the stability of oxidized wax was compared to that of unoxidized wax (as received). As Table 3.5 indicates, the oxidized wax system is up to 50% more stable than the unoxidized system based on the time each system takes to reach a conductance peak.

Table 3.5 Correlation of time to reach conductance peak and viscosity for 3 wt%, xGnP-15 systems with 0 wt% ODPA.

Type of Wax	Mixing Time [hr]	Time to Reach Conductance Peak [min]	Viscosity [Pa-s]
Paraffin	1	11.2	0.0084
Paraffin (Ox)	1	11.6	0.0086
50/50 Composite	1	17.8	0.0120
50/50 Composite (Ox)	1	18.2	0.0198
50/50 Composite	24	21.8	0.0165
50/50 Composite (Ox)	24	31.7	0.0194
Microcrystalline	1	32.3	0.0520
Microcrystalline (Ox)	1	51.5	0.0550

Viscosity measurements show that oxidation of the wax increases viscosity up to 65% as well as indicate a correlation between the viscosity of the system and the settling rate. Although

there is not a direct linear relationship, as the viscosity increases, the stability generally increases as well. However, it is noted that purely oxidizing the wax does not provide a significant increase viscosity of the system or increase in stability; after 3 hours both oxidized paraffin and oxidized microcrystalline wax settle out.

Next, the effect on stability of ODPA mixed with an oxidized wax system was explored. When oxidizing the wax, oxygen groups are introduced to the system. By introducing hydroxyl groups of ODPA, the intention was to improve stability through chemical interactions initiated by the oxygen. As Figure 3.22 indicates, ODPA does improve the stability of xGnP-15 as previously reported for an unoxidized system.

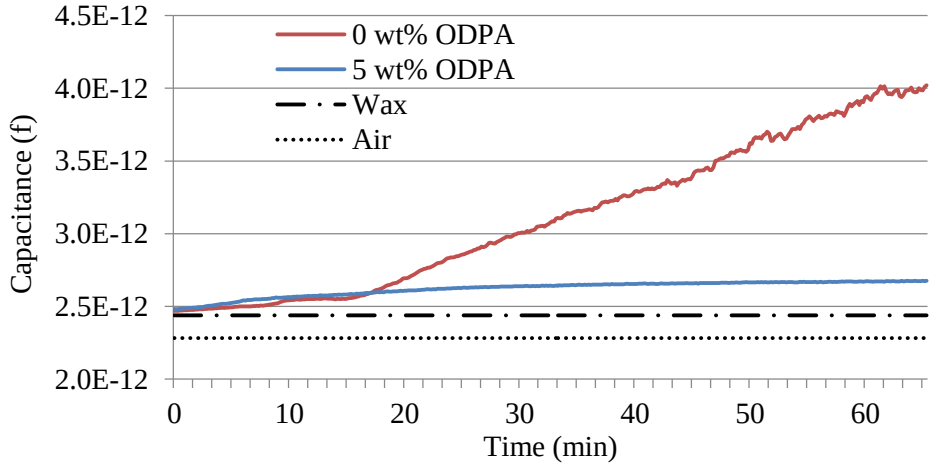

Figure 3.22 Capacitance data for a 3 wt% xGnP-15 oxidized microcrystalline system, 1 hour mix with and without ODPA.

In an oxidized system with the addition of ODPA, mixing time and viscosity once again have an effect on the stability of the system. As can be seen in Figure 3.23 through Figure 3.25 for 3 wt% xGnP-15 systems with 5 wt% ODPA, 24 hour mixing surpasses 1 hour mixing time (Figure 3.23 and Figure 3.24). Additionally, the higher viscosity microcrystalline wax is more stable than the paraffin wax (Figure 3.23 and Figure 3.25). In addition to visual inspection, this

conclusion is based on the smaller increase in capacitance, Figure 3.26, and no conductance path, Figure 3.27, for the microcrystalline wax, which indicates slower precipitation.

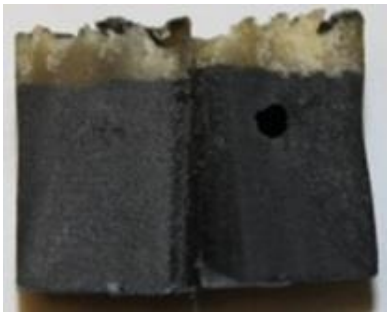

Figure 3.23 Oxidized microcrystalline, 1 hour mix; after 4 hours.

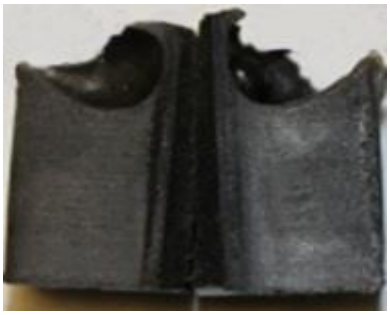

Figure 3.24 Oxidized microcrystalline, 24 hour mix; after 10.3 hours.

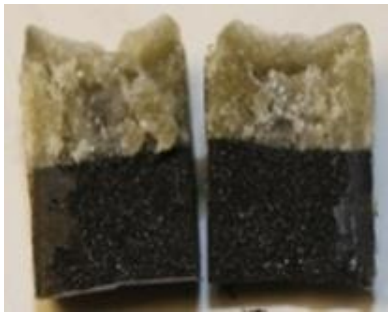

Figure 3.25 Oxidized paraffin, 1 hour mix; after 3 hours.

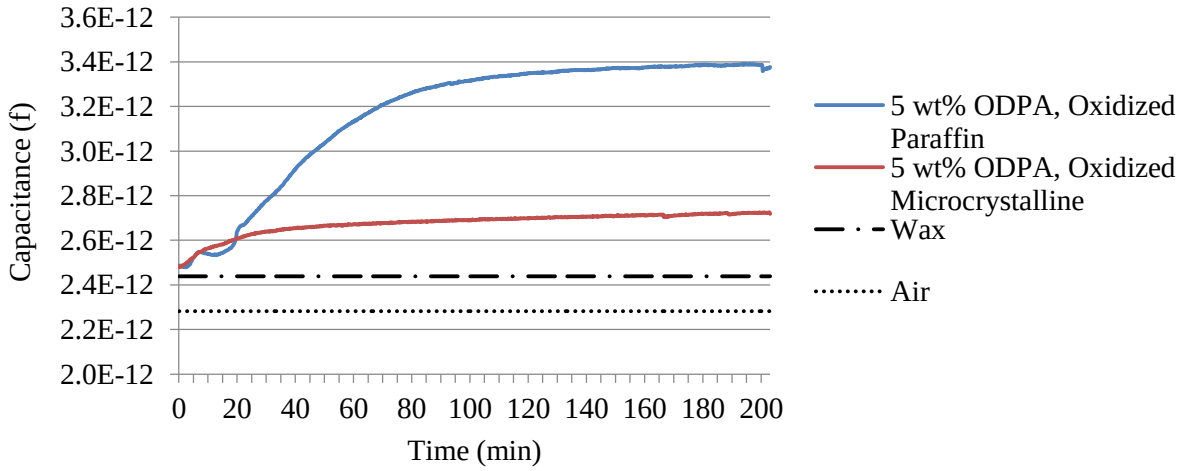

Figure 3.26 Capacitance data for 3 wt% xGnP, 1 hour mixed systems Figure 3.23 and Figure 3.25.

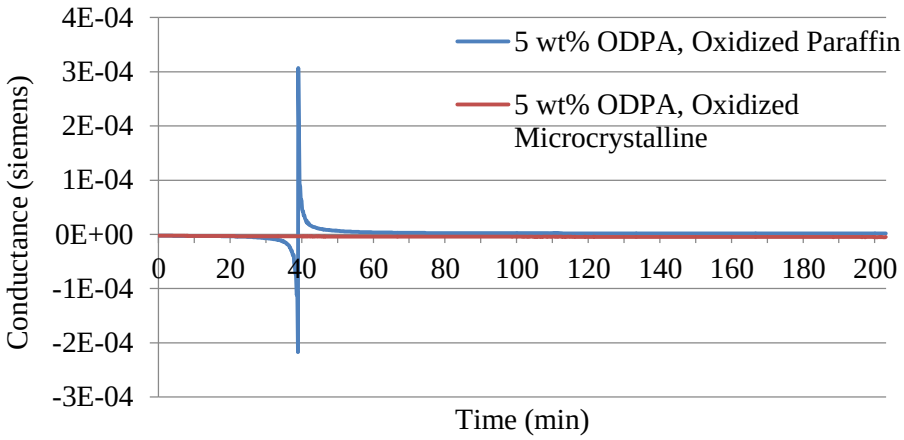

Figure 3.27 Conductance data for 3 wt% xGnP, 1 hour mixed systems Figure 3.23 and Figure 3.25.

Figure 3.28 shows that with 24 hour mixing, microcrystalline wax with 5 wt% ODPA is the most stable system for both oxidized and unoxidized wax. Images reflect stability after 50 hours in the molten state. Based on visual inspection, oxidized wax is slightly more stable than unoxidized wax as indicated by the white lines superimposed on the figure.

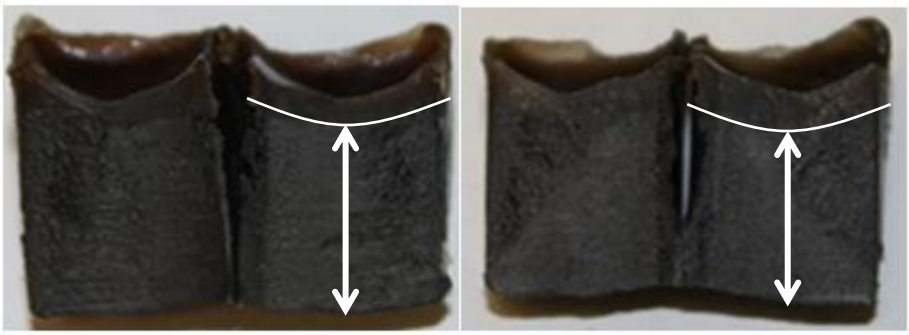

Figure 3.28 3 wt% xGnP-15, 5 wt% ODPA, microcrystalline wax, 24 hour mix: oxidized (left) and unoxidized (right) after 50 hours.

3.5.4. Stabilization Summary

The stability of graphite nanoplatelet/wax composites for phase change thermal energy storage depends greatly on particle size, dispersion of the platelets, viscosity of the wax, and chemical interactions within the system. The comparison of xGnP-1 and xGnP-15 stability

indicates that the xGnP-1 is more stable, though, for the majority of work reported, xGnP-15 was used due to its superior electrical and thermal conductivity. Experiments with both unoxidized and oxidized wax indicate that mixing time and viscosity impact the stability of the system. Through capacitance and conductance measurements as well as visual inspection, it is concluded that a 24-hour mixing time and high viscosity wax greatly improves the stability of an xGnP-15, wax system. It is posited that the long mixing time more effectively disperses and breaks up agglomerated particles in addition to a more viscous system that reduces the rate of precipitation. It is noted that simply oxidizing the wax does not significantly increase stability of the system.

The impact on stability from the addition of ODPA to an xGnP-15, wax system was also reported. Although the addition of ODPA increases viscosity, which in turn enhances stability, Raman spectroscopy and XPS were used as analysis techniques to confirm chemical interaction of the graphite and ODPA to further decrease the precipitation rate. It was shown that the use of ODPA along with control of viscosity, mixing time and oxidation was able to increase the stability as measured by capacitance sedimentation and visual inspection from 11 minutes to 50 hours. The following section discusses how these changes to the pure PCM system, specifically ODPA addition, oxidation, and concentration of xGnP, impact the thermal conductivity of the system.

3.6. Thermal Conductivity and Latent Heat of Wax-xGnP systems

The thermal conductivity was measured for unoxidized and oxidized microcrystalline and paraffin wax as well as wax systems mixed with 3 wt% xGnP and a combination of 3 wt% xGnP and 5 wt% ODPA. The results are presented in Figure 3.29. It is interesting to note the slight difference between response of the unoxidized and oxidized systems with the addition of xGnP

and ODPA. For both of the oxidized systems, the addition of 3 wt% xGnP doubles the thermal conductivity and further enhancement is seen with the addition of ODPA. The unoxidized systems see an increase in thermal conductivity of about 60% with the addition of 3 wt% xGnP, but then a slight decrease with the addition of ODPA. Even though this is an interesting response, it is noted that a small range exists for the thermal conductivity of each of the corresponding systems (i.e. thermal conductivity of 3 wt% xGnP ranges from 0.44 $Wm^{-1}K^{-1}$ to 0.51 $Wm^{-1}K^{-1}$).

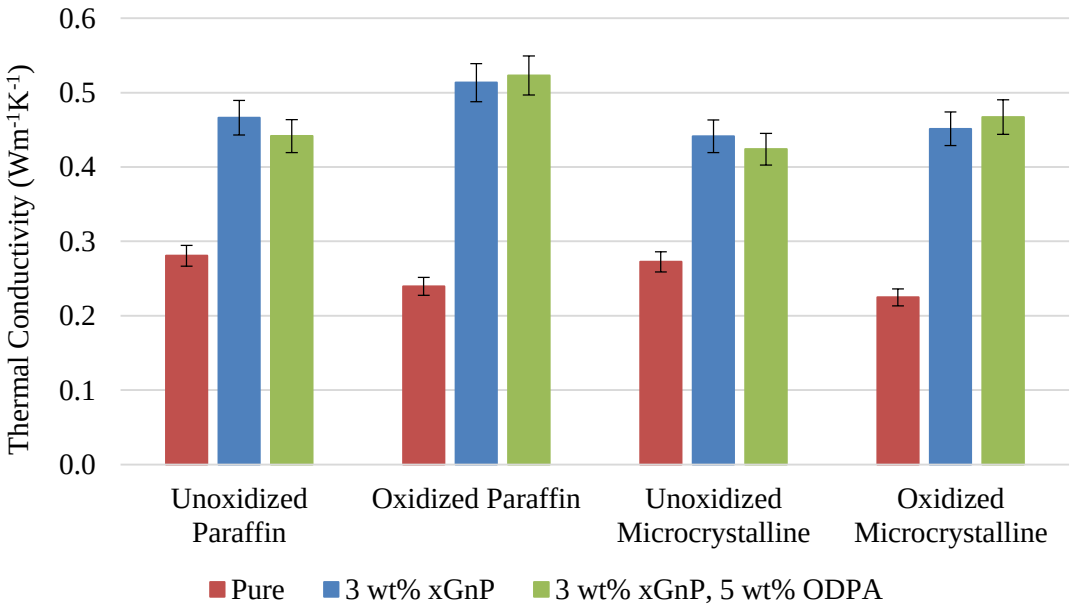

Figure 3.29 Thermal conductivity of various experimental systems.

The latent heat and melting temperature was then measured with DSC. Figure 3.30 and Figure 3.31 present DSC curves for paraffin and microcrystalline wax. The measurement process starts on the bottom left of the graph. Heat was gradually added (5°C per minute) until both the sample and the reference reach 80°C, which is indicated by the lower portion of the graph. Then the sample was cooled back to the original temperature, which can be seen by the upper portion of each graph. The latent heat can be calculated by the area under the largest peak (during either

the endothermic or exothermic process) and the melting temperature is measured as the temperature at the top of the peak. The following aspects of the curves are of interest:

A – Smaller peaks occur at solid-solid transition where the orthorhombic crystal structure (hard and brittle) of the paraffin transforms in a hexagonal crystal structure (softer, shows plasticity). Microcrystalline waxes do not exhibit a solid-solid transition. This peak was not used in the latent heat or melting temperature calculations.

B – As previously mentioned, crystalline polymers give rise to very broad melting peaks because of the size distribution of the crystallites as discussed in Section 1.3. The latent heat and melting temperature are measured based on the size and location of this peak. The broad peak of the microcrystalline wax reflects the difference in the molecular structure between linear chain paraffin wax and branched chain microcrystalline waxes. This data is summarized in Table 3.6 and Table 3.7.

C – This indicates the sample that was oxidized with 3 wt% xGnP and 5 wt% ODPA. As shown Figure 3.30 and Figure 3.31 as well Table 3.6 and Table 3.7, oxidation reduces both the melting temperature and latent heat.

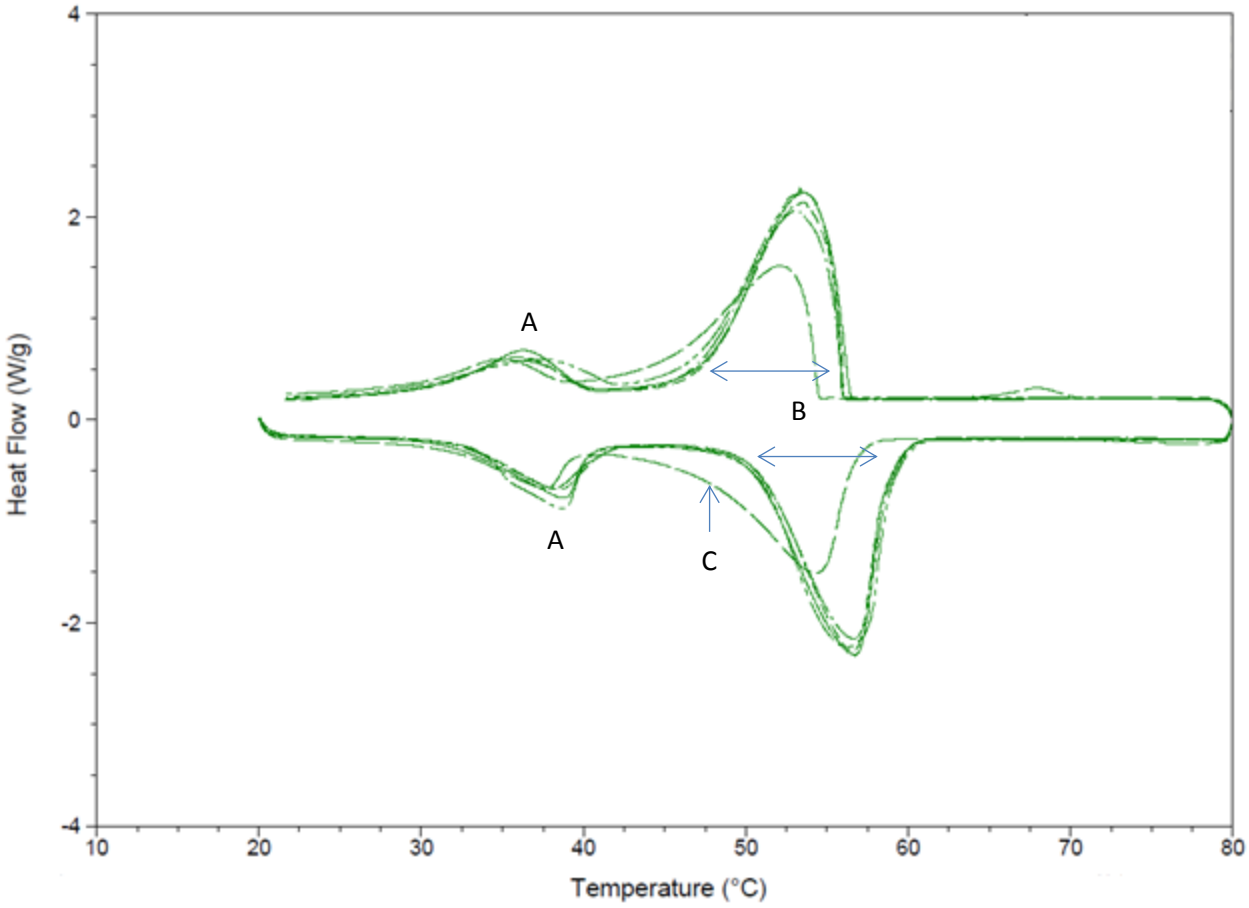

Figure 3.30 DSC curve for paraffin wax.

Table 3.6 DSC data for paraffin wax.

Paraffin Wax	Pure Paraffin	Paraffin with 3 wt% xGnP	Paraffin with 3 wt% xGnP and 5 wt% ODPA	Oxidized Paraffin with 3 wt% xGnP and 5 wt% ODPA
Melt Peak [°C]	56.39	56.72	56.64	54.45
Melting enthalpy [Jg^{-1}]	147.80	141.80	133.40	96.96
Cryst. Peak [°C]	53.32	53.69	53.66	52.22
Cryst. Enthalpy [Jg^{-1}]	145.10	143.00	135.00	97.72

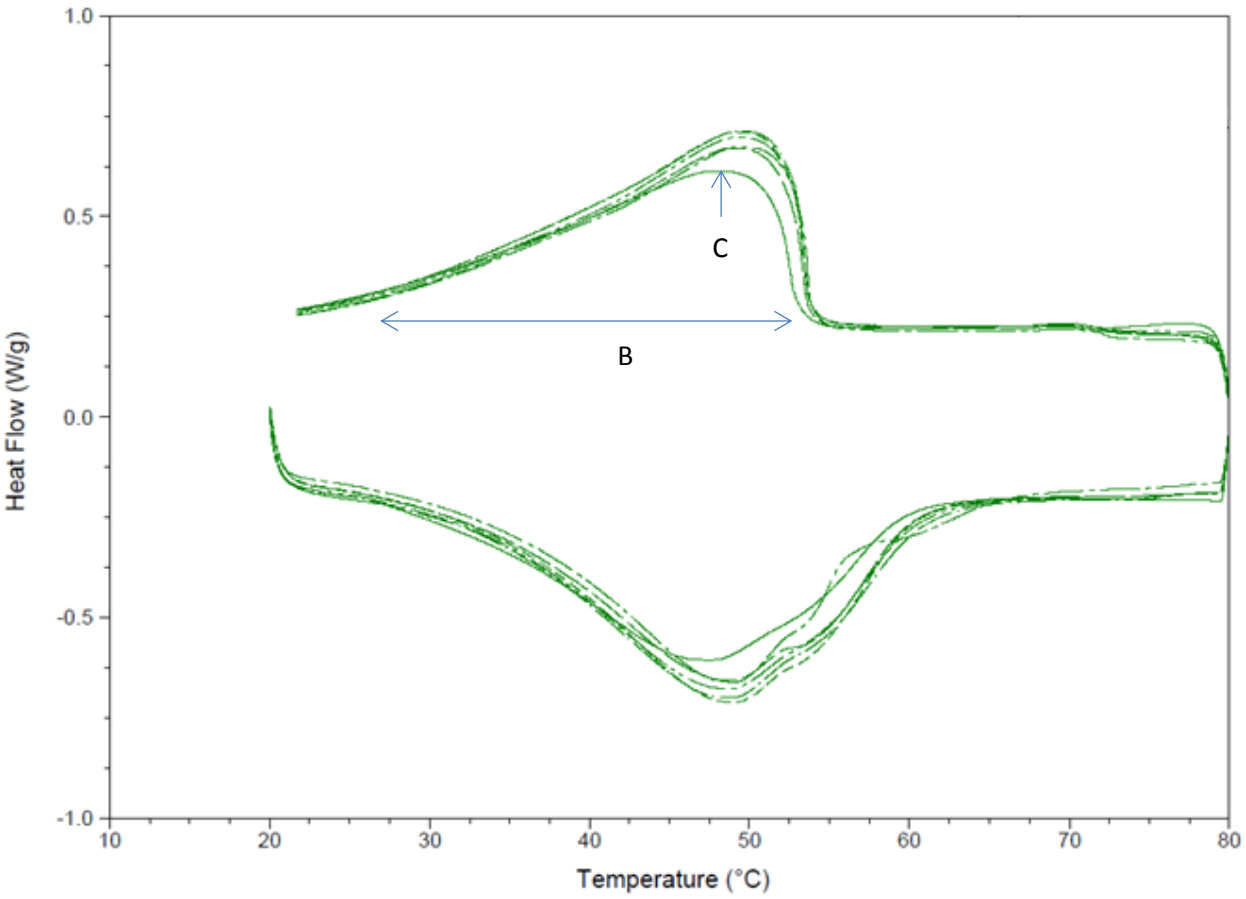

Figure 3.31 DSC curve for microcrystalline wax.

Table 3.7 DSC data for microcrystalline wax.

Microcrystalline Wax	Pure Micro	Micro with 3 wt% xGnP	Micro with 3 wt% xGnP and 5 wt% ODPA	Oxidized Micro with 3 wt% xGnP and 5 wt% ODPA
Melt Peak [°C]	48.77	48.93	48.66	47.50
Melting enthalpy [Jg^{-1}]	103.50	103.70	100.30	88.87
Cryst. Peak [°C]	49.67	49.90	49.86	48.60
Cryst. Enthalpy [Jg^{-1}]	90.16	87.29	83.99	71.49

Based on visual inspection of the oxidized systems with 3 wt% xGnP and 5 wt% ODPA, these systems were reported to have a slight performance enhancement over a similar system with unoxidized wax. However, since oxidization reduces latent heat by 30% for paraffin and 15% for microcrystalline wax, it is posited that an unoxidized system with 3 wt% xGnP and 5

wt% ODPA is superior to the oxidized system. It is noted that the addition of ODPA reduces the latent heat of the system by 10% for paraffin and 3% for microcrystalline wax, but for all systems, paraffin wax has a larger latent heat than microcrystalline wax. Additionally, no effect on the melting temperature is reported except for a slight decrease with oxidation of the wax.

Based on the above results, it is understood that system of 3 wt% xGnP and 5 wt% ODPA with unoxidized paraffin or microcrystalline wax is a superior system based on thermal conductivity, latent heat, and melting temperature measurements. Next, the impact of concentration is discussed of unoxidized systems up to 10 wt% xGnP. The wt% of ODPA remains at 5 wt% for minimal impact on latent heat. Thermal conductivity for systems up to 10 wt% is shown in Figure 3.32 in the solid state. Note that thermal conductivity values of paraffin and microcrystalline were averaged for simplicity due to their similar thermal conductivity response to the addition of ODPA and xGnP. Systems with ODPA are indicated by the diamond pattern on the bars on the right of the figure. The increase in thermal conductivity is linear with a maximum at 1.1 $Wm^{-1}K^{-1}$ at 10 wt% xGnP, 5 wt% ODPA.

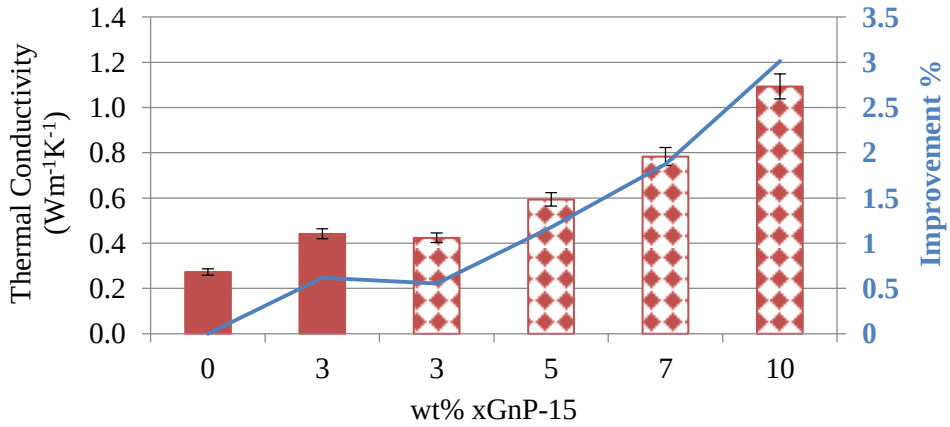

Figure 3.32 Thermal conductivity values for systems up to 10 wt% xGnP. Presence of ODPA is indicated by the diamond pattern.

DSC measurements were also conducted for each of the systems in Figure 3.32 and presented in Figure 3.33. Note that this figure presents latent heat data for microcrystalline wax, but a similar rate of decrease was demonstrated by paraffin wax. Figure 3.33 presents a decrease of 16% for the latent heat for the 10 wt% xGnP with 5 wt% ODPA samples, but also a linear increase in thermal conductivity.

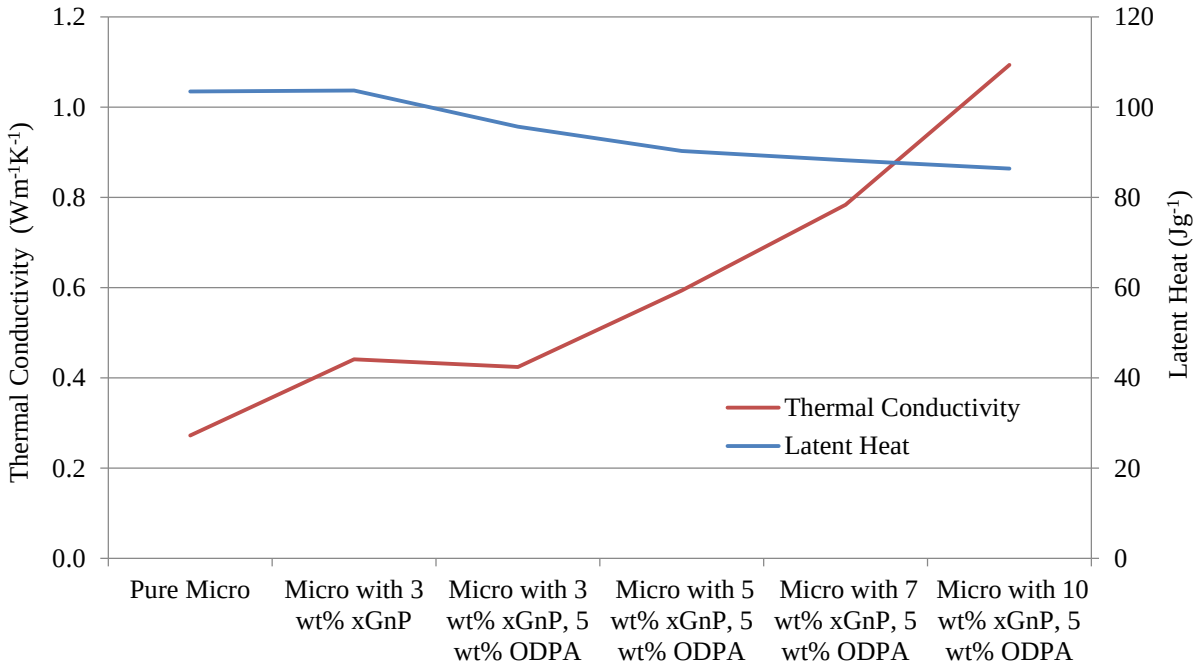

Figure 3.33 Comparison of thermal conductivity and latent heat for various composite systems.

3.7. Summary

A method of maintaining a stable suspension of xGnP in the molten state was developed. Settling was measured through both visual inspection and a capacitance technique that quantifies the settling. This is critical to retaining composite properties, such as thermal conductivity, as the material moves through a solid-liquid phase change when used as a thermal energy storage medium. This work also indicates that not only thermal conductivity should be considered when considering the use of xGnP to increase the rate of thermal charging, but also the stability of

graphite. For example, as shown by the graph in Figure 3.34, the thermal conductivity of octadecane is about twice that of paraffin, but when compared to paraffin in a stability steady, xGnP in octadecane settles in about 90 seconds. Note that the thermal conductivity of paraffin/5 wt% xGnP composite is 0.6 $Wm^{-1}K^{-1}$, similar to the experimental values reported in Figure 3.32.

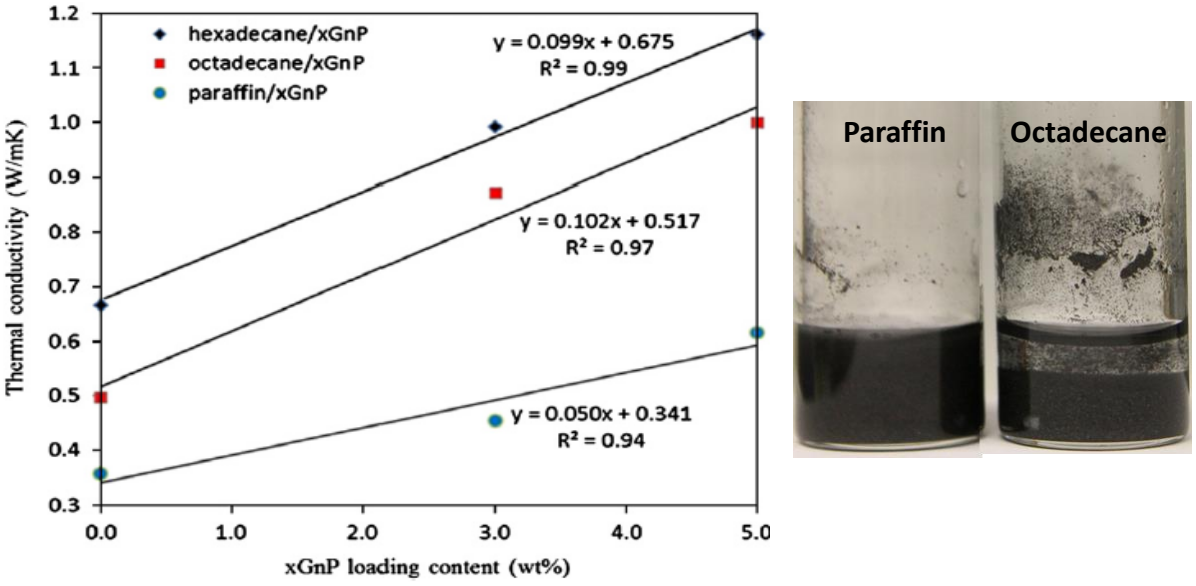

Figure 3.34 Thermal conductivity as a function of wt% for various PCM (left) [85]; stability of xGnP in paraffin and octadecane after 90 seconds (right).

Through the addition of octadecylphosphonic acid as well as control of viscosity and mixing time, the precipitation of xGnP in paraffin wax in the molten state is minimized. With this combination of processing steps, increase in the stability or settling time of the paraffin/graphite composites was increased by a factor of 270 over composites without any treatment. This finding is documented as GTRC ID 6185, "Stability Enhancement of Paraffin/Exfoliated Graphite Nanoplatelet Composites for Latent Heat Thermal Storage Systems".

Thermal conductivity, latent heat, and melting temperature measurements were reported for the stable paraffin wax and microcrystalline wax composites. Based on these results, it is posited that xGnP stabilized with ODPA mixed with unoxidized paraffin or microcrystalline wax is a superior system based on thermal conductivity, latent heat, and melting temperature measurements. Additionally, though microcrystalline wax is more viscous than paraffin wax, paraffin wax has a higher latent heat, which would be reflected in the thermal energy stored during phase change.

As discussed at the end of Chapter 2, the second phase of research focuses on the impact of thermal conductivity on thermal charging. The common metric used in literature to describe the impact of xGnP addition on wax is increase on thermal conductivity. Chapter 4 focuses on thermal charging experiments to correlate thermal conductivity of xGnP systems to their thermal response.

CHAPTER 4: THERMAL CHARGING PERFORMANCE EVALUCATION OF NANOPARTICLES AND METAL FOAMS

4.1. Introduction

Thermal charging enhancement of paraffin wax can be achieved through the introduction of high conductivity foams or nanoparticles to increase the thermal conductivity of the PCM [30, 51, 52]. Increasing the thermal conductivity of paraffin wax through dispersion of xGnP was explored in Chapter 3. It was noted that effective thermal conductivity enhancement with this method is dependent on the concentration (wt%) and nanoparticle stability within the liquid PCM. Chapter 3 discussed methods to stabilize the xGnP as well as the impact of concentration on the thermal conductivity and latent heat of the composite. Comparison of these two characteristic thermal properties is a common performance metric [52, 82, 98]. However, the non-linear phase change process introduces a need for comparative thermal charging experiments to understand the rate of thermal response as a function of the thermal conductivity, weight percentage, and geometry of enhancement material.

This chapter explores the influence of thermal conductivity on the rate of thermal charging of PCM composites. With non-phase change systems, the composite thermal conductivity is used to describe the rate at which thermal energy enters the system. The relationship between thermal conductivity and thermal charging has been extrapolated to PCM composites. This chapter will study the relationship between thermal conductivity and thermal charging rate to highlight the factors that are significant to the thermal charging rate for PCM thermal storage systems.

Initial experiments will discuss the impact on the thermal charging of paraffin wax due to the dispersion of xGnP stabilized with ODPA as discussed in Chapter 3. By applying two

different constant heat fluxes to the sample, thermal charging response is quantified by measuring the temperature of the bottom of the sample over time and then comparing to the composite thermal conductivity. Next, the thermal charging of compressed expanded graphite foams of similar weight percent and thermal conductivity will be compared to that of xGnP. Finally, the use of xGnP in aluminum foams, necessary for applications that require structural support, to increase the baseline thermal charging performance of these materials will be explored. By using a standard experimental sample for all three systems, comparisons are readily made between various methods of thermal charging enhancement by increasing the thermal conductivity of PCM composites.

4.2. Summary of Thermal Charging Experiments

Composite properties of graphite systems were first measured using a hot disk thermal analyzer (Hot Disk TPS2500S) for the thermal conductivity at 20°C and a DSC (TA Instruments Q2000) for the latent heat and melting temperature by ramping from 20°C to 80°C at 5°C per minute. Thermal charging experiments were then conducted by applying a constant heat flux to a rectangular sample and comparing the rate at which the composites increased in temperature to quantify the thermal charging performance of the each system.

The thermal charging test container was made from Acrylite® FF Acrylic Sheet with a thickness of 1.27 cm purchased from US Plastic Corp. The test container measured 5.08 cm x 5.08 cm x 2.54 cm and was designed in two separate pieces, each 5.08 cm x 5.08 cm and 1.27 cm thick, for simple loading and unloading of the samples as shown in Figure 4.1 (left). The top acrylic piece was made with a 2.54 cm x 2.54 cm hole into which the xGnP composite was poured. The bottom acrylic piece was solid. Thin film heaters with an adhesive backing and

maximum output of 1.55 Wcm^{-2} were obtained from McMaster-Carr. The heaters were attached to a square 0.15 cm thick aluminum plate and then placed on top of the sample. K-type thermocouples of diameter 0.025 cm were used in conjunction with an Agilent 34972A Data Acquisition unit via an Agilent 20-channel Armature Multiplexer to record the thermocouple temperatures. The heaters were powered using an Agilent E3649A DC power supply. Figure 4.1 (right) presents a schematic of the test sample.

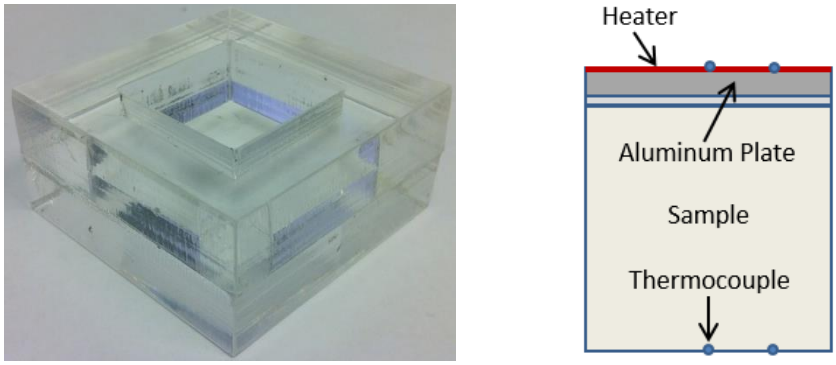

Figure 4.1 Test setup (left); Schematic of test setup for thermal charging experiments (right).

For all experiments, two thermocouples were placed under the heater to measure the top temperature of the sample and two additional thermocouples were placed at the bottom of the sample as shown in Figure 4.1 (right). A piece of oil resistant rubber was then placed on top of the heater to prevent leakage and minimize convective losses. Finally, the entire system was placed inside of an insulated box. For each constant heat flux experiment, the top and bottom temperatures of the sample were recorded over time.

4.3. Graphite Composites

4.3.1. Thermal Charging Enhancement using Graphite Nanoplatelets (xGnP)

The xGnP/paraffin wax composites described in Chapter 3 were reheated and poured into acrylic test containers shown in Figure 4.1. Thermal charging experiments were conducted under

both 1.55 Wcm^{-2} and 0.39 Wcm^{-2} to compare the various systems under a high and low heat flux conditions. Graphite nanoplatelets composites used in thermal charging experiments are summarized in Table 4.1.

Table 4.1 Summary of xGnP composites used in thermal charging experiments.

	Thermal Conductivity [$Wm^{-1}K^{-1}$]
Paraffin Wax	0.28
3 wt% xGnP/5 wt% ODPA Microcrystalline Wax	0.43
3 wt% xGnP/5 wt% ODPA Paraffin Wax	0.44
10 wt% xGnP/5 wt% ODPA Paraffin Wax	1.09

Thermal charging results are presented in Figure 4.2, Figure 4.3, and Figure 4.4. A baseline case of paraffin exposed to 1.55 Wcm^{-2} (left) and 0.39 Wcm^{-2} (right) is represented by the data in Figure 4.2. The poor thermal charging performance of paraffin wax is implied by the difference in the rate of temperature change between the top and the bottom temperatures. The experiment was terminated when the top temperature reached the 100°C limit for the acrylic material.

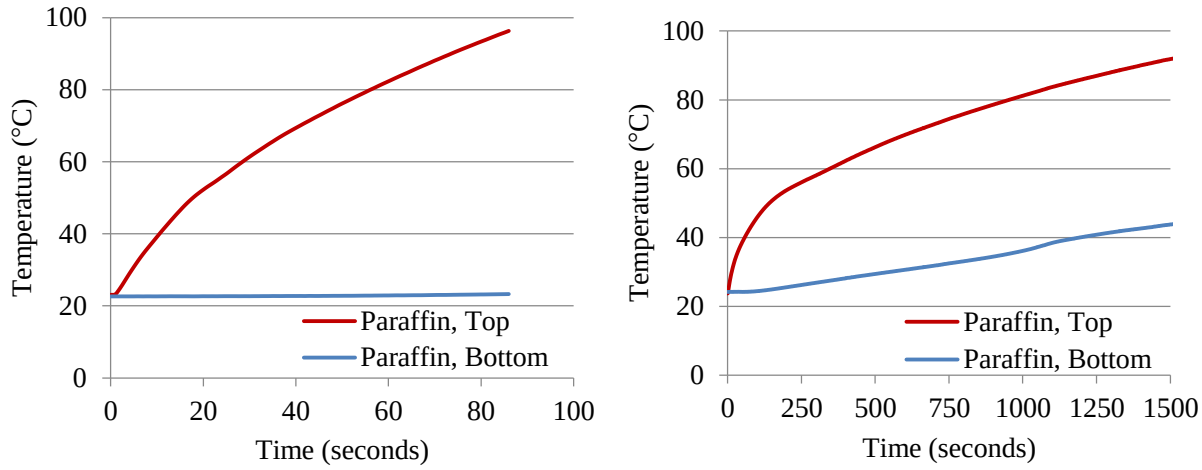

Figure 4.2 Baseline thermal charging performance data for paraffin wax; 1.55 Wcm^{-2} (left), 0.39 Wcm^{-2} (right).

Thermal charging data for the systems summarized in Table 4.1 are shown in Figure 4.3 exposed to 1.55 Wcm^{-2} and Figure 4.4 exposed to 0.39 Wcm^{-2}. The percent temperature increase, calculated by the difference between the initial and final temperature divided by the initial temperature for each experiment, is shown in Table 4.2 for both boundary conditions. This is used as a comparison metric since no sample undergoes solid-liquid phase change within the experimental period. For both heat fluxes, the rate of temperature increase of the 10 wt% xGnP is slightly higher than the other samples. Additionally, it is shown that the microcrystalline and paraffin composites exhibit similar trends in temperature increase with 3 wt% xGnP. Since these two systems have a similar effective thermal conductivity, this performance suggests a relationship between thermal charging and thermal conductivity.

Though none of the samples undergo solid-liquid phase change, the impact of solid-solid phase change can be seen in Figure 4.4. As previously shown in Figure 3.30 and Figure 3.31, paraffin wax undergoes distinct solid-solid and solid-liquid phase change periods whereas microcrystalline wax undergoes a solid-liquid phase change over a wide temperature range. The

paraffin wax composite lines of Figure 4.4 have inflections in the temperature data around 35°C, which corresponds to the solid-solid phase change temperature of paraffin wax. The microcrystalline composite line of Figure 4.4 remains linear as a result of the of latent heat distribution over the entire temperature range.

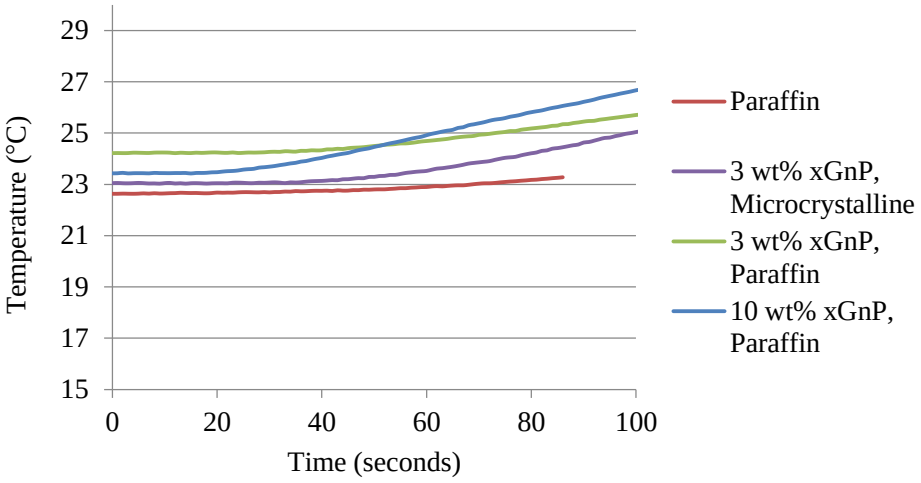

Figure 4.3 Bottom temperature of xGnP thermal charging experiments under 1.55 Wcm^{-2}; all xGnP samples with 5 wt% ODPA.

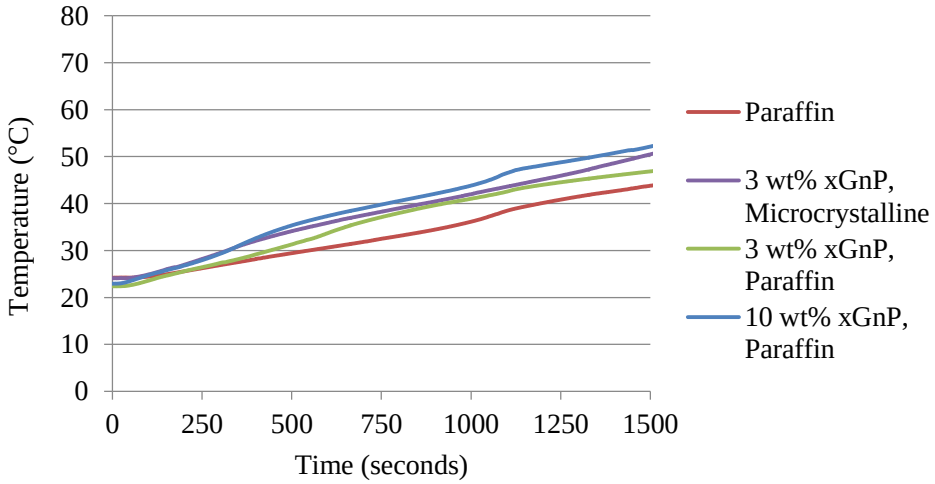

Figure 4.4 Bottom temperature of xGnP thermal charging experiments under 0.39 Wcm^{-2}; all xGnP samples with 5 wt% ODPA.

Table 4.2 Percent increase in temperature of data in Figure 4.3 and Figure 4.4.

	1.55 Wcm^{-2}	**0.39 Wcm^{-2}**
Paraffin Wax	3%	81%
3 wt% xGnP/5 wt% ODPA Microcrystalline Wax	6%	109%
3 wt% xGnP/5 wt% ODPA Paraffin Wax	9%	109%
10 wt% xGnP/5 wt% ODPA Paraffin Wax	14%	127%

To compare the impact of increase in thermal conductivity to the increase in temperature, Figure 4.5 displays the percent increase in temperature reported in Table 4.2 with the thermal conductivity of each composite reported in Table 4.1. Figure 4.5 indicates that thermal conductivity and rate of temperature response are not linearly related. For both heat fluxes, the increase in temperature starts to level at 1.1 Wm^{-1}K^{-1}. Especially for the small thermal charging improvement for 1.55 Wcm^{-2} between 0.43 Wm^{-1}K^{-1} and 1.1 Wm^{-1}K^{-1}, this data indicates that the 100% increase thermal conductivity has little impact on the rate of thermal response.

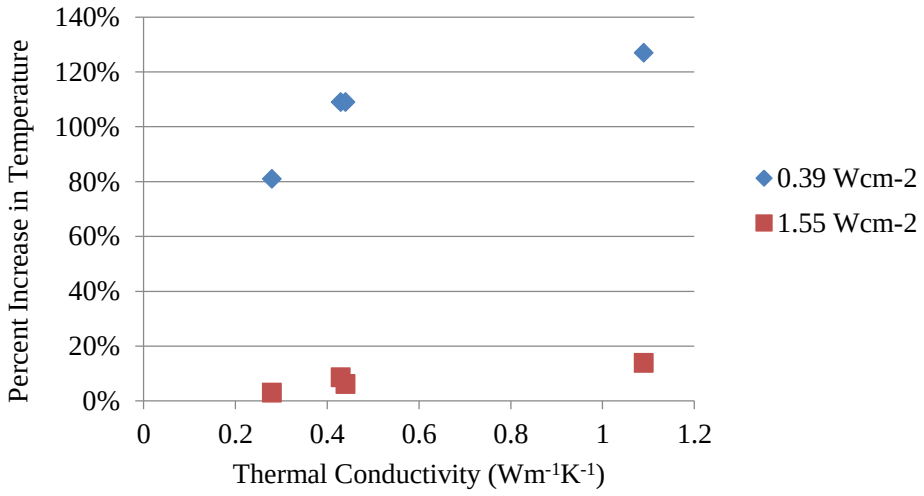

Figure 4.5 Percent increase in temperature as a function of thermal conductivity for low and high heat fluxes.

Thermal charging experiments with various xGnP concentrations indicate that graphite nanoplatelets have more impact under high heat fluxes; however, the addition of graphite in any concentration has limited impact on thermal charging. A comparison of the impact of 3 wt% xGnP mixed with paraffin and microcrystalline indicates that, although thermal conductivity is not linearly related to thermal charging, systems of similar effective thermal conductivity will charge at similar rates. The next section will explore other graphite materials, specifically compressed expanded natural graphite, to better understand the impact of thermal conductivity, concentration, and geometry on rate of thermal charging.

4.3.2. Thermal Charging Enhancement using Graphite Foam

As discussed in Section 2.4.2, compressed expanded natural graphite (CENG) foam phase change composites are characterized by latent heat and thermal conductivity measurements as a function of the bulk density of the CENG. While latent heat of the PCM decreases due to the addition of graphite as well voids formed during the compression process [72], thermal conductivity of the PCM increases [52, 72, 77]. In addition to studying the influence of CENG bulk density on the storage properties of the PCM composite, applications such as thermal management of a battery pack [52], thermal storage in a solar hot water system [77, 99], and general application in constant temperature conditions [61] have been considered. In these applied experiments, Mills *et al.* [52], Haillot *et al.* [99], and Zhong *et al.* [61] studied PCM composites enhanced by CENG foam with bulk densities of 210 kgm-3, 150 kgm-3, and 70 kgm-3, respectively. These three experiments discussed thermal charging of the PCM/CENG composites, but comparison of the effectiveness of the CENG on the thermal response of the PCM remains a function of the thermal conductivity. Thermal charging experiments are required to compare the impact of the various geometries of graphite, specifically CENG and xGnP,

without relying solely on thermal conductivity measurements. To compare to the results of Section 4.3.1, CENG composites with similar weight percentage and thermal conductivity are prepared and compared to the thermal charging performance of equivalent xGnP composites.

The production of expanded graphite is discussed in Section 2.4.2.1. Exfoliated graphite was purchased from Anthracite Industries, Inc. This expandable graphite was heated in a 1000W microwave for two 30 second intervals to complete the expansion process. An optical image of the expanded graphite (EG) and an SEM image are shown in Figure 4.6. Each worm of expanded graphite is approximately 1.5-2.0 mm long and about 0.4 mm wide.

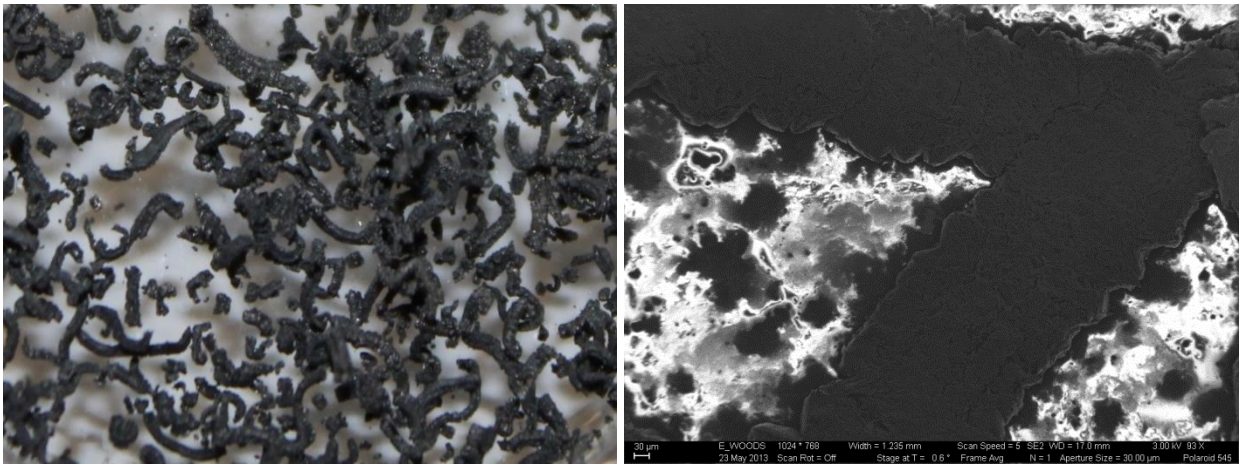

Figure 4.6 Optical image of EG (left); SEM image of EG at 93x magnification (right).

Each expanded graphite worm is an accordion style connection of graphene layers that have been separated through acid intercalation and subsequent introduction to high temperature. A progression of pictures with increasing magnification is shown in Figure 4.7 and Figure 4.8.

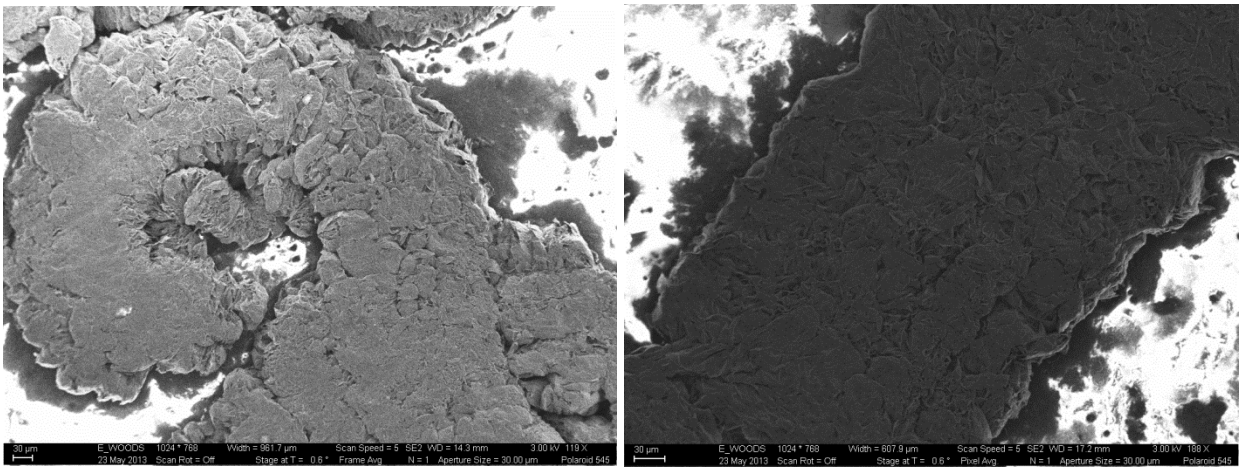

Figure 4.7 SEM images of EG at 119x (left) and 188x (right) magnification.

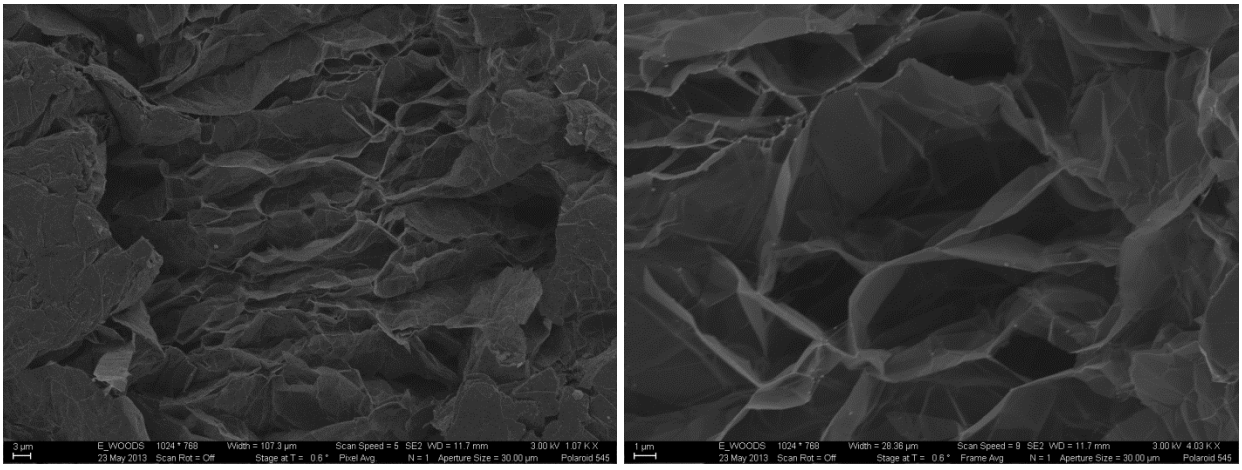

Figure 4.8 SEM images of EG at 1080x (left) and 4030x (right) magnification.

After the expansion process, the EG was manually compacted to the desired bulk density using the compression system shown in Figure 4.9 (right). EG was loaded into the container and then compressed until the pressing die was flush to the top of the container, forming a sample of volume 120 cm^3. By measuring the mass of EG in the compression system, samples with bulk densities of 23 kgm^{-3} (3 wt% graphite) and 11 kgm^{-3} (1.5 wt% graphite) were formed.

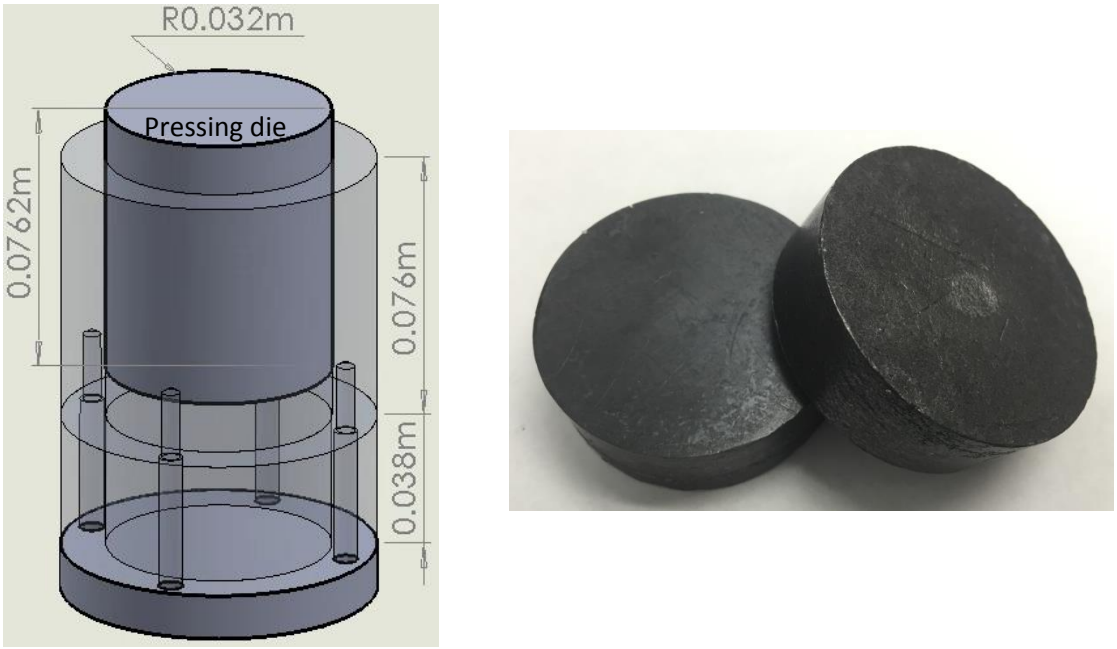

Figure 4.9 Compression system used to form samples (left); experimental sample cut in half (right).

The pressing die was then removed and a block of solid paraffin wax was placed on top of the CENG in the bottom section of the compression system. Paraffin wax properties are presented in

Table 3.1. The setup was placed inside of a vacuum furnace at 80°C and then the furnace was evacuated. As discussed in Section 2.4.2.2, fully saturating the foam is of concern due to the potential to close pores during the compression process. Saturation of the composite was quantified by the percent void, a measurement of the mass of paraffin in the composite compared to the predicted mass of paraffin based on the volume and density. Both CENG composites soaked for 14.5 hours, which resulted in full saturation (0% void).

The CENG composites were used in thermal conductivity and latent heat measurements as well as thermal charging experiments. Thermal charging experimental samples were prepared by cutting 2.54 cm x 2.54 cm x 1.27 cm blocks of the CENG composite. Samples were placed in the test setup of Figure 4.1 and prepared similar to the xGnP thermal charging experiments with the aluminum plate and heater placed on top. A summary of the CENG composite properties compared to those of the xGnP composites is shown in Table 4.3. The increased thermal conductivity of the CENG composite is a result of the additional surface area of the graphite exposed during the expansion process. The percent decrease in latent heat indicates that both 3 wt% graphite systems have a similar reduction in latent heat and that the addition of ODPA to stabilize the xGnP further decreases the latent heat of the composite as reported in Section 3.6.

Table 4.3 Comparison of xGnP to CENG composites; *note that 3 wt% xGnP/0 wt% ODPA is 4%.

	Thermal Conductivity [$Wm^{-1}K^{-1}$]	**Percent Decrease in Latent Heat**
3 wt% xGnP/5 wt% ODPA Paraffin Wax	0.4	10%*
3 wt% CENG Paraffin Wax	2.3	3%
10 wt% xGnP/5 wt% ODPA Paraffin Wax	1.1	15%
1.5 wt% CENG Paraffin Wax	1.1	1%

4.3.2.1. Comparison of graphite composites of similar concentration

Thermal charging response of 3 wt% CENG compared to 3 wt% xGnP is shown in Figure 4.10 (1.55 Wcm^{-2}) and Figure 4.11 (0.39 Wcm^{-2}). The percent temperature increase, as calculated for the xGnP experiments of Section 4.3.1, is shown in Table 4.4. For both heat fluxes, the 3 wt% CENG bottom temperature increases at a faster rate than the 3 wt% xGnP. Percent increase in temperature data in Table 4.4 indicates that the higher thermal conductivity of the CENG composite has a greater impact on the thermal charging rate for the high heat flux as compared to the low heat flux. The solid-solid phase change is shown in Figure 4.11 by the inflection in the temperature data around 35°C, which corresponds to the solid-solid phase change temperature of paraffin wax.

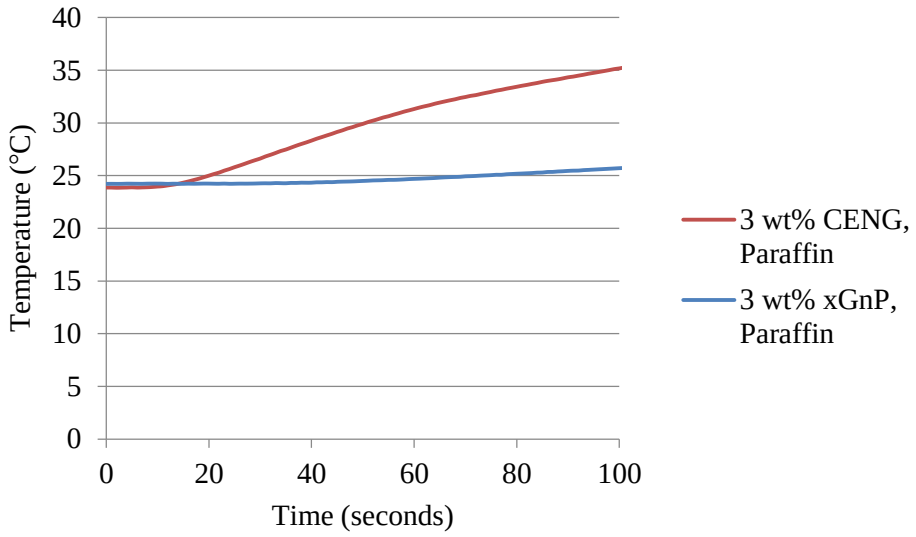

Figure 4.10 Bottom temperature of thermal charging experiments under 1.55 Wcm^{-2}; xGnP sample with 5 wt% ODPA.

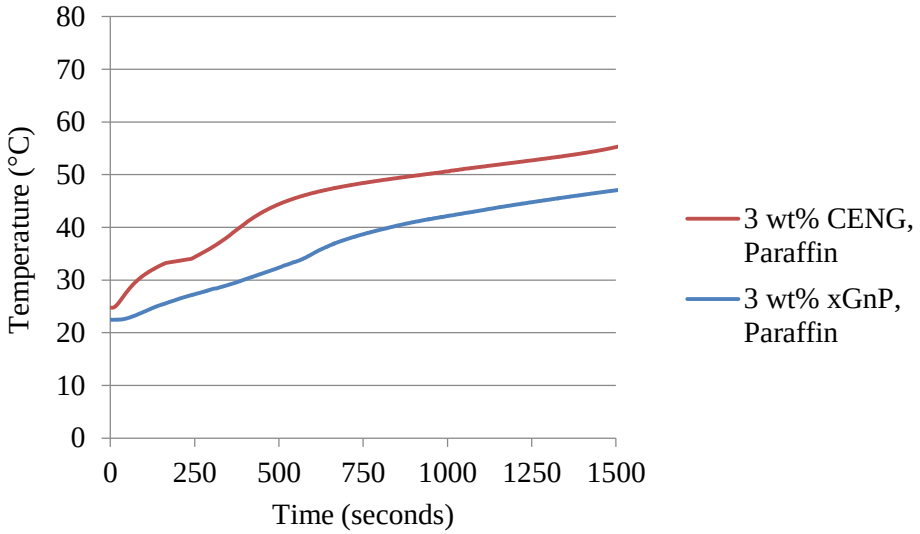

Figure 4.11 Bottom temperature of thermal charging experiments under 0.39 Wcm^{-2}; xGnP sample with 5 wt% ODPA.

Table 4.4 Percent increase in temperature of data in Figure 4.10 and Figure 4.11.

	1.55 Wcm^{-2}	**0.39 Wcm^{-2}**
Paraffin Wax	3%	81%
3 wt% xGnP/5 wt% ODPA Paraffin Wax	6%	109%
3 wt% CENG Paraffin Wax	47%	123%

This comparison between 3 wt% CENG and 3 wt% xGnP composites indicates that material geometry and boundary condition, not only weight percentage, impacts thermal response of the composite. By comparing the response under high and low heat fluxes in Table 4.4, it is indicated that for a high heat flux, the CENG outperforms the xGnP by 41%, but under the low heat flux, the difference is only 14% between the two systems. It could be posited for even lower heat fluxes, xGnP may be superior to CENG on the impact on thermal charging performance. However, at such low heat fluxes, the addition of either CENG or xGnP would not have a significant impact compared to pure paraffin wax and would not be beneficial when considering the decrease in latent heat.

4.3.2.2. Comparison of graphite composites of similar thermal conductivity

Thermal charging response of 1.5 wt% CENG compared to 10 wt% xGnP is shown in Figure 4.12 (1.55 Wcm^{-2}) and Figure 4.13 (0.39 Wcm^{-2}). Both composites have a thermal conductivity of 1.1 $Wm^{-1}K^{-1}$. The percent temperature increase, as calculated for the xGnP experiments of Section 4.3.1, is shown in Table 4.5. Though there is some variation in the percent increase, the samples with the same thermal conductivity perform similarly. The solid-solid phase change is shown in Figure 4.13 by the inflection in the temperature data around 35°C, which corresponds to the solid-solid phase change temperature of paraffin wax. The difference in the melting curves of the xGnP composite compared to the CENG is attributed to the addition of ODPA, which affects the DSC curve.

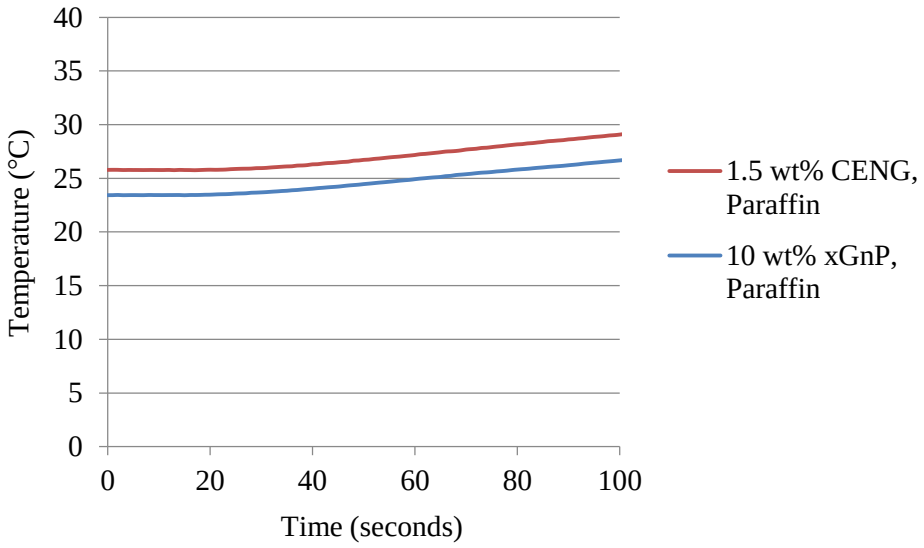

Figure 4.12 Bottom temperature of thermal charging experiments under 1.55 Wcm^{-2}; xGnP sample with 5 wt% ODPA.

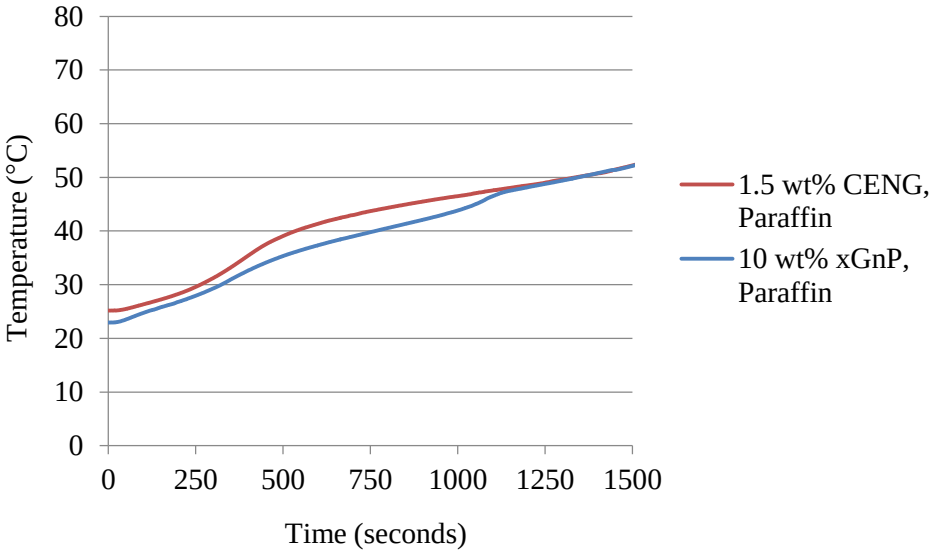

Figure 4.13 Bottom temperature of thermal charging experiments under 0.39 Wcm^{-2}; xGnP sample with 5 wt% ODPA.

Table 4.5 Percent increase in temperature of data in Figure 4.12 and Figure 4.13.

	1.55 Wcm^{-2}	**0.39 Wcm^{-2}**
Paraffin Wax	3%	81%
10 wt% xGnP/5 wt% ODPA Paraffin Wax	14%	127%
1.5 wt% CENG Paraffin Wax	11%	107%

This comparison between 1.5 wt% CENG and 10 wt% xGnP samples indicates that thermal conductivity of the graphite composite provides a good estimation of how the system will perform under constant heat flux thermal charging. This performance was tested under two different heat fluxes. Due to the limited impact on latent heat of the 1.5 wt% CENG samples, this work also suggests that material geometry is important to consider when choosing thermal performance enhancement materials. While the 10 wt% xGnP/5 wt% ODPA samples decreased the latent heat by 15%, the 1.5 wt% CENG composite only decreased it by 1%.

Recall that initial investigation of xGnP was motivated by the objective of reducing impact on latent heat. While xGnP addition has historically been based on the percolation threshold of 3 wt%, literature discussing CENG does not study systems less than 6 wt% (50 kgm^{-3}) due to structural concerns. It is posited that this difference in material concentration supported the conclusion regarding the impact on latent heat. However, when considering the necessity of ODPA to stabilize the graphite, as well as the ability to encase CENG composites in a shell to prevent structural decay, it is concluded that CENG is superior to xGnP as a standalone system.

4.3.2.3. Cost Comparison of CENG and xGnP composites

The thermal performance of xGnP and CENG samples has been compared in 4.3.2.1 and 4.3.2.2, but to fully understand the impact of these materials, comparison must also be conducted on a cost basis. Bulk material costs were obtained from manufactures and are listed in Table 4.6. The composite cost is calculated by multiplying the cost of the bulk material by its respective weight percent in each composite system. By considering the reduction in latent heat of each enhancement material, an energy storage cost has been calculated.

Table 4.6 Cost comparison of graphite systems; *Sum of xGnP and ODPA

	Bulk Material Cost [$kg^{-1}]	wt% in Composite	Composite Cost [$kg^{-1}]	Reduction in Latent Heat	Energy Storage Cost [$J^{-1}]
Expandable Graphite	3				
11 kg/m^3		1.5%	0.045	1%	0.030
23 kg/m^3		3.0%	0.09	3%	0.020
xGnP	50				
3 wt% xGnP		3.0%	1.5	10%	0.135*
10 wt% xGnP		10.0%	5	15%	0.248*
ODPA	10	5.0%	0.5	-	-

The analysis indicates that the energy storage cost of xGnP is an order of magnitude greater than CENG. This is a result of additional processing and small tolerances required of consistent xGnP production as well as the need for ODPA to stabilize the xGnP. It is further confirmed that CENG is a superior thermal enhancement material as compared to xGnP.

4.3.3. Summary of Graphite Composites

Thermal charging experiments with graphite composites indicate that material geometry, boundary conditions, and thermal conductivity impact the response of the system. Experiments with xGnP composites indicate that percent increase in temperature does not have a direct relationship to thermal conductivity. This suggests that thermal conductivity of the composite is an insufficient metric to compare the influence of nanoparticles on the rate of thermal energy storage of the PCM composite as they are not linearly related.

In comparisons with similar graphite concentration, CENG systems outperformed xGnP systems due to the CENG high thermal conductivity. Exposure to a high heat flux resulted in greater improvement by the CENG as compared to xGnP or pure paraffin wax. In experiments with composites of comparable thermal conductivity, the systems performed similarly. This

indicates that, although thermal conductivity is not linearly related to the rate of thermal charging, composites of similar thermal conductivity can be expected to perform the same in thermal charging applications. By comparing percent increase in temperature, 10 wt% could be considered superior, but this comes at a significant cost of latent heat capacity. This comparison of latent heat storage capacity also explains why 10 wt% system slightly outperformed the 1.5 wt% CENG; the inability to store as much latent heat means that the system will move out of the solid-solid phase change period earlier and, therefore, increase in temperature faster during sensible heating until the system reaches solid-liquid phase change.

In general, the results presented in this section indicate that CENG is superior to xGnP as a method to increase thermal charging of PCM based on both performance and energy storage cost. Additional work should be completed to understand the impact of CENG concentration on the rate of thermal charging and latent heat capacity. As shown in Table 4.4 and Table 4.5, 3 wt% CENG outperforms 1.5 wt%, but the associated impact varies for high and low heat fluxes. Since the xGnP results indicate that the different in performance is not linearly related to the material concentration, a similar study should be completed for CENG composites.

4.4. Aluminum Foam Composites

A potential issue with CENG composites is that the compressed graphite does not produce a structurally supportive material. For some applications, the additional rigidity of aluminum foams is necessary. Though the production of CENG does not allow the integration of this composite in aluminum foams, xGnP composites can easily be incorporated by pouring paraffin wax premixed with xGnP and ODPA into the foam. The following section studies the

use of stable graphite nanoplatelet composites in improving the thermal charging performance of aluminum foams.

4.4.1. Thermal Charging Enhancement using Aluminum Foam

Aluminum foams are an attractive thermal enhancement material due to their stiffness/strength properties paired with high thermal conductivity, high surface area densities, and continuous interconnected pore structure [30, 63]. They are a promising thermal enhancement material for latent heat thermal storage systems that require structural support, though weight can become a concern for larger systems as aluminum is denser than graphite. As discussed in Section 2.4.1, foams are described by their pore density and relative density. Both of these parameters impact the natural convection and conduction within the PCM/foam system, which then impact the rate of thermal charging. In general, the introduction of aluminum foam may impede natural convection depending on orientation of the heat source, but the conductive foam network greatly improves the thermal charging as compared to the influence from natural convection within a pure PCM system. However, an additional complexity of natural convection within the pore is of concern. As the surface area increases to promote conduction within the system, the size of the pore decreases, therefore, limiting the natural convection within the pore.

This brief summary of the tradeoffs between natural convection and conduction as a function of the relative density and pore density introduces the complexity of studying the impact on thermal charging of foams under different boundary conditions. In addition to the geometry of the foam, another way to increase the rate of thermal charging is to increase the thermal conductivity of the paraffin wax with which the aluminum is saturated. Paraffin wax mixed with xGnP stabilized with ODPA is studied as a method of increasing the rate of thermal charging.

Thermal charging experiments were performed for three aluminum foam pore densities under 1.55 Wcm^{-2} with varying weight percentages of xGnP. The graphite nanoplatelets/paraffin wax composites described in Chapter 3 were used to saturate 9% relative density aluminum foams, which were acquired from ERG Aerospace in three different pore densities, 10, 20, and 40 PPI. Foam samples were cut into rectangular portions with sides of 2.54 cm with a thickness of 1.27 cm and then permanently bonded to an aluminum plate with Epoxy Technology thermal epoxy. Figure 4.14 (left) depicts the aluminum before and after the epoxy process.

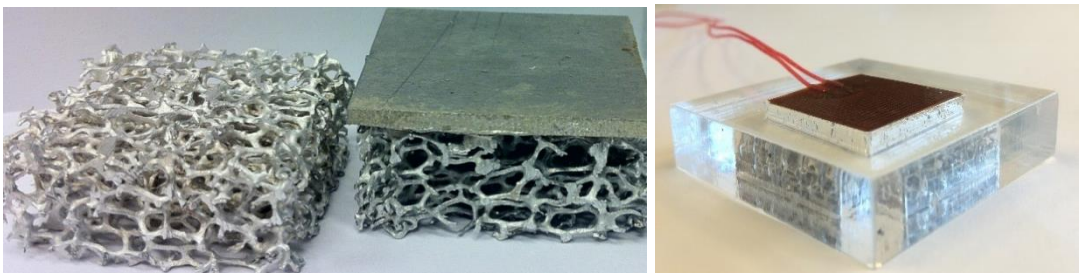

Figure 4.14 Aluminum foam before and after the attachment of the aluminum plate (left); Sample with heater attached to aluminum plate, foam saturated with PCM, and integrated into acrylic container (right).

To saturate the aluminum foams with the PCM composite, each sample was heated on a hotplate at 100°C for 10 minutes and then immediately placed into the top portion of the test setup of Figure 4.1. The setup was oriented upside down with the aluminum plate on the bottom, and liquid paraffin/xGnP mixture was poured into the foam. A piece of aluminum foil was immediately placed on top and then the solid side of the test container was placed on top of the aluminum foil. The sample was immediately turned over, so that the heater was on the top. This process was completed to remove any air bubbles in the system and to ensure that the PCM filled all pores of the foam. The sample was allowed to cool and excess PCM was removed. The final product is show in Figure 4.1 (right).

Comparison between the baseline aluminum foams saturated with paraffin wax and those enhanced with xGnP is made graphically through the temperature response as well as numerically by calculating the melting time. Example baseline data is shown by the pure paraffin data of Figure 4.15. The initial steep temperature slope indicates the sensible heating portion of paraffin followed by a lesser temperature change during the solid-solid and then solid-liquid phase change portion of the heating process. The shift to a steeper slope around 56°C indicates the period when phase change melting process has ended and the paraffin continues storing heat as sensible heat. The impact on thermal performance is measured by the time of this change from solid-liquid latent to sensible heat storage. This metric is referred to as time to end of melt. To find the time to end of melt for each system, the maximum difference between the top and bottom temperature of the sample was calculated. The time and top and bottom temperatures associated when this maximum temperature difference occurred were recorded and used to compare the systems. Note that a shorter time to end of melt coincides with better thermal charging.

Bottom temperature data recorded for 40 PPI aluminum foam saturated with pure paraffin and 3 wt% xGnP is shown in Figure 4.15. Temperature measurements indicate that the addition of 3 wt% xGnP decreases the time to end of melt by 7%. Similar results are shown by 10 PPI and 20 PPI foams, shown in Figure 4.16, which displays a 6% and an 8% decrease in time to end of melt with the addition of 3 wt% xGnP stabilized with ODPA. The difference in initial temperatures, specifically noticeable for 10 PPI and 20 PPI experiments, was unavoidable due to uncontrollable ambient lab temperatures. It is noted that the samples that began at lower temperatures were those mixed with xGnP. Therefore, the percent decrease in time to end of melt for these systems may be lower than the calculated values.

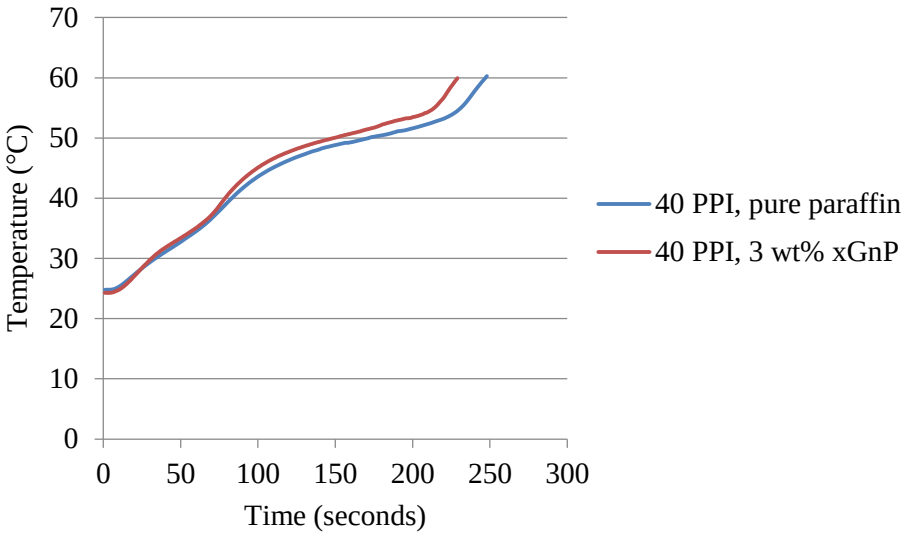

Figure 4.15 Bottom temperature data for 40 PPI aluminum foam saturated with pure paraffin and 3 wt% xGnP/5 wt% ODPA exposed to 1.55 Wcm^{-2}.

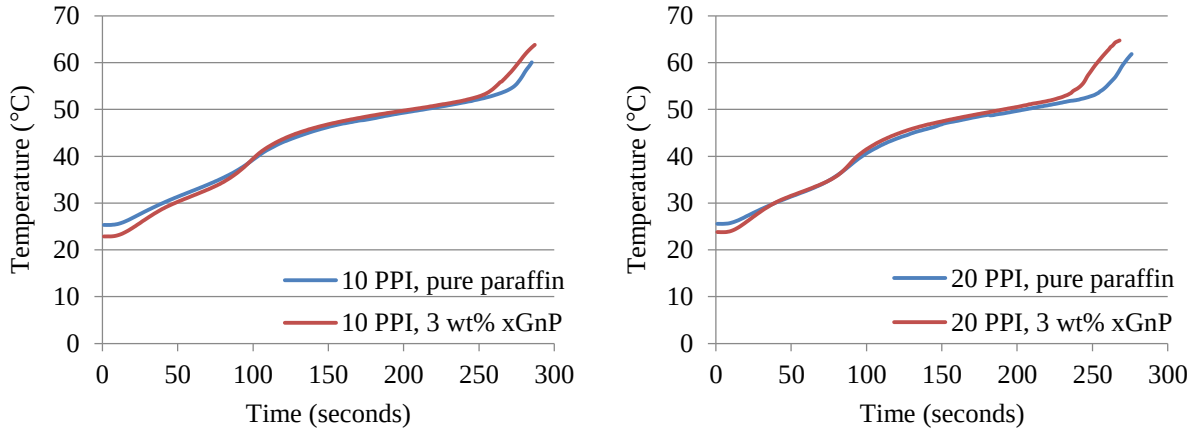

Figure 4.16 Bottom temperature data for 10 PPI and 20 PPI aluminum foam saturated with pure paraffin and 3 wt% xGnP/5 wt% ODPA exposed to 1.55 Wcm^{-2}.

Data presented in Figure 4.15 and Figure 4.16 is summarized in Table 4.7. The top temperature refers to the temperature of the top of the sample at the time to end of melt. In addition to the decrease in time to end of melt, the top temperature decreases for samples with graphite nanoplatelets. The decrease of both of these values indicates that the addition of xGnP increases the rate of charging by distributing heat more evenly through the composite. The decrease in the top temperature is specifically of interest for thermal management systems where

the PCM system not only stores heat, but also limits the junction temperature to prevent harm to electronics. Even if considered within the margin of error for each of the respective measurements, this work suggests that the addition of xGnP offers a method to reduce the bulk density of the aluminum foam, while providing similar thermal charging performance.

Table 4.7 Summary of data presented in Figure 4.15 and Figure 4.16.

	Time to End of Melt [sec]	**Top Temperature [°C]**
40 PPI, pure paraffin	225	78.3
40 PPI, 3 wt% xGnP	209	77.6
20 PPI, pure paraffin	253	85.0
20 PPI, 3 wt% xGnP	233	83.7
10 PPI, pure paraffin	271	86.5
10 PPI, 3 wt% xGnP	254	84.8

A cycling study was performed to study the performance of the aluminum foam/xGnP composite when exposed to 1.55 Wcm^{-2} until the top temperature reached the acrylic limit of 100°C, allowed to naturally cool, and then reheated. This process was completed 8 times. Data is presented in Figure 4.17 and Table 4.8. Due to uncontrollable ambient lab temperatures, Figure 4.17 compares Trial 4 through Trial 8 because all began with initial bottom temperatures between 24.3°C and 25.6°C. Data indicates that the thermal charging performance, as measured by time to end of melt, varies less than 4% for Trial 4 through Trial 8. This variation can be attributed to slight variation in the initial temperature condition.

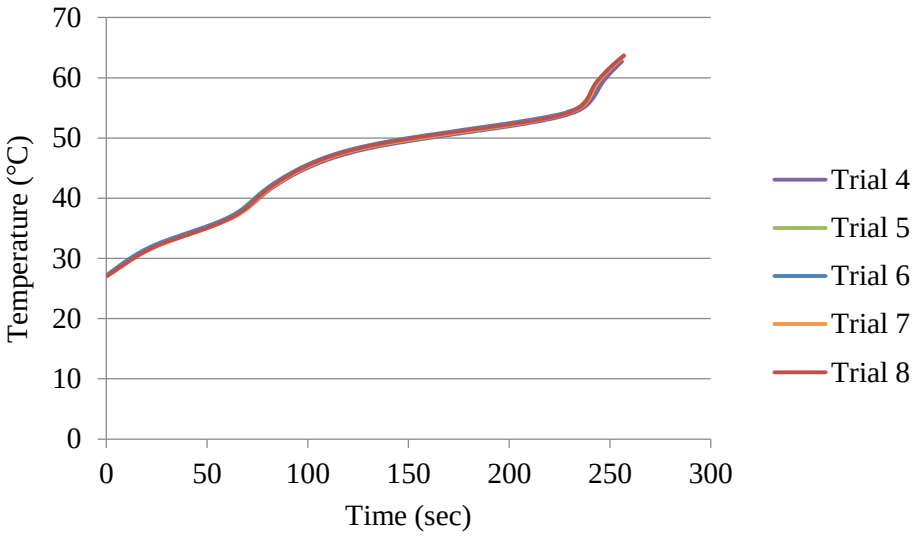

Figure 4.17 Bottom temperature data for 10 PPI aluminum foam/3 wt% xGnP/5 wt% ODPA cycling study exposed to 1.55 Wcm^{-2}.

Table 4.8 Summary of thermal charging cycling trials

Trial	Time to End of Melt [sec]	Initial Bottom Temperature [°C]
1	254	22.9
2	243	26.7
3	263	22.7
4	250	25.4
5	251	24.6
6	256	24.3
7	248	25.6
8	246	25.6

As discussed in Table 4.3 and Section 4.3.2, the addition of 3 wt% xGnP and 5 wt% ODPA decreases the latent heat by 10%, but it also increases the thermal charging rate of aluminum foams by about 7% when exposed to high heat flux as shown in Table 4.7. For applications where additional aluminum is not an option due to cost or size constraints, the addition of xGnP provides a cost effective alternative to using aluminum foams of high relative density.

CHAPTER 5: CONCLUSIONS AND FUTURE WORK

5.1. Summary of Contributions

The development of thermally responsive systems with high energy density for storing waste heat is a critical link between energy production and utilization in the effort to reduce overall energy demand. Phase change materials offer high energy storage capacity due to the latent heat storage. While the temperature at which phase change can occur covers a wide range based on chemical structure, the phase change process typically spans a small temperature range. This allows the PCM to be tuned for specific applications. Solid-liquid PCMs have a high latent heat capacity as well as exhibit small volume changes. Organic solid-liquid PCMs are chemically stable, non-toxic, and non-corrosive. The main issue with organic solid-liquid PCMs is their characteristic low thermal conductivity, which limits the rate at which thermal energy can be stored.

This thesis focused on the addition of high conductivity foams or nanoparticles within PCM to improve thermal performance of the composite. The study was motivated by the goal to increase the thermal charging rate while having limited impact on latent heat capacity as well as on the time and energy required for composite production. Graphite was used due to its high thermal conductivity and low density, while paraffin wax and microcrystalline wax were used as two common types of organic solid-liquid PCMs.

Effective thermal conductivity enhancement with highly conductive nanoparticles in PCM is dependent on stability of these suspensions during melting and solidification. This thesis made an original contribution by studying methods of stabilizing graphite nanoplatelets in liquid PCM and is the first to incorporate a dispersant with xGnP, which increased stability from 11

minutes to 50 hours as measured by both visual inspection and capacitance sedimentation measurements. It was also determined that the stability depends greatly on particle size, dispersion of the platelets, and viscosity of the wax, while oxidation of the wax has little impact. This study included characterizing the properties of the wax using NMR and Raman spectroscopy as well as measuring the thermal conductivity, melting temperature, and latent heat to understand the impact of the xGnP and dispersant on the properties of the PCM.

The primary performance metric traditionally used to compare graphite nanoplatelet systems is thermal conductivity of the composite measured in the solid state. An original contribution of this thesis was the further investigation of such systems based on thermal charging and energy storage cost metrics. Thermal charging experiments under various heat fluxes were completed for xGnP composites to compare the thermal response of each system as a function of the measured thermal conductivity in the solid state. These experiments showed that thermal response does not have a linear relationship to thermal conductivity. For example, a 150% increase in thermal conductivity resulted in a 28% increase in charging rate, but a 450% increase in thermal conductivity only saw an increase in 46% of the thermal charging rate. This suggests that thermal conductivity of the composite is an insufficient metric to solely compare the influence of nanoparticles on the rate of thermal energy storage of the PCM composite.

To advance the study of the impact of thermal conductivity, graphite concentration, and material geometry on the thermal response of PCM, compressed expanded graphite foam composites of similar material concentrations and thermal conductivities as the xGnP samples were prepared. Because of the increased surface area and distribution of the CENG, a much smaller weight percentage of graphite was required to obtain a comparable sample in terms of thermal conductivity of xGnP. For example, both a 10 wt% xGnP composite and a 1.5 wt%

CENG composite had thermal conductivities of 1.1 $Wm^{-1}K^{-1}$. Comparison between the thermal charging curve of 1.5 wt% CENG and 10 wt% xGnP samples indicated that thermal conductivity of the graphite composite provides a good estimation of how the system will perform under constant heat flux conditions. Although there is a direct relationship between conductivity and charging, CENG results reaffirmed that this result is not linear. Due to the limited impact on latent heat of the 1.5 wt% CENG samples, this work also suggests that material geometry is important to consider when choosing thermal performance enhancement materials. While the 10 wt% xGnP/5 wt% ODPA samples decreased the latent heat by 15%, the 1.5 wt% CENG composite only decreased it by 1%.

In general, CENG has less impact on the composite latent heat and exhibits a better thermal response due to the material foam geometry as compared to nanoparticles. Latent heat is significantly affected due to the higher concentration of xGnP required to reach thermal conductivities comparable to CENG as well as the addition of ODPA to stabilize the nanoparticles. Additionally, because of less stringent production restrictions as well as no dispersant required to improve stability, CENG has a lower energy storage cost than xGnP, which is calculated as a function of the bulk material cost, material concentration, and impact on latent heat.

When used as a discrete system, CENG is considered a superior thermal enhancement material as compared to xGnP. However, when the structural rigidity of metal foam is required, CENG foams are not a feasible option. Aluminum foams are a common solution for enhancing the thermal performance of PCM in such conditions, however, compared to graphite, this adds considerable expense to the system. The stable xGnP/paraffin wax composite was introduced for the first time to aluminum foam to study the impact of increasing the thermal conductivity of the

baseline aluminum foam/paraffin wax system. It was found that this proposed composite offers a method of increasing the performance of aluminum foams without the further cost or weight of additional aluminum.

5.2. Future Work

For low-grade waste heat applications, CENG foams offer a promising alternative to nanoparticles or metal foams. The production of this lightweight, low cost system is scalable and the foam is easily molded to conform to many geometries. However, similar to work with xGnP, the main comparison metrics used in literature are the impact on thermal conductivity and latent heat as a function of material concentration. As discussed in this thesis, the additional concerns of thermal charging performance, energy storage cost, and stability are of equal significance and need to be addressed. Future work should focus on the impact of CENG concentration and system boundary condition on the thermal charging performance of CENG composites. Stability of CENG should also be confirmed through cyclic studies. Further efforts should focus on modelling the CENG systems with experimental validation to study various geometries of latent heat thermal storage systems.

For applications that require metallic foams, additional work needs to be focused on the potential of combining two thermal enhancement materials into one system. This combination would allow for a minimization of metal foam to conform only to structural requirements. Excess metal to increase thermal transport would not be required because of enhanced thermal transport from the PCM with a lightweight or more cost effective option such as graphite nanoparticles. This type of hybrid system requires a more robust study on the cyclic stability and

performance as well as how boundary conditions and xGnP concentration affect thermal charging stability and performance.

REFERENCES

[1] L. L. N. Laboratory and U. D. o. Energy, "Estimated US Energy Use in 2011: ~97.3 Quads," ed, 2012.

[2] I. BCS, "Waste Heat Recovery: Technology and Opportunities in U.S. Industry," 2008.

[3] G. J. Zhang, M. Cai, and A. Hu, "Energy consumption and the unexplained winter warming over northern Asia and North America," *Nature Climate Change*, 2013.

[4] C. C. S. Reddy, S. V. Naidu, and G. P. Rangaiah, "Waste Heat Recovery Methods And Technologies," *Chemical Engineering*, vol. 120, pp. 28-38, 2013.

[5] G. Shu, Y. Liang, H. Wei, H. Tian, J. Zhao, and L. Liu, "A review of waste heat recovery on two-stroke IC engine aboard ships," *Renewable & Sustainable Energy Reviews*, vol. 19, pp. 385-401, 2013.

[6] C. R. Kumar, A. Sonthalia, and R. Goel, "EXPERIMENTAL STUDY ON WASTE HEAT RECOVERY FROM AN INTERNAL COMBUSTION ENGINE USING THERMOELECTRIC TECHNOLOGY," *Thermal Science*, vol. 15, pp. 1011-1022, 2011.

[7] W. C. Ltd. (4/19). *Hybrid Power Generation Systems*. Available: http://www.mpoweruk.com/hybrid_power.htm

[8] I. Dincer and M. Rosen, *Thermal energy storage: systems and applications*, 2 ed.: Wiley, 2011.

[9] B. Zalba, H. Mehling, J. M. Marín, and L. F. Cabeza, "Review on thermal energy storage with phase change: materials, heat transfer analysis and applications," *Materials, heat transfer analysis and applications*, vol. 23, pp. 251-283, 2003.

[10] A. Sharma, V. V. Tyagi, C. R. Chen, and D. Buddhi, "Review on thermal energy storage with phase change materials and applications," *Renewable & Sustainable Energy Reviews*, vol. 13, pp. 318-345, 2009.

[11] S. D. Sharma and K. Sagara, "Latent heat storage materials and systems - A review," vol. 2, pp. 1-56, 2005.

[12] "Phase Changes."

[13] A. Shukla, D. Buddhi, and R. L. Sawhney, "Solar water heaters with phase change material thermal energy storage medium: A review," *Renewable and Sustainable Energy Reviews*, vol. 13, pp. 2119-2125, 2009.

[14] M. M. Farid, "review on phase change energy storage," *materials and applications*, vol. 45, pp. 1597-1615, 2004.

[15] S. M. Hasnain, "Review on sustainable thermal energy storage technologies, Part I: heat storage materials and techniques," *Energy Conversion and Management*, vol. 39, 1998.

[16] G. A. Lane, "Solar heat storage: Latent heat materials," 1983.

[17] F. Agyenim, "A review of materials, heat transfer and phase change problem formulation for latent heat thermal energy storage systems (LHTESS)," *Renewable & Sustainable Energy Reviews*, vol. 14, pp. 615-628, 2010.

[18] N. Sarier and E. Onder, "Organic phase change materials and their textile applications: an overview," *Thermochimica Acta*, 2012.

[19] A. Sarı, H. Sarı, and A. Önal, "Thermal properties and thermal reliability of eutectic mixtures of some fatty acids as latent heat storage materials," *Energy Conversion and Management*, vol. 45, pp. 365-376, 2004.

[20] A. Malfliet, G. Deferme, L. Stappers, and J. Fransaer, "Synthesis and characterization of composite coatings for thermal actuation," *Journal of The Electrochemical Society,* vol. 154, pp. D50-D56, 2007.
[21] C. Hoogendoorn and G. Bart, "Performance and modelling of latent heat stores," *Solar energy,* 1992.
[22] M. Liu, W. Saman, and F. Bruno, "Review on storage materials and thermal performance enhancement techniques for high temperature phase change thermal storage systems," *Renewable and Sustainable Energy Reviews,* vol. 16, pp. 2118-2132, 2012.
[23] Y.-T. Yang and Y.-H. Wang, "Numerical simulation of three-dimensional transient cooling application on a portable electronic device using phase change material," *International Journal of Thermal Sciences,* vol. 51, pp. 155-162, 2012.
[24] K. Ki-bum, C. Kyung-wook, K. Young-jin, L. Ki-hyung, and L. Kwan-soo, "Feasibility study on a novel cooling technique using a phase change material in an automotive engine," *Energy,* vol. 35, pp. 478-484.
[25] W.-f. Wu, N. Liu, W.-l. w. u. e. c. Cheng, and Y. Liu, "Study on the effect of shape-stabilized phase change materials on spacecraft thermal control in extreme thermal environment," *Energy Conversion & Management,* vol. 69, pp. 174-180, 2013.
[26] G. Guyonvarch, R. Haller, and L. Lepetit, "Cold storage and thermal comfort in stop-start vehicles and urban driving cycles," *Revue de l'Electricite et de l'Electronique,* pp. 80-84, 2005.
[27] F. Sai Cheong, T. Fock Lai, and S. Chong Chai, "EXPERIMENTAL INVESTIGATIONS ON THE COOLING OF A MOTORCYCLE HELMET WITH PHASE CHANGE MATERIAL," *Thermal Science,* vol. 15, pp. 807-816, 2011.
[28] (2012). *Statistical Review of World Energy*. Available: http://www.bp.com/sectionbodycopy.do?categoryId=7500&contentId=7068481
[29] M. A. Brown, *Climate change and global energy security : technology and policy options*. MIT Press: Cambridge, Mass., 2011.
[30] S. Jegadheeswaran and S. D. Pohekar, "Performance enhancement in latent heat thermal storage system: A review," *Renewable and Sustainable Energy Reviews,* vol. 13, pp. 2225-2244, 2009.
[31] M. Lacroix, "Study of the heat transfer behavior of a latent heat thermal energy storage unit with a finned tube," *International journal of heat and mass transfer,* vol. 36, pp. 2083-2092, 1993.
[32] M. Gharebaghi and I. Sezai, "Enhancement of heat transfer in latent heat storage modules with internal fins," *Numerical Heat Transfer, Part A: Applications,* vol. 53, pp. 749-765, 2007.
[33] Y. Zhang, Z. Chen, Q. Wang, and Q. Wu, "Melting in an enclosure with discrete heating at a constant rate," *Experimental thermal and fluid science,* vol. 6, pp. 196-201, 1993.
[34] B. J. Jones, D. Sun, S. Krishnan, and S. V. Garimella, "Experimental and numerical study of melting in a cylinder," *International journal of heat and mass transfer,* vol. 49, pp. 2724-2738, 2006.
[35] K. Ng, Z. Gong, and A. Mujumdar, "Heat transfer in free convection-dominated melting of a phase change material in a horizontal annulus," *International communications in Heat and mass transfer,* vol. 25, pp. 631-640, 1998.
[36] F. Tan, "Constrained and unconstrained melting inside a sphere," *International communications in Heat and mass transfer,* vol. 35, pp. 466-475, 2008.

[37] C. Liu and D. Groulx, "Numerical Study of the Effect of Fins on the Natural Convection Driven Melting of Phase Change Material," in *COMSOL Conference 2011*, 2011.
[38] M. Lacroix and M. Benmadda, "Analysis of natural convection melting from a heated wall with vertically oriented fins," *International Journal of Numerical Methods for Heat & Fluid Flow,* vol. 8, pp. 465-478, 1998.
[39] H. Ettouney, H. El-Dessouky, and E. Al-Kandari, "Heat transfer characteristics during melting and solidification of phase change energy storage process," *Industrial & engineering chemistry research,* vol. 43, pp. 5350-5357, 2004.
[40] R. Akhilesh, A. Narasimhan, and C. Balaji, "Method to improve geometry for heat transfer enhancement in PCM composite heat sinks," *International journal of heat and mass transfer,* vol. 48, pp. 2759-2770, 2005.
[41] M. Lacroix and M. Benmadda, "Numerical simulation of natural convection-dominated melting and solidification from a finned vertical wall," *Numerical Heat Transfer, Part A Applications,* vol. 31, pp. 71-86, 1997.
[42] V. Shatikian, G. Ziskind, and R. Letan, "Numerical investigation of a PCM-based heat sink with internal fins," *International journal of heat and mass transfer,* vol. 48, pp. 3689-3706, 2005.
[43] K. C. Nayak, S. K. Saha, K. Srinivasan, and P. Dutta, "A numerical model for heat sinks with phase change materials and thermal conductivity enhancers," *International Journal of Heat and Mass Transfer,* vol. 49, pp. 1833-1844, 2006.
[44] S. Krishnan, S. V. Garimella, and S. S. Kang, "A novel hybrid heat sink using phase change materials for transient thermal management of electronics," *Components and Packaging Technologies, IEEE Transactions on,* vol. 28, pp. 281-289, 2005.
[45] J. C. Kurnia, A. P. Sasmito, S. V. Jangam, and A. S. Mujumdar, "Improved design for heat transfer performance of a novel phase change material (PCM) thermal energy storage (TES)," *Applied Thermal Engineering,* 2012.
[46] L. Tan, Y. Kwok, A. Date, and A. Akbarzadeh, "Numerical Study of Natural Convection Effects in Latent Heat Storage using Aluminum Fins and Spiral Fillers."
[47] Z. Chen, L. Cao, G. Fang, and F. Shan, "Synthesis and Characterization of Microencapsulated Paraffin Microcapsules as Shape-Stabilized Thermal Energy Storage Materials," *Nanoscale & Microscale Thermophysical Engineering,* vol. 17, pp. 112-123, 2013.
[48] B. Li, T. Liu, L. Hu, Y. Wang, and L. Gao, "Fabrication and Properties of Microencapsulated Paraffin@SiO2 Phase Change Composite for Thermal Energy Storage," *ACS Sustainable Chemistry & Engineering,* vol. 1, pp. 374-380, 2013/03/04 2013.
[49] M. Zhang, X.-M. Tong, H. Zhang, and J.-H. Qiu, "Preparation and characterization of Poly (MMA-co-AA)/Paraffin microencapsulated phase change material for thermal energy storage," *Energy Sources, Part A: Recovery, Utilization, and Environmental Effects,* vol. 34, pp. 396-403, 2012.
[50] Y. Wang, H. Shi, T. D. Xia, T. Zhang, and H. X. Feng, *Fabrication and performances of microencapsulated paraffin composites with polymethylmethacrylate shell based on ultraviolet irradiation-initiated.*
[51] L. Fan and J. M. Khodadadi, "Thermal conductivity enhancement of phase change materials for thermal energy storage: A review," *Renewable and Sustainable Energy Reviews,* vol. 15, pp. 24-46, 2011.

[52] A. Mills, S. Al-Hallaj, M. Farid, and J. R. Selman, "Thermal conductivity enhancement of phase change materials using a graphite matrix," *Applied Thermal Engineering,* vol. 26, pp. 1652-1661, 2006.
[53] E.-B. S. Mettawee and G. M. R. Assassa, "Thermal conductivity enhancement in a latent heat storage system," *Solar Energy,* vol. 81, pp. 839-845, 2007.
[54] J. Y. Long, "Study on Phase-change Temperature and Latent Heat of Organic Phase-change Nano-fluid," *Advanced Materials Research,* vol. 152-153, pp. 1591-1594, 2010.
[55] J. Y. Long, "Study on Thermal Conductivity of Organic Phase-Change Nano-Fluid," *Advanced Materials Research,* vol. 152-153, pp. 1579-1582, 2010.
[56] S.-T. Hong and D. R. Herling, "Effects of surface area density of aluminum foams on thermal conductivity of aluminum foam-phase change material composites," *Advanced Engineering Materials,* vol. 9, pp. 554-557, 2007.
[57] J. A. Molefi, A. S. Luyt, and I. Krupa, "Investigation of thermally conducting phase-change materials based on polyethylene/wax blends filled with copper particles," *Journal of Applied Polymer Science,* vol. 116, pp. 1766-1774, 2010.
[58] W. Yu, H. Xie, and X. Wang, "Enhanced Thermal Conductivity of Liquid Paraffin Based Nanofluids Containing Copper Nanoparticles," *Journal of Dispersion Science and Technology,* vol. 32, pp. 948-951, 2011.
[59] C. Y. Zhao, W. Lu, and Y. Tian, "Heat transfer enhancement for thermal energy storage using metal foams embedded within phase change materials (PCMs)," *Solar Energy,* vol. 84, pp. 1402-1412, 2010.
[60] A. Siahpush, J. O'Brien, and J. Crepeau, "Phase Change Heat Transfer Enhancement Using Copper Porous Foam," *Journal of Heat Transfer,* vol. 130, p. 082301, 2008.
[61] Y. Zhong, S. Li, X. Wei, Z. Liu, Q. Guo, J. Shi, *et al.*, "Heat transfer enhancement of paraffin wax using compressed expanded natural graphite for thermal energy storage," *CARBON,* vol. 48, pp. 300-304, 2010.
[62] E. Aerospace. (2011). *The Basics of Duocel® Foam*. Available: http://www.ergaerospace.com/Descriptors.htm
[63] C. Y. Zhao, "Review on thermal transport in high porosity cellular metal foams with open cells," *International Journal of Heat and Mass Transfer,* vol. 55, pp. 3618-3632, 2012.
[64] C. Y. Zhao, "Heat transfer enhancement of high temperature thermal energy storage using metal foams and expanded graphite," *Solar Energy Materials & Solar Cells,* vol. 95, pp. 636-643, 2011.
[65] Z. Chen, M. Gu, and D. Peng, "Heat transfer performance analysis of a solar flat-plate collector with an integrated metal foam porous structure filled with paraffin," *Applied Thermal Engineering,* vol. 30, pp. 1967-1973, 2010.
[66] K. Lafdi, O. Mesalhy, and S. Shaikh, "Experimental study on the influence of foam porosity and pore size on the melting of phase change materials," *Journal of Applied Physics,* vol. 102, pp. 083549-083549-6, 2007.
[67] W. Li, Z. Qu, Y. He, and W. Tao, "Experimental and numerical studies on melting phase change heat transfer in open-cell metallic foams filled with paraffin," *Applied Thermal Engineering,* vol. 37, pp. 1-9, 2012.
[68] Y. Tian, "Numerical investigation of heat transfer in phase change materials (PCMs) embedded in porous metals," *Energy,* vol. 36, pp. 5539-5546, 2011.

[69] J. M. Marín, B. Zalba, L. F. Cabeza, and H. Mehling, "Improvement of a thermal energy storage using plates with paraffin–graphite composite," *International Journal of Heat and Mass Transfer,* vol. 48, pp. 2561-2570, 2005.
[70] R. Pokhrel, "Analysis and Design of a Paraffin/Graphite Composite PCM Integrated in a Thermal Storage Unit," *Journal of Solar Energy Engineering,* vol. 132, pp. 041006:1-04041006, 2010.
[71] D. Haillot, X. Py, V. Goetz, and M. Benabdelkarim, "Storage composites for the optimisation of solar water heating systems," *Chemical Engineering Research and Design,* vol. 86, pp. 612-617, 2008.
[72] X. Py, "Paraffin/porous-graphite-matrix composite as a high and constant power thermal storage material," *International Journal of Heat and Mass Transfer,* vol. 44, pp. 2727-2737, 2001.
[73] S. Pincemin, R. Olives, X. Py, and M. Christ, "Highly conductive composites made of phase change materials and graphite for thermal storage," *Solar Energy Materials and Solar Cells,* vol. 92, pp. 603-613, 2008.
[74] A. Sari and A. Karaipekli, "Thermal conductivity and latent heat thermal energy storage characteristics of paraffin/expanded graphite composite as phase change material," *Applied Thermal Engineering,* vol. 27, pp. 1271-1277, 2007.
[75] H. Yin, "Experimental research on heat transfer mechanism of heat sink with composite phase change materials," *Energy Conversion & Management,* vol. 49, pp. 1740-1746, 2008.
[76] L. Xia, "Preparation and thermal characterization of expanded graphite/paraffin composite phase change material," *Carbon,* vol. 48, pp. 2538-2548, 2010.
[77] D. Haillot, V. Goetz, X. Py, and M. Benabdelkarim, "High performance storage composite for the enhancement of solar domestic hot water systems: Part 1: Storage material investigation," *Solar energy,* vol. 85, pp. 1021-1027, 2011.
[78] J. Long, "Preparation of uniform and stable organic phase-change nano-fluid of paraffin and nano-aluminum for thermal storage," in *Proceedings: 2010 International Conference on Digital Manufacturing & Automation*, 2010, pp. 110-113.
[79] W. Wang, "Enhanced thermal conductivity and thermal performance of form-stable composite phase change materials by using β-Aluminum nitride," *Applied Energy,* vol. 86, pp. 1196-1200, 2009.
[80] K. Chintakrinda, R. D. Weinstein, and A. S. Fleischer, "A direct comparison of three different material enhancement methods on the transient thermal response of paraffin phase change material exposed to high heat fluxes," *International Journal of Thermal Sciences,* vol. 50, pp. 1639-1647, 2011.
[81] J. Xiang and L. T. Drzal, "Investigation of exfoliated graphite nanoplatelets (xGnP) in improving thermal conductivity of paraffin wax-based phase change material," *Solar Energy Materials & Solar Cells,* vol. 95, pp. 1811-1818, 2011.
[82] S. Kim and L. T. Drzal, "High latent heat storage and high thermal conductive phase change materials using exfoliated graphite nanoplatelets," *Solar Energy Materials & Solar Cells,* vol. 93, pp. 136-142, 2009.
[83] W. Cheng, R.-m. Zhang, K. Xie, N. Liu, and J. Wang, "Heat conduction enhanced shape-stabilized paraffin/HDPE composite PCMs by graphite addition: Preparation and thermal properties," *Solar Energy Materials and Solar Cells,* vol. 94, pp. 1636-1642, 2010.

[84] O. Sanusi, R. Warzoha, and A. S. Fleischer, "Energy storage and solidification of paraffin phase change material embedded with graphite nanofibers," *International Journal of Heat and Mass Transfer,* vol. 54, pp. 4429-4436, 2011.
[85] J. Jeon, S.-G. Jeong, J.-H. Lee, J. Seo, and S. Kim, "High thermal performance composite PCMs loading xGnP for application to building using radiant floor heating system," *Solar Energy Materials and Solar Cells,* vol. 101, pp. 51-56, 2012.
[86] Z. G. Zhang and X. M. Fang, "Study on paraffin/expanded graphite composite phase change thermal energy storage material," *Energy Conversion and Management,* vol. 47, pp. 303-310, 2006.
[87] A. Elgafy and K. Lafdi, "Effect of carbon nanofiber additives on thermal behavior of phase change materials," *CARBON,* vol. 43, pp. 3067-3074, 2005.
[88] Y. Cui, C. Liu, S. Hu, and X. Yu, "The experimental exploration of carbon nanofiber and carbon nanotube additives on thermal behavior of phase change materials," *Solar Energy Materials and Solar Cells,* vol. 95, pp. 1208-1212, 2011.
[89] (2013). *Uses of NMR spectroscopy*. Available: http://chem.ch.huji.ac.il/nmr/whatisnmr/whatisnmr.html
[90] R. A. Williams, C. G. Xie, R. Bragg, and W. P. K. Amarasinghe, "Experimental techniques for monitoring sedimentation in optically opaque suspensions," *Colloids and Surfaces,* vol. 43, pp. 1-32, 1990.
[91] X. Li, T. Lei, W. Wang, Q. Xu, and J. Zhao, "Capacitance sensors for measuring suspended sediment concentration," *CATENA,* vol. 60, pp. 227-237, 2005.
[92] E. Salazar-Neumann, Y. Nahmad-Molinari, J. C. Ruiz-Suarez, P.-L. Ardisson, C. A. Arancibia-Bulnes, and R. Rechtman, "Size distribution of a metallic polydispersion through capacitive measurements in a sedimentation experiment," *Applied Physics Letters,* vol. 79, pp. 406-408, 2001.
[93] T. M. Shi, S. J. R. Simons, F. J. Dickin, and R. A. Williams, "Electrical sensing of dispersion behaviour," *Colloids and Surfaces A: Physicochemical and Engineering Aspects,* vol. 77, pp. 9-27, 1993.
[94] C. G. Xie, R. A. Williams, S. J. R. Simons, M. S. Beck, and R. Bragg, "A novel sedimentation analyser," *Measurement Science and Technology,* vol. 1, p. 1216, 1990.
[95] M. C. Prado, R. Nascimento, L. G. Moura, M. J. S. Matos, M. S. C. Mazzoni, L. G. Cancado, *et al.*, "Two-Dimensional Molecular Crystals of Phosphonic Acids on Graphene," *ACS Nano,* vol. 5, pp. 394-398, 2011/01/25 2010.
[96] A. Moshkovith, V. Perfiliev, A. Verdyan, I. Lapsker, R. Popovitz-Biro, R. Tenne, *et al.*, "Sedimentation of IF-WS2 aggregates and a reproducibility of the tribological data," *Tribology International,* vol. 40, pp. 117-124, 2007.
[97] A. C. Ferrari, "Raman spectroscopy of graphene and graphite: Disorder, electron–phonon coupling, doping and nonadiabatic effects," *Solid State Communications,* vol. 143, pp. 47-57, 2007.
[98] S. Yu, S.-G. Jeong, O. Chung, and S. Kim, "Bio-based PCM/carbon nanomaterials composites with enhanced thermal conductivity," *Solar Energy Materials and Solar Cells,* vol. 120, Part B, pp. 549-554, 2014.
[99] D. Haillot, F. Nepveu, V. Goetz, X. Py, and M. Benabdelkarim, "High performance storage composite for the enhancement of solar domestic hot water systems: Part 2: Numerical system analysis," *Solar energy,* vol. 86, pp. 64-77, 2012.